IOPscience iopscience.iop.org

Home Search Collections Journals About Contact us My IOPscience

Stability of coupled tearing modes in tokamaks

This content has been downloaded from IOPscience. Please scroll down to see the full text.

1993 Nucl. Fusion 33 1533

(http://iopscience.iop.org/0029-5515/33/10/I11)

View the table of contents for this issue, or go to the journal homepage for more

Download details:

IP Address: 128.83.61.231
This content was downloaded on 11/03/2015 at 21:10

Please note that terms and conditions apply.

STABILITY OF COUPLED TEARING MODES IN TOKAMAKS

R. FITZPATRICK, R.J. HASTIE, T.J. MARTIN, C.M. ROACH
AEA Fusion,
UKAEA/Euratom Fusion Association,
Culham Laboratory,
Abingdon, Oxfordshire,
United Kingdom

ABSTRACT. The general coupled tearing-mode dispersion relation is investigated in tokamaks. A differential rotation of rational surfaces in high temperature devices is found to decouple low amplitude modes, so that they only reconnect magnetic flux at one surface in the plasma and behave ideally at the remaining surfaces. Above a threshold mode amplitude, the rational surfaces start to lock together, permitting modes to develop which simultaneously reconnect magnetic flux at more than one surface. Such modes are generally more unstable than uncoupled modes. Ideal rational surfaces, on which there is no reconnection, located close to the plasma edge are found to shield free-boundary tearing modes from the destabilizing influence of external-kink modes. The threshold mode amplitude required to lock coupled rational surfaces decreases rapidly with increasing machine dimensions.

1. INTRODUCTION

In a high temperature tokamak plasma the determination of tearing-mode stability reduces to an asymptotic matching problem [1]. The system is conventionally divided into two regions. In the 'outer' region, which comprises most of the plasma, the tearing perturbation is described by the marginally stable equations of ideal magnetohydrodynamics (MHD). However, these equations become singular on mode rational surfaces. In the 'inner' region, which is strongly localized around the rational surfaces, non-ideal effects such as resistivity, inertia and viscosity become important. The growth rate and rotation frequency of the reconnected magnetic flux at a given rational surface in the plasma (labelled j) are fixed by matching a quantity Δ_j, which is determined by the resistive layer solution in the inner region, to the ideal MHD solution in the outer region. In tokamaks, magnetic perturbations with different poloidal mode numbers are coupled together via toroidicity and the shaping of equilibrium flux surfaces [2]. The quantities Δ_j for each rational surface in the plasma are interrelated via a matrix equation [3–5].

This paper attempts some general analysis of the coupled tearing-mode problem, starting from the basic form of the dispersion relation and some simple physics based assumptions regarding the resistive layers. The differential rotation of tearing modes resonant on different rational surfaces in the plasma is found to affect their mutual interactions profoundly [6]. A model containing both electromagnetic and fluid elements is developed to deal with the problem in the non-linear regime.

This paper also presents results from the recently developed code T7, which determines the general tearing-mode dispersion relation by standard shooting techniques for a large aspect ratio tokamak with non-circular surfaces. Both free boundary and fixed boundary calculations are possible. The ordering adopted for T7 is such that only *seven* coupled poloidal harmonics are retained for each rational surface in the plasma. In principle, the techniques used to develop the code can be extended to finite aspect ratios, but this would involve the retention of a large number of poloidal harmonics in the calculation. The analysis presented here represents an intermediate stage between a purely cylindrical calculation and a toroidal calculation carried out at realistic values of aspect ratio. In fact, the code T7 possesses many of the advantages of a cylindrical code, in that it is relatively undemanding in computer time and has extremely good convergence properties, even at finite pressure. The code enables the relative strengths of mutual mode couplings to be estimated. Trends can also be spotted: for example, whether toroidicity, pressure, ellipticity or triangularity are stabilizing or destabilizing under certain conditions.

As an example of the use of the code T7, the stability of the (2, 1) tearing mode is investigated for $q_0 > 1$. The interaction of this mode with the (3, 1) external-kink mode is of particular interest in this study. The general analysis presented in the early

part of the paper is found to be extremely useful in the interpretation of the code output.

This paper is arranged as follows. The general analysis of the coupled tearing-mode dispersion relation is given in Section 2, and the results from the code T7 are presented in Section 3. Most of the technical details of the code T7 are relegated to the four appendices. Appendix A describes the derivation of the T7 equations. Appendix B is concerned with the properties of these equations, in particular their behaviour in the vicinity of mode rational surfaces and their angular momenum conserving properties. Appendix C describes the boundary conditions applied at the edge of the plasma. Finally, Appendix D describes the construction of the tearing-mode dispersion relation. The paper is summarized in Section 4.

2. THE TEARING-MODE DISPERSION RELATION

2.1. Introduction

The general tearing-mode dispersion relation (see Appendix D) is written as

$$(\Delta - \mathbf{E})\Psi = 0 \tag{1}$$

where Δ is the diagonal matrix of the Δ_j values at each of the N (say) rational surfaces in the plasma, $\mathbf{E}$ is a *real symmetric* $N \times N$ matrix referred to as the E matrix and Ψ is a $1 \times N$ vector whose elements (Ψ_j) are the reconnected magnetic fluxes at the various rational surfaces. Here, Δ_j is the dimensionless tearing stability index of the resistive layer at the jth surface (see Section B.2.3). The exact definition of the reconnected fluxes Ψ_j is given in Appendix B (see Eqs (91a, b), (107a–c), (120a, b) (122)).

2.2. The linear tearing-mode dispersion relation

2.2.1. *Introduction*

Consider a plasma containing two rational surfaces of radii r_1 and r_2, with $r_1 < r_2$. The resistive layers at both surfaces are assumed to lie in the *linear* regime.

2.2.2. *Linear layer physics*

Let ω_1 and ω_2 be the 'natural' rotation frequencies of tearing modes at surfaces 1 and 2, respectively [7–9]. These frequencies are determined by the local equilibrium $\boldsymbol{E} \times \boldsymbol{B}$ and diamagnetic fluid velocities.

The *linear* response of the resistive layer at surface j ($j = 1$ or 2) to a magnetic perturbation with an $\exp(-i\omega t)$ time dependence is given (see Refs [8–10]) by

$$\Delta_j = -i(\omega - \omega_j)\tau_j \tag{2}$$

where τ_j is the local 'visco-resistive' reconnection time-scale. This time-scale is given by

$$\tau_j \simeq 2.1\, \frac{\tau_H^{1/3}(r_j)\tau_R^{5/6}(r_j)}{\tau_V^{1/6}(r_j)} \tag{3}$$

where $\tau_H = (R_0/B_0)\sqrt{\rho}/ns$ is the hydromagnetic time-scale, $\tau_V = r^2\rho/\mu_\perp$ is the viscous diffusion time-scale and $\tau_R = r^2/\eta_\parallel$ is the resistive diffusion time-scale. Here, n is the toroidal mode number of the tearing perturbation, $\rho(r)$ the mass density, $\eta_\parallel(r)$ the parallel resistivity, $\mu_\perp(r)$ the perpendicular viscosity and $s(r) \equiv rq'/q$ the magnetic shear. The quantity R_0 is the average major radius of the outermost plasma flux surface (see Eq. (71a)), and B_0 is the vacuum toroidal magnetic field strength at this radius (see Section A.1). The 'visco-resistive' regime (in which anomalous viscosity and resistivity are important in the layer, but in which inertia is negligible) is the relevant tearing regime for most ohmically heated tokamak plasmas [9].

Equations (1) and (2) give a linear tearing dispersion relation of the form

$$\frac{\Psi_1}{\Psi_2} = \frac{E_{12}}{-i(\omega - \omega_1)\tau_1 - E_{11}} = \frac{-i(\omega - \omega_2)\tau_2 - E_{22}}{E_{12}} \tag{4}$$

2.2.3. *Stability in a differentially rotating plasma*

In many tokamak plasmas the differences between the various natural frequencies are much larger than the layer reconnection rates, so that $|\omega_1 - \omega_2|\tau_j \gg 1$ (see Section 3.4) [6, 9]. In this limit, the linear dispersion relation yields the following two modes:

$$\omega \simeq \omega_1 - \frac{E_{12}^2}{(\omega_1 - \omega_2)\tau_1\tau_2} + i\,\frac{E_{11}}{\tau_1} \tag{5a}$$

with $|\Psi_2| \ll |\Psi_1|$, and

$$\omega \simeq \omega_2 + \frac{E_{12}^2}{(\omega_1 - \omega_2)\tau_1\tau_2} + i\,\frac{E_{22}}{\tau_2} \tag{5b}$$

where $|\Psi_1| \ll |\Psi_2|$. These are termed the 'unreconnected' modes associated with surfaces 1 and 2, respectively. Note that the off-diagonal element of the $\mathbf{E}$ matrix gives rise to a small frequency shift such as to bring the two mode frequencies closer together. The unreconnected mode associated with surface 1 rotates

close to the natural frequency of surface 1 and effectively behaves *ideally* at surface 2 (i.e. $\Psi_2 \simeq 0$), and vice versa.

2.2.4. *Stability in a uniformly rotating plasma*

Consider the special case when $\omega_1 = \omega_2$. Suppose that $\tau_2 \ll \tau_1$, which is quite likely, especially if surface 2 lies close to the edge of the plasma. In this limit, the two modes obtained from the linear dispersion relation are

$$\omega \simeq \omega_2 + \mathrm{i}\,\frac{E_{22}}{\tau_2} \qquad |\Psi_1| \ll |\Psi_2| \tag{6a}$$

$$\omega \simeq \omega_2 + \mathrm{i}\,\frac{F_{11}^{-1}}{\tau_1} \qquad \Psi_2 \simeq -\frac{E_{12}}{E_{22}}\,\Psi_1 \tag{6b}$$

The first mode is the unreconnected mode associated with surface 2 (i.e. the surface with the faster reconnection rate). The second mode is termed the 'fully reconnected' mode associated with surface 1 (i.e. the surface with the slower reconnection rate). Here, F_{jj} is a diagonal element of the F matrix, $\mathbf{F} \equiv \mathbf{E}^{-1}$. The fully reconnected mode associated with surface 1 effectively acts as if there is a vacuum at surface 2 (i.e. $\Delta_2 \simeq 0$).

2.2.5. *Discussion*

The simple model outlined above suggests that, in a tokamak plasma with widely dispersed natural frequencies, linear stability analysis yields the so called 'unreconnected' modes, which only reconnect magnetic flux one rational surface at a time. The unreconnected mode associated with the jth rational surface satisfies $\Psi_{k\neq j} = 0$. For such a mode, the tearing-mode dispersion relation (1) reduces to

$$\Delta_j = E_{jj} \tag{7}$$

It is also convenient to define the 'fully reconnected' mode associated with the jth rational surface. This has a vacuum-like behaviour at all other rational surfaces, so that $\Delta_{k\neq j} = 0$. For such a mode the tearing-mode dispersion relation (1) reduces to

$$\Delta_j = F_{jj}^{-1} \tag{8}$$

Consider a plasma in which all of the natural frequencies are identical, but the reconnection rates at the different rational surfaces are widely separated. According to the simple model outlined above, linear stability analysis yields the fully reconnected mode associated with the rational surface possessing the slowest reconnection rate, and the unreconnected mode associated with the surface possessing the fastest reconnection rate. For a general surface j with an intermediate reconnection rate, the associated mode achieves 'full reconnection' (i.e. $\Delta_k = 0$) at surfaces with faster reconnection rates, and behaves ideally (i.e. $\Psi_k = 0$) at surfaces with slower rates. Such a mode is termed 'partially reconnected', and the appropriate dispersion relation is written as

$$\Delta_j = (F'_{jj})^{-1} \tag{9}$$

Here, the reduced F matrix, $\mathbf{F}'$, is obtained by deleting the rows and columns of the E matrix associated with the unreconnected surfaces, to form a reduced E matrix, $\mathbf{E}'$, and then inverting.

2.3. The non-linear tearing-mode dispersion relation

2.3.1. *Introduction*

The significance of the unreconnected and the fully reconnected modes is further illustrated by the following simple model. Consider, again, a plasma containing two rational surfaces, radii r_1 and r_2, with $r_1 < r_2$. Tearing at surface 1 is assumed to be *saturated*, with reconnected flux Ψ_1, whereas surface 2 is assumed to be intrinsically *tearing stable* (i.e. $E_{22} < 0$).

According to the tearing-mode dispersion relation (1), the reconnected flux driven at surface 2 is given by

$$\Psi_2 = \frac{E_{12}}{\Delta_2 - E_{22}}\,\Psi_1 \tag{10}$$

and tearing at surface 1 is governed by

$$\Delta_1 = E_{11} + \frac{E_{12}^2}{\Delta_2 - E_{22}} \tag{11}$$

2.3.2. *Electromagnetic and viscous torques*

Now, the magnetic reconnection driven at surface 2 gives rise to equal and opposite toroidal electromagnetic torques acting in the vicinity of each rational surface (see Section B.3). Thus, using Eq. (177),

$$\delta T_{\phi\mathrm{EM}}(r_1) = -\delta T_{\phi\mathrm{EM}}(r_2) = 2n\pi^2 R_0 E_{12}\,\mathrm{Im}(\Psi_2 \Psi_1^*) \tag{12}$$

which reduces to

$$\delta T_{\phi\mathrm{EM}}(r_1) = 2n\pi^2 R_0\,\frac{E_{12}^2\,\mathrm{Im}(\Delta_2^*)}{|\Delta_2 - E_{22}|^2}\,|\Psi_1|^2 \tag{13}$$

with the aid of Eq. (10).

The electromagnetic torques that develop in the plasma modify the bulk toroidal rotation [7–9, 11]. (It is assumed that any modifications to the bulk

poloidal rotation are prevented by strong poloidal flow damping.) Such modifications are opposed by the action of perpendicular plasma viscosity. For a steady state plasma, the change in the toroidal angular rotation velocity $\Omega_\phi(r)$ satisfies

$$\frac{\mathrm{d}}{\mathrm{d}r}\left((r\mu_\perp)\frac{\mathrm{d}\Omega_\phi}{\mathrm{d}r}\right) = 0 \tag{14}$$

where $\mu_\perp(r)$ is the (anomalous) coefficient of perpendicular viscosity [8, 9]. The toroidal rotation of the plasma is assumed to be 'clamped' at the edge ($r = a$) [8, 9, 12], so that

$$\Omega_\phi(a) = 0 \tag{15}$$

The viscous torques that develop in the vicinity of the rational surfaces are given by

$$\delta T_{\phi \mathrm{VS}}(r_j) = 4\pi^2 R_0 \left[(r\mu_\perp R_0^2)\frac{\mathrm{d}\Omega_\phi}{\mathrm{d}r}\right]_{r_j-}^{r_j+} \tag{16}$$

The rotation profile that satisfies Eqs (14) and (15), and also yields equal and opposite viscous torques acting at the rational surfaces, has the form

$$\Omega_\phi(r) = \Omega_\phi(r_1) \tag{17a}$$

for $r < r_1$,

$$\Omega_\phi(r) = \Omega_\phi(r_1)\int_r^{r_2}\frac{\mathrm{d}r}{r\mu_\perp(r)}\Big/\int_{r_1}^{r_2}\frac{\mathrm{d}r}{r\mu_\perp(r)} \tag{17b}$$

for $r_1 \le r \le r_2$ and

$$\Omega_\phi(r) = 0 \tag{17c}$$

for $r_2 < r$.

Note that the plasma rotation is only modified inside surface 2. According to Eq. (17), the viscous torques acting at the two rational surfaces take the form

$$\delta T_{\phi \mathrm{VS}}(r_1) = -\delta T_{\phi \mathrm{VS}}(r_2) = -4\pi^2 R_0 \Omega_\phi(r_1) R_0^2 \Big/\int_{r_1}^{r_2}\frac{\mathrm{d}r}{r\mu_\perp(r)} \tag{18}$$

2.3.3. *Layer physics*

The saturated magnetic island at surface 1 is required to rotate at the associated natural frequency [8, 9]. However, this frequency is Doppler shifted with respect to the unperturbed natural frequency ω_1 by the changes induced in the bulk plasma rotation. Thus, the rotation frequency of the magnetic island, which is also the rotation frequency of the tearing perturbation as a whole, is given by

$$\omega = \omega_1 - n\Omega_\phi(r_1) \tag{19}$$

The *linear* response of the resistive layer at surface 2 is given by (see Eq. (2))

$$\Delta_2 = -\mathrm{i}(\omega - \omega_2)\tau_2 \tag{20}$$

Note that since there is no modification to the plasma rotation velocity at surface 2, there is no Doppler shifting of the associated natural frequency. The use of the *linear* response at surface 2 is obviously only valid as long as relatively little reconnection is driven there.

2.3.4. *Torque balance*

The steady state rotation frequency of the magnetic perturbation ω is determined by the balance of electromagnetic and viscous torques at the rational surfaces. Thus,

$$\delta T_{\phi \mathrm{EM}}(r_1) + \delta T_{\phi \mathrm{VS}}(r_1) = 0 \tag{21}$$

yielding

$$\frac{1}{4}\frac{|\Psi_1|^2}{\Lambda^2}\frac{\hat{\omega}}{\alpha^2 + \hat{\omega}^2} = 1 - \hat{\omega} \tag{22}$$

where

$$\hat{\omega} = \frac{\omega - \omega_2}{\omega_1 - \omega_2} \tag{23a}$$

$$\alpha = \frac{-E_{22}}{|\omega_1 - \omega_2|\tau_2} \tag{23b}$$

$$\Lambda^2 = \frac{(B_0 r_1 s_1)^2}{2E_{12}^2}(\omega_1 - \omega_2)^2\tau_2\frac{\tau_{\mathrm{H}}^2(r_1)}{\tau_{\mathrm{V}}(r_1)}\Big/\int_{r_1}^{r_2}\frac{\mu_\perp(r_1)}{r\mu_\perp(r)}\mathrm{d}r \tag{23c}$$

and $s_j \equiv s(r_j)$. Equation (22) is similar to that obtained for the 'slip frequency' of a simple induction motor and possesses bifurcated solutions for $\alpha^2 < 1/27$ [13, 14].

In many tokamak plasmas the differences between the various natural frequencies are much larger than the layer reconnection rates, so that $|\omega_1 - \omega_2|\tau_2 \gg 1$ (see Section 3.4) [6, 9]. This implies that the parameter α is small. In the asymptotic limit $\alpha \ll 1$, Eq. (22) yields

$$\omega \simeq \frac{1}{2}(\omega_1 + \omega_2) + \frac{1}{2}(\omega_1 - \omega_2)\sqrt{1 - \frac{|\Psi_1|^2}{\Lambda^2}} \tag{24}$$

for $|\Psi_1| \le \Lambda$, and

$$\omega \simeq \omega_2 + 4\alpha^2(\omega_1 - \omega_2)\frac{\Lambda^2}{|\Psi_1|^2} \tag{25}$$

for $|\Psi_1| > \Lambda$. Thus, for $|\Psi_1| \ll \Lambda$ the tearing perturbation rotates close to the natural frequency of surface 1. As $|\Psi_1|$ is gradually increased, there is a gradual change in the rotation frequency until, at $|\Psi_1| = \Lambda$, it lies

midway between the natural frequencies of surfaces 1 and 2. Any further increase leads to a discontinuous change in the rotation frequency to a value that is very close to the natural frequency of surface 2. This process is termed the mutual 'locking' of surfaces 1 and 2.

It follows from Eqs (10), (11) and (20) that prior to locking

$$|\Delta_2| \gg 1 \qquad |\Psi_2| \ll |\Psi_1| \qquad \Delta_1 \simeq E_{11} \tag{26}$$

whereas after locking

$$|\Delta_2| \ll 1 \qquad \Psi_2 \simeq -\frac{E_{12}}{E_{22}}\Psi_1 \qquad \Delta_1 \simeq F_{11}^{-1} \tag{27}$$

Thus, if the amplitude of the reconnected flux at surface 1, $|\Psi_1|$, lies below the critical value, Λ, then there is virtually no reconnection at surface 2 and Δ_1 takes on its unreconnected value, E_{11}. However, if $|\Psi_1|$ lies above the critical value, then there is substantial tearing at surface 2 and Δ_1 takes on its fully reconnected value, F_{11}^{-1}. In this case the reconnected flux driven at surface 2 is approximately the so called 'fully reconnected' flux (i.e. that required to make Δ_2 exactly zero) [7]. The critical amplitude, Λ, at which tearing is induced at surface 2 is a function of the off-diagonal element of the E matrix coupling surfaces 1 and 2 (i.e. E_{12}), as well as the difference between the two natural frequencies, various characteristic time-scales at surfaces 1 and 2, and the viscosity profile between the two surfaces.

After locking, the resistive layer at surface 2 probably enters the non-linear regime, since a substantial amount of reconnected magnetic flux is driven there. As has been previously noted, in the non-linear regime the reconnected flux is forced to rotate at the associated natural frequency, implying that after locking the tearing perturbation rotates at *exactly* ω_2. However, this minor modification to the theory does not affect any of the other results. The use of the linear response at surface 2 to obtain the locking threshold is justified because very little magnetic flux is driven there prior to locking.

2.3.5. *Locking*

When $|\Psi_1|$ reaches the threshold value, Λ, the steady state rotation frequency of the reconnected flux at surface 1 makes a sudden transition from an initial value $\omega = (\omega_1 + \omega_2)/2$ to a final value $\omega \simeq \omega_2$. This process is termed the mutual locking of surfaces 1 and 2. The time-scale for locking can be estimated as follows.

The time dependent fluid equation of angular motion is written [15] as

$$\rho \frac{d\Omega_\phi}{dt} = \frac{1}{r}\frac{d}{dr}\left((r\mu_\perp)\frac{d\Omega_\phi}{dr}\right) \tag{28}$$

where any flux surface averaged metric elements have been absorbed into the definitions of $\rho(r)$ and $\mu_\perp(r)$. Assuming that $\Omega_\phi(r,t) \equiv \Omega_\phi(r)\exp(t/\tau_{lock})$ during locking, the associated rotation profile takes the form

$$\Omega_\phi(r) \simeq \Omega_\phi(r_1)\exp\left[\sqrt{\frac{\tau_V(r_1)}{\tau_{lock}}}\left(\frac{r}{r_1} - 1\right)\right] \tag{29a}$$

for $r \leq r_1$ and

$$\Omega_\phi(r) \simeq \Omega_\phi(r_1)\exp\left[\sqrt{\frac{\tau_V(r_1)}{\tau_{lock}}}\left(1 - \frac{r}{r_1}\right)\right] \tag{29b}$$

for $r_1 < r$, provided that $\tau_{lock} \ll \tau_V(r_1)$. It follows from Eq. (16) that the viscous torque acting at surface 1 is

$$\delta T_{\phi VS}(r_1) \simeq -4\pi^2 R_0 2n(B_0 r_1 s_1)^2 \times \sqrt{\frac{\tau_V(r_1)}{\tau_{lock}}}(\omega_1 - \omega_2)\frac{\tau_H^2(r_1)}{\tau_V(r_1)}(1 - \hat{\omega}) \tag{30}$$

The electromagnetic torque acting at surface 1 is given by

$$\delta T_{\phi EM}(r_1) \simeq 4\pi^2 R_0 \frac{n}{4}(B_0 r_1 s_1)^2(\omega_1 - \omega_2) \times \frac{\tau_H^2(r_1)}{\tau_V(r_1)}\frac{\hat{\omega}}{\alpha^2 + \hat{\omega}^2}\Big/\int_{r_1}^{r_2}\frac{\mu_\perp(r_1)}{r\mu_\perp(r_1)}\,dr \tag{31}$$

where use has been made of Eqs (13), (20) and (23), and of $|\Psi_1| \simeq \Lambda$.

The locking time-scale is estimated by balancing the viscous torque against the maximum electromagnetic torque, which occurs when $\hat{\omega} = \alpha$. This yields

$$\tau_{lock} \simeq \left(16\alpha\int_{r_1}^{r_2}\frac{\mu_\perp(r_1)}{r\mu_\perp(r)}\,dr\right)^2\tau_V(r_1) \tag{32}$$

which is valid provided that the term in large round brackets is much less than unity. In tokamaks with widely separated natural frequencies, where $\alpha \ll 1$, this is probably the case. Equation (32) implies that the locking time-scale is much less than the global viscous relaxation time-scale.

Note from Eq. (29) that the modification to the fluid velocity profile during locking is strongly localized around rational surface 1. After locking, the velocity profile relaxes to a steady state profile of the form (17) on a viscous diffusion time-scale (τ_V).

2.3.6. *Forced reconnection*

The tearing dispersion relation at surface 2 is written as

$$\Delta_2 = E_{22} + E_{12}\frac{\Psi_1}{\Psi_2} \tag{33}$$

Just before locking, the reconnected flux at surface 1 does not rotate at the natural frequency of surface 2, and there is consequently very little driven reconnection at the latter surface:

$$\frac{\Psi_2}{\Psi_1} \simeq \mathrm{i}\,\frac{2E_{12}}{(\omega_1 - \omega_2)\tau_2} \tag{34}$$

(see Eqs (20), (24) and (33)). Just after locking, the flux at surface 1 is left co-rotating *in phase* with the driven flux at surface 2 (see Section 2.3.7), so that

$$\frac{\Psi_2}{\Psi_1} \simeq \frac{2E_{12}}{|\omega_2 - \omega_2|\tau_2} \tag{35}$$

In the *linear* regime, forced reconnection at surface 2 obeys

$$\frac{\Psi_2}{\Psi_2^{\mathrm{full}}} = \left[1 - \left(1 + \frac{2E_{22}}{|\omega_1 - \omega_2|\tau_2}\right)\exp\left(\frac{E_{22}t}{\tau_2}\right)\right] \tag{36}$$

where use has been made of Eqs (20), (33) and (35). Here,

$$\Psi_2^{\mathrm{full}} = -\frac{E_{12}}{E_{22}}\Psi_1 \tag{37}$$

is the fully reconnected flux, and $t = 0$ just after locking. Full reconnection is achieved for $t \gg \tau_{\mathrm{rec}} = \tau_2/(-E_{22})$. For $t \ll \tau_{\mathrm{rec}}$, Eq. (36) yields

$$\frac{\Psi_2}{\Psi_1} \simeq \frac{2E_{12}}{|\omega_1 - \omega_2|\tau_2}\left(1 + \frac{|\omega_1 - \omega_2|t}{2} + \ldots\right) \tag{38}$$

Note that the initial growth rate is independent of the layer reconnection time-scale at surface 2.

In reality, the layer is likely to enter the non-linear regime long before full reconnection is achieved. Thus, according to standard non-linear theory [16], the time-scale for full reconnection is given by $\tau_{\mathrm{rec}} \simeq (W_2^{\mathrm{full}}/r_2)\tau_{\mathrm{R}}(r_2)$, where W_2^{full} is the island width corresponding to the reconnected flux Ψ_2^{full}.

In some situations, forced reconnection gives rise to evolution on the Sweet-Parker time-scale, $\tau_{\mathrm{SP}} = \tau_{\mathrm{R}}^{1/2}\tau_{\mathrm{H}}^{1/2}$, owing to the persistence of the ideal current sheet into the non-linear regime [17]. This only occurs if the layer is 'non-constant ψ' (i.e. the growth rate exceeds the current diffusion rate across the layer) as it enters the non-linear regime. In the above calculation, it is easily demonstrated that the layer is already 'constant ψ' immediately after locking (i.e. whilst the layer is still linear) provided that

$$|\omega_1 - \omega_2| \ll \frac{\tau_{\mathrm{V}}^{1/3}(r_2)}{\tau_{\mathrm{H}}^{2/3}(r_2)\tau_{\mathrm{R}}^{2/3}(r_2)} \tag{39}$$

which is probably the case in ohmically heated tokamaks [9]. Since the rate of forced reconnection decreases with time (see Eq. (36)), whilst the layer width stays constant (see Eq. (52)), the layer remains 'constant ψ' throughout its linear (and subsequent non-linear) phase. Thus, evolution on the Sweet-Parker time-scale is not expected to occur.

2.3.7. *Unlocking*

After locking, the layer at surface 2 is likely to enter the non-linear regime. According to the simplest non-linear theory [16], the dispersion relation becomes

$$\tau_{\mathrm{R}}(r_2)\frac{\mathrm{d}}{\mathrm{d}t}\left(\frac{IW_2}{r_2}\right) = \mathrm{Re}(\Delta_2) \tag{40}$$

where $I = 0.8227$ and W_2 is the island width [9]. Thus, the steady state reconnected flux driven at surface 2 is

$$|\Psi_2| = |\Psi_2^{\mathrm{full}}|\cos(\Delta\varphi) \tag{41}$$

where use has been made of Eqs (33) and (37). Here,

$$\Delta\varphi = \arg(\Psi_2) - \arg(\Psi_1) - \arg(E_{12}) \tag{42}$$

is the phase difference between the islands at the two rational surfaces. Zero phase difference is defined as the orientation in which the islands have the maximum destabilizing effect on one another. Using Eqs (12) and (41), the electromagnetic torque acting at surface 2 takes the form

$$\delta\mathrm{T}_{\phi\mathrm{EM}}(r_2) = -n\pi^2 R_0\frac{E_{12}^2}{-E_{22}}|\Psi_1|^2\sin(2\Delta\varphi) \tag{43}$$

This viscous torque is given by

$$\delta\mathrm{T}_{\phi\mathrm{VS}} = 4n\pi^2 R_0(B_0 r_1 s_1)^2 \times \frac{\tau_{\mathrm{H}}^2(r_1)}{\tau_{\mathrm{V}}(r_1)}(\omega_1 - \omega_2)\left|\int_{r_1}^{r_2}\frac{\mu_\perp(r_1)}{r\mu_\perp(r)}\,\mathrm{d}r\right| \tag{44}$$

where use has been made of Eqs (18) and (19), and of $\omega = \omega_2$.

The steady state phase difference between the two islands is obtained by balancing the viscous and electromagnetic torques at surface 2. Thus, using Eqs (23), (43) and (44),

$$\sin(2\Delta\hat{\varphi}) = 8\alpha\frac{\Lambda^2}{|\Psi_1|^2} \tag{45}$$

where $\Delta\hat{\varphi} \equiv \mathrm{sgn}(\omega_1 - \omega_2)\Delta\varphi$. It can easily be shown that any solutions to Eq. (45) with $\Delta\hat{\varphi} > \pi/4$ are unstable [9]. For a tokamak with widely differing

natural frequencies, where $\alpha \ll 1$, the phase difference just above the locking threshold ($|\Psi_1| = \Lambda$) is very small:

$$\Delta\hat{\varphi}_{\rm lock} \simeq 4\alpha \tag{46}$$

Furthermore, once locking has taken place, $|\Psi_1|$ must be reduced significantly below the locking threshold Λ before the reverse process, 'unlocking', occurs. In fact,

$$|\Psi_1|_{\rm unlock} = \sqrt{8\alpha}\Lambda \tag{47}$$

since for $|\Psi_1|^2 > 8\alpha\Lambda^2$ no solutions of Eq. (45) are possible. The critical phase difference at unlocking is

$$\Delta\hat{\varphi}_{\rm unlock} = \pi/4 \tag{48}$$

2.3.8. *Saturated island at surface 2*

Consider, finally, the case where surface 2 is intrinsically *tearing unstable*, with saturated reconnected flux Ψ_2 and island width W_2. Since the layer is now in the non-linear regime, the reconnected flux is required to rotate at the associated natural frequency, ω_2 [9].

According to Eqs (33) and (40), there is a periodic modulation in the width of the magnetic island at surface 2 due to the differential rotation of the coupled island at surface 1. This gives rise to an associated modulation in the amplitude of the reconnected flux of the form

$$|\tilde{\Psi}_2| = \frac{2E_{12}}{(IW_2/r_2)(\omega - \omega_2)\tau_{\rm R}(r_2)} |\Psi_1| \sin[(\omega - \omega_2)t] \tag{49}$$

where ω (given by Eq. (19)) is the rotation frequency of the island at surface 1. Here, it has been assumed that the modulations in island width are relatively small and that $W_2 \propto \sqrt{\tilde{\Psi}_2}$ [9].

According to Eqs (12) and (49), the modulations in the island width at surface 2 give rise to a *steady* electromagnetic torque acting to bring the two islands into co-rotation:

$$\delta T_{\phi{\rm EM}}(r_1) = -\delta T_{\phi{\rm EM}}(r_2)$$

$$\simeq 2n\pi^2 R_0 \frac{E_{12}^2}{(IW_2/r_2)(\omega - \omega_2)\tau_{\rm R}(r_2)} |\Psi_1|^2 \tag{50}$$

There is also a much larger *oscillatory* electromagnetic torque giving rise to a slightly non-uniform rotation of the two islands, but in conventional tokamak plasmas this effect is relatively unimportant [9].

A comparison of Eqs (13), (20) and (50) indicates that the rotating island at surface 2 acts like a linear layer with an effective dispersion relation

$$\Delta_2 \simeq -{\rm i}(\omega - \omega_2)\tau_{\rm R}(r_2)\frac{IW_2}{r_2}$$

$$\equiv -{\rm i}(\omega - \omega_2)\tau_2 \frac{IW_2}{\delta_2} \tag{51}$$

where

$$\frac{\delta_2}{r_2} = 2.1 \frac{\tau_{\rm H}^{1/3}(r_2)}{\tau_{\rm V}^{1/6}(r_2)\tau_{\rm R}^{1/6}(r_2)} \tag{52}$$

is the characteristic width of the visco-resistive layer [9]. The derivation of Eq. (51) is valid provided that $|\Delta_2| \gg 1$, which also ensures that the modulation in island width is relatively small. Note that the non-linear dispersion relation (51) merges with the linear dispersion relation (20) as IW_2, the equivalent layer width of the saturated magnetic island, approaches the linear layer width δ_2. According to Eqs (20) and (51), the layer at surface 2 has an equivalent dispersion relation to a slab of conducting material, of thickness δ_2 in the linear regime and IW_2 in the non-linear regime, with the same resistivity as the plasma, but rotating at the natural frequency, ω_2 [14, 18].

By analogy with the analysis of Section 2.3.4, in the non-linear regime ($IW_2 \gg \delta_2$) there is a critical amplitude of the reconnected flux at surface 1 required to lock the magnetic island at surface 2. This amplitude is expressed as

$$\Lambda^* = \sqrt{\frac{IW_2}{\delta_2}}\,\Lambda \tag{53}$$

where Λ is the critical amplitude in the linear regime ($IW_2 \ll \delta_2$). Note that as the saturated island width at surface 2 increases, locking becomes progressively more difficult. For $|\Psi_1| \ll \Lambda^*$ the island at surface 1 rotates close to its natural frequency, ω_1. The island at surface 2 always rotates at its natural frequency, ω_2. As $|\Psi_1|$ is gradually increased, there is a gradual change in the rotation frequency of island 1 until, at $|\Psi_1| = \Lambda^*$, it lies midway between the natural frequencies of surfaces 1 and 2. Any further increase leads to a sudden change in rotation frequency such that both islands end up co-rotating at ω_2 in a mutually destabilizing configuration.

2.3.9. *Discussion*

The above analysis can readily be extended to the case of a plasma containing many rational surfaces. It is assumed that the various frequencies are widely separated. Consider the tearing mode associated with a general rational surface j. If the reconnected flux, $|\Psi_j|$, lies below a certain threshold value, $\Lambda_j^{(0)}$, then

none of the other surfaces are locked. The mode consequently behaves (almost) *ideally* at these surfaces, with (nearly) zero reconnected flux. In this case, the mode is effectively unreconnected, and the appropriate dispersion relation at surface j is given by Eq. (7). If $|\Psi_j|$ lies above a certain critical value, $\Lambda_j^{(0)}$ ($\Lambda_j^{(1)} \geq \Lambda_j^{(0)}$), then *all* of the other surfaces are locked, and (assuming that these surfaces are intrinsically stable to tearing modes) the driven reconnected fluxes attain their fully reconnected values (i.e. such as to make $\Delta_{k\neq j} = 0$). In this situation, the mode is effectively fully reconnected and the appropriate dispersion relation is given by Eq. (8). Finally, for $\Lambda_j^{(0)} < |\Psi_j| < \Lambda_j^{(1)}$, only *some* of the other surfaces are locked. In this case, the mode is partially reconnected, and the appropriate dispersion relation is given by Eq. (9). The threshold values, $\Lambda_j^{(0)}$ and $\Lambda_j^{(1)}$, are functions of the off-diagonal elements of the E matrix, the differences between the natural frequencies, various layer quantities evaluated at the rational surfaces, and the plasma viscosity profile.

3. RESULTS FROM THE CODE T7

3.1. Specification of the plasma equilibrium

In T7 the locus of the outermost plasma flux surface (in dimensionless cylindrical polar co-ordinates) is given by

$$R = 1 - \epsilon\cos\omega + \epsilon E_a\cos\omega - \epsilon T_a\cos 2\omega + O(\epsilon^3)$$
$$Z = \epsilon\sin\omega + \epsilon E_a\sin\omega + \epsilon T_a\sin 2\omega + O(\epsilon^3) \qquad (54)$$

where ϵ is the inverse aspect ratio of the equilibrium, E_a the (non-dimensional) ellipticity and T_a the (non-dimensional) triangularity. The T7 ordering scheme implies that ϵ, E_a and T_a are all small compared with unity (see Sections A.1 and A.2).

The safety factor profile $q(r)$ and the pressure profile $p(r)$ are both specified as functions of a radius-like non-dimensional flux surface label r (where $r = 0$ on the magnetic axis and $r = 1$ on the outermost plasma flux surface). For the example calculations presented in this paper, the safety factor profile is assumed to have the general form

$$q(r) = q_a\frac{r^2}{1-(1-r^2)^{q_a/q_0}} - q_a\frac{\lambda}{2}r^{2k}(1-r^2) \qquad (55)$$

where q_0 is the central safety factor, q_a is the edge safety factor and k is a positive integer. The $O(\epsilon^2)$ edge shear parameter λ is iterated until the constraint (128) is satisfied (i.e. until the edge current is zero). In the cylindrical limit, this q profile corresponds to a toroidal current profile of the form $j(r) = j_0(1-r^2)^{q_a/q_0-1}$.

The plasma pressure profile is assumed to have the general form

$$p = p_0(1-r^2)^2 \qquad (56)$$

where p_0 is the central pressure. Note that the constraints (127) are automatically satisfied by such a profile. Together, the constraints (127) and (128) ensure that the equilibrium plasma current is zero [to $O(\epsilon^2)$] at the plasma–vacuum boundary. The central plasma pressure is conveniently parametrized by the (cylindrical) poloidal beta,

$$\beta_p = 4\frac{q_a^2}{\epsilon^2 B_0^2}\int_0^1 rp(r)\,dr \qquad (57)$$

The T7 ordering scheme implies that $\epsilon\beta_p$ is small compared with unity.

3.2. Toroidal equilibrium with shaped plasma cross-sections

For the model q profile (55), the effects of toroidicity, pressure and flux surface shaping tend to broaden the associated current profile, leading to the development of an unphysical non-zero edge current. There is, by design, zero edge current in the cylindrical limit. A judicious choice of the edge shear parameter (e.g. $\lambda = \lambda_c$) allows a redistribution of the toroidal current such that the edge value is again zero. This redistribution conserves the central q profile, the edge q profile and the integrated toroidal plasma current (to $O(\epsilon^2)$). For low values of the parameter k in Eq. (55) (e.g., $k = 1$) the current redistribution extends well into the plasma interior, but for higher values (e.g., $k = 4$) the redistribution only affects the outer regions.

Figure 1 shows the flux surfaces, the q profile and the normalized parallel current profile ($\hat{J}_\parallel \equiv (R_0q_0/2B_0) \times \langle R^2\boldsymbol{J}\cdot\boldsymbol{B}/R_0^2B_0\rangle$, see Section C.1) for a typical zero-β equilibrium before and after a current redistribution with $k = 4$. It can be seen that, in this case, there is relatively little change to the plasma equilibrium inside the $q = 2$ surface.

In the T7 ordering scheme, equilibrium quantities can be expressed as power series in the various expansion parameters. A general quantity λ can be written as

$$\lambda = \lambda^{(0)} + \lambda^{(1)}\epsilon^2 + \lambda^{(2)}\epsilon^2\beta_p^2 + \lambda^{(3)}\epsilon^2\beta_p + \lambda^{(4)}E_a^2 + \lambda^{(5)}T_a^2 + O(\epsilon^3) \qquad (58)$$

where $\lambda^{(0)}$ is the cylindrical limit, $\lambda^{(1)}$ is a toroidicity correction, $\lambda^{(2)}$ is a pressure correction, $\lambda^{(3)}$ is a correction due to combined toroidal and pressure effects,

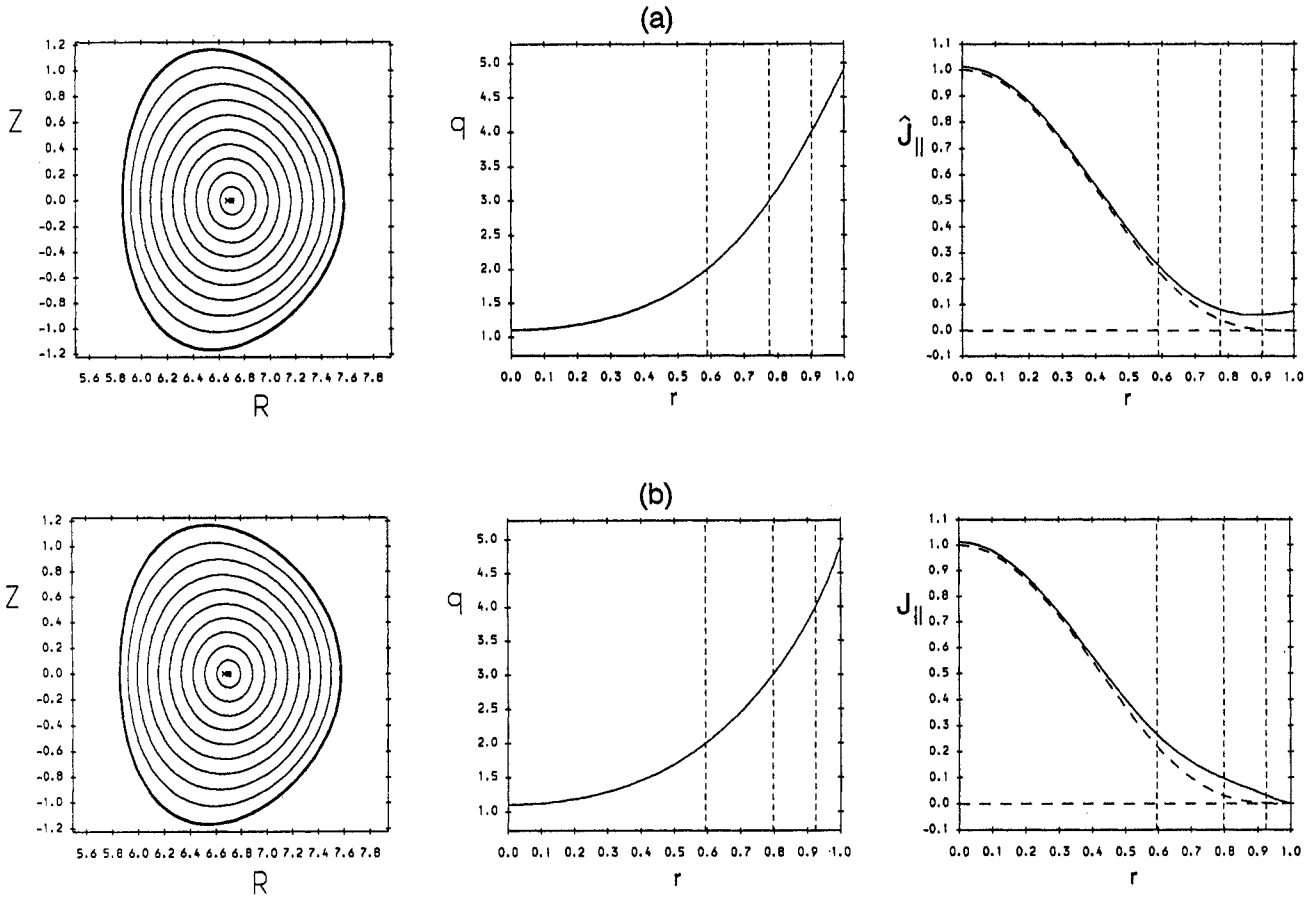

FIG. 1. Flux surfaces, q profile and parallel current profile for a typical zero β T7 equilibrium: (a) before any current redistribution, (b) after a current redistribution with k = 4. The equilibrium parameters are $\epsilon = 0.15$, $E_a = 0.15$, $T_a = 0.05$, $q_0 = 1.1$ and $q_a = 4.9$. The flux surfaces are plotted in the poloidal plane with the minor radius of the outermost flux surface normalized to unity. The current profile is normalized with respect to the cylindrical current on the magnetic axis. The positions of the q = 2, q = 3 and q = 4 surfaces are indicated in the q(r) and $\hat{J}_{\|}(r)$ plots. In the $\hat{J}_{\|}(r)$ plot, the solid curve is the total current and the dashed curve is the cylindrical contribution.

$\lambda^{(4)}$ is an ellipticity correction and $\lambda^{(5)}$ is a triangularity correction. Figure 2 shows the coefficients of such an expansion for the integrated plasma current I_ϕ (normalized to the cylindrical current $I_\phi^{(0)} = 2\pi\epsilon^2 R_0 B_0/q_a$), the critical edge shear parameter λ_c and the total plasma inductance $l_i \equiv 2\int B_p^2\, dV/I_\phi^2 R_0$ before and after a current redistribution with $k = 4$, calculated for a set of equilibria with $q_0 = 1.1$ and q_a in the range 2.5 to 5.2.

At fixed edge q, the effects of toroidicity, pressure and flux surface shaping all tend to increase the cross-sectional area of the plasma, leading to a corresponding increase in the plasma current (see Fig. 2). The critical shear parameter λ_c is independent of the localization parameter k (since the edge magnetic shear, $s_a = 2 + \lambda$, does not depend on k) and increases monotonically with increasing toroidicity, pressure and shaping (see Fig. 2).

The broadening of the current profile due to, for example, toroidal effects gives rise to a corresponding reduction in l_i (see Fig. 2). The current redistribution needed to maintain physical boundary conditions at the plasma edge leads to a peaking of the current profile, with an associated increase in l_i. However, for localized redistributions (e.g., $k = 4$) this increase in l_i is relatively small (see Fig. 2).

3.3. Stability of the (2, 1) tearing mode for $q_0 > 1$

3.3.1. Introduction

The code T7 has been used to investigate the stability of the (2, 1) tearing mode for $q_0 > 1$. This study is relevant to the current rise phase in conventional

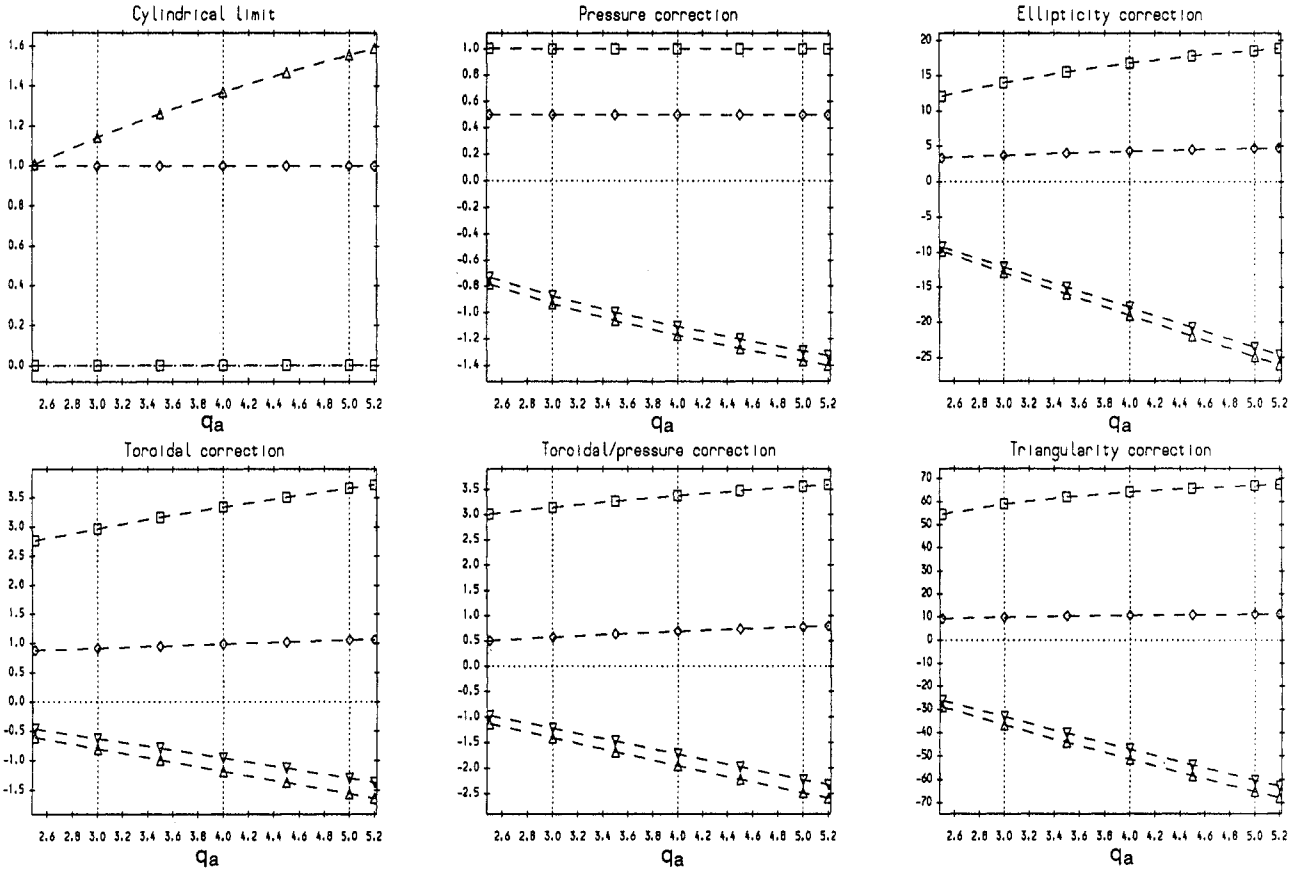

FIG. 2. The integrated plasma current (◇), critical edge shear parameter (□) and total plasma inductance before (△) and after (▽) a current redistribution with k = *4, calculated for a set of equilibria with* q_0 = *1.1 and* q_a *in the range 2.5 to 5.2. The plasma current is normalized with respect to the cylindrical plasma current. The six subplots show the coefficients of each equilibrium quantity in a general expansion of the form given in Eq. (58). Thus, the 'cylindrical limit' corresponds to* $\lambda^{(0)}$, *the 'toroidal correction' to* $\lambda^{(1)}$ *and so on.*

tokamaks, which is characterized by sudden transient bursts of rotating MHD activity as low mode number rational surfaces cross the plasma boundary [19]. Such behaviour is thought to be due to interaction between tearing modes and free-boundary external-kink modes. In JET, it is generally observed that if the rotating MHD activity reaches a sufficient amplitude to 'lock' to the vacuum vessel, then it persists, and eventually triggers a major disruption [20].

The interaction of the (2, 1) tearing mode with the (3, 1) external-kink mode has been investigated by scanning q_a in the range 2.5 to 5.2, at fixed q_0. Scans have been performed for q_0 = 1.01 and 1.1. The q_0 = 1.01 scan lies well away from the ideal stability boundary for the (3, 1) external-kink mode, whereas the q_0 = 1.1 scan just grazes the stability boundary at q_a = 3 [21]. The (3, 1) tearing mode, is stable throughout both scans.

In the T7 ordering scheme, the tearing stability indices for the unreconnected and fully reconnected (2, 1) modes can both be expressed as a power series of the form (58), provided $q_0 > 1$. For $q_0 < 1$, coupling between the (2, 1) tearing mode and the (1, 1) internal-kink mode gives rise to a more complicated scaling with the expansion parameters [4, 22].

3.3.2. *The cylindrical limit*

Figure 3 shows the cylindrical (2, 1) tearing stability index as a function of q_a, for q_0 = 1.01 and 1.1. Data are displayed for both free-boundary (i.e. no wall) and fixed-boundary (i.e. a perfectly conducting wall located at r = 1) calculations. In the cylindrical limit, there is no distinction between the fully reconnected and the unreconnected modes (for a monotonic q profile), since there is no coupling between the different poloidal

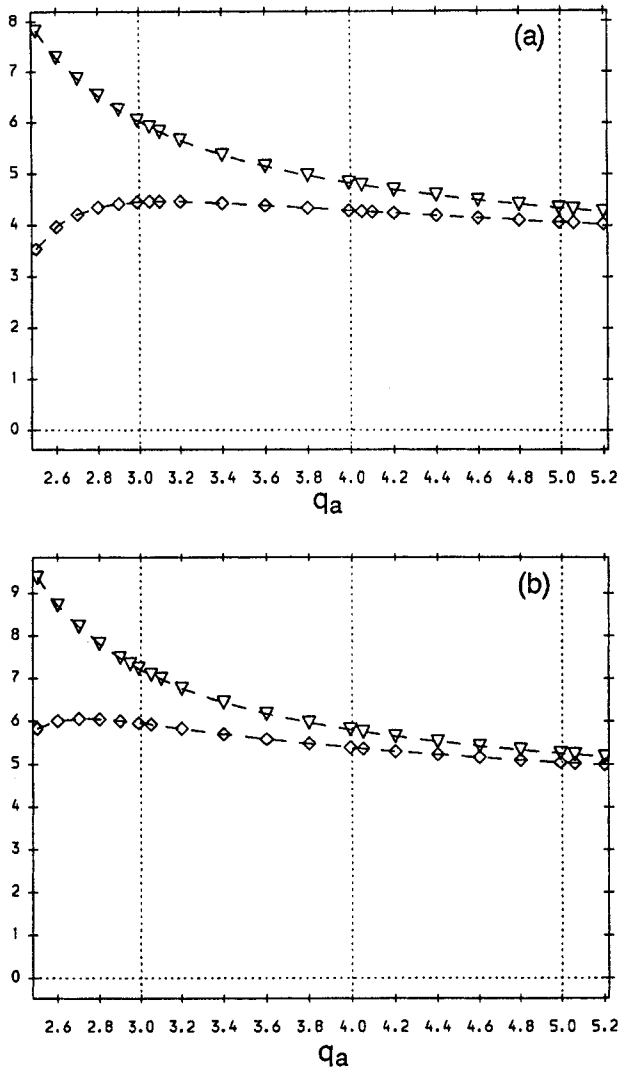

FIG. 3. The (2, 1) tearing stability index (normalized to the minor radius of the $q = 2$ *surface) in the cylindrical limit (i.e.* $\lambda^{(0)}$ *in Eq. (58)) as a function of* q_a *(with* $k = 4$*) for (a)* $q_0 = 1.01$*, (b)* $q_0 = 1.1$*. Data are shown for free-boundary (∇) and fixed-boundary (◇) calculations.*

harmonics. It can be seen that the fixed-boundary mode is more stable than the free-boundary mode, but that this is only a significant effect for $q_a \lesssim 3$. Raising q_0 clearly has a destabilizing effect on the (2, 1) mode.

3.3.3. *The effect of toroidicity*

Figure 4 shows the toroidal correction to the (2, 1) tearing stability index as a function of q_a, for $q_0 = 1.01$. Figure 4(a) shows data for the unreconnected and the fully reconnected *fixed-boundary* modes. It can be seen that for both modes toroidicity is *stabilizing* and that the effect is strongest at low edge q. For $q_a > 3$, the stability curve for the unreconnected mode (for which the toroidally coupled $m = 3$ harmonic does not reconnect any magnetic flux at the $q = 3$ surface) bifurcates from the curve for the fully reconnected mode (for which the $m = 3$ harmonic achieves full reconnection at $q = 3$). The fully reconnected mode is clearly always more unstable than the unreconnected mode. According to the analysis of Section 2.3, the (2, 1) mode does not reconnect magnetic flux at the $q = 3$ surface below a certain critical amplitude, but as the critical amplitude is exceeded there is a sudden transition to full reconnection at $q = 3$. Figure 4(a) implies that this transition has a *destabilizing* effect on the mode.

Figure 4(b) shows data for the unreconnected and the fully reconnected *free-boundary* modes. With full reconnection at the $q = 3$ surface, the free-boundary mode is significantly destabilized by toroidicity with respect to the fixed-boundary mode (see also Fig. 4(c)). This destabilizing effect is peaked around $q_a = 3$: clear evidence that it is due to interaction with the (3, 1) external-kink mode. This is confirmed by Fig. 5, which shows the toroidal correction to the (2, 1) tearing stability index for $q_0 = 1.1$. The proximity of the (3, 1) external-kink stability boundary leads to extreme destabilization of the fully reconnected free-boundary (2, 1) tearing mode around $q_a = 3$. This effect reaches a maximum for q_a which is larger than 3: i.e. when the $q = 3$ surface lies just *inside* the plasma. With no reconnection at the $q = 3$ surface, there is relatively little difference between the effect of toroidicity on the stability of the fixed-boundary and free-boundary modes (see Figs 4(d) and 5(d)).

Figure 6 shows typical fully reconnected and unreconnected tearing eigenfunctions, for free-boundary and fixed-boundry (2, 1) modes, calculated for $q_0 = 1.1$ and $q_a = 3.05$. The fully reconnected and free-boundary mode has a substantial $m = 3$ toroidally coupled side-band due to interaction with the (3, 1) external-kink mode. In fact, as q_0 is gradually increased, so that the ideal stability boundary is approached, the $m = 3$ harmonic increases in importance until the eigenfunction eventually resembles the (3, 1) external-kink eigen-function. On the other hand, the unreconnected free-boundary mode only has a fairly modest $m = 3$ toroidally coupled sideband, which is very similar in form to that of the fixed-boundary modes. Clearly, the presence of an unreconnected $q = 3$ surface in the plasma effectively 'shields' the (2, 1) free-boundary tearing mode from the influence of the (3, 1) external-kink mode.

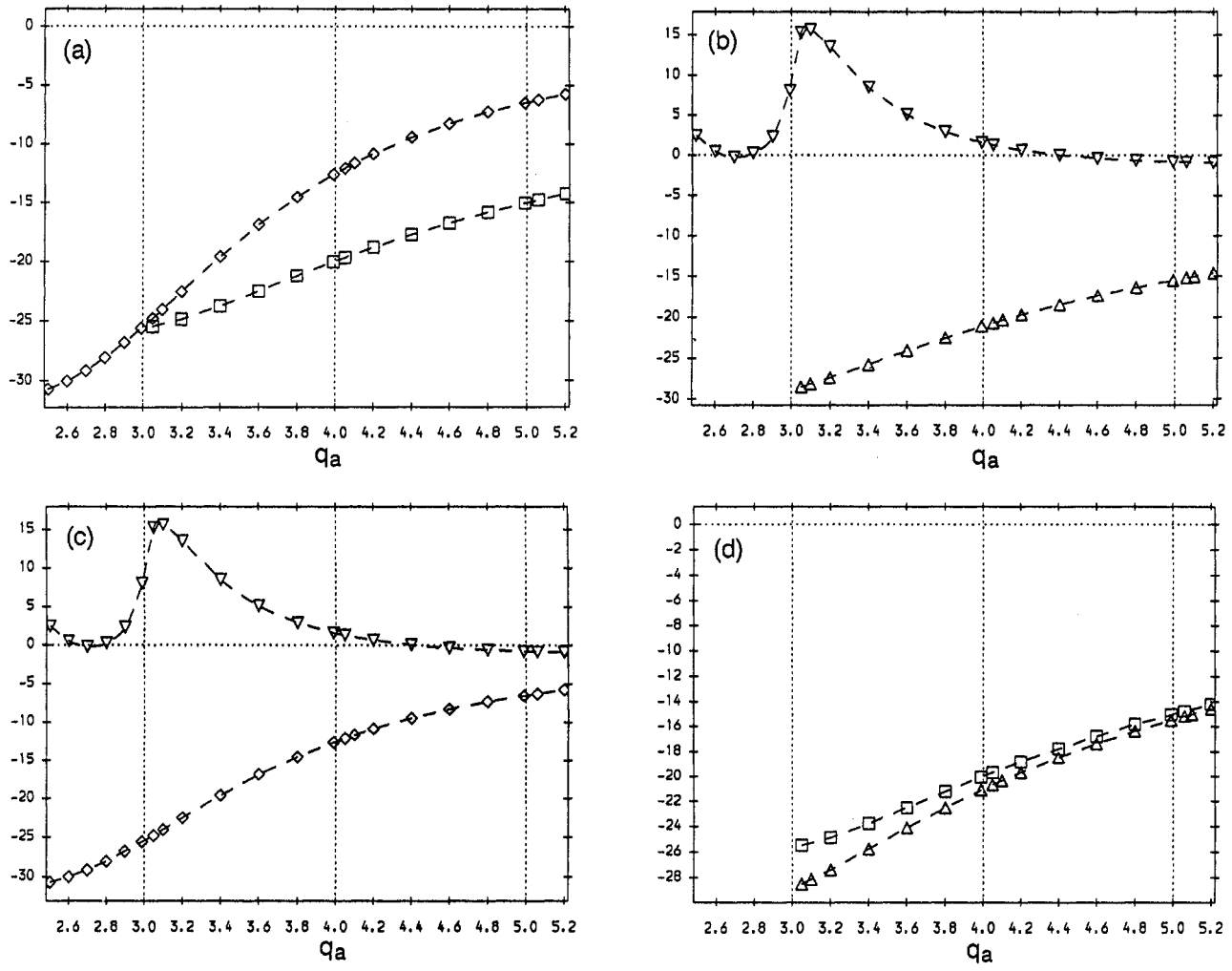

FIG. 4. The toroidal correction (i.e. $\lambda^{(1)}$ in Eq. (58)) to the (2, 1) tearing stability index (normalized to the minor radius of the q = 2 surface) as a function of q_a, for $q_0 = 1.01$ (with k = 4). Data are shown for the fixed-boundary fully reconnected mode (◇), the fixed-boundary unreconnected mode (□), the free-boundary fully reconnected mode (▽) and the free-boundary unreconnected mode (△). Data for the unreconnected modes are only plotted when they differ from those for the fully reconnected modes. Subplot (a) compares data for the fixed-boundary modes, subplot (b) compares data for the free-boundary modes, subplot (c) compares data for the fully reconnected modes and subplot (d) compares data for the unreconnected modes.

This shielding effect can be overcome in two different ways. Firstly, the (2, 1) mode can exceed the critical amplitude for locking the $q = 3$ surface, and, secondly, the $q = 3$ surface can leave the plasma (i.e. $q_a < 3$). In the first case, the observable consequence would be a discontinuous change in the rotation frequency of the (2, 1) mode, as locking occurred, followed by a sudden increase in the saturated amplitude. In the second case, the loss of the $q = 3$ surface from the plasma would trigger a dramatic increase in the saturated amplitude.

For a free-boundary plasma, a current ramp-up with full reconnection at the $q = 3$ surface should appear significantly different from one with no reconnection at $q = 3$. In the former case, the destabilizing effect of the external-kink mode peaks for q_a just above 3, but also extends well beyond $q_a \simeq 4$ (see Figs 4 and 5). Thus, as the current is ramped up, and q_a decreases, the amplitude of the saturated (2, 1) mode should increase *continuously*, reaching a maximum just *before* the $q = 3$ surface leaves the plasma. The propagation frequency of the mode is given by the unperturbed natural frequency of the outermost locked rational surface, so there should be *discontinuous* changes in the frequency as coupled rational surfaces leave the

plasma. In the latter case, toroidicity is stabilizing for $q_a \geq 3$, and strongly destabilizing for $q_a < 3$. Therefore, there should be no effect until the $q = 3$ surface leaves the plasma, after which there should be a dramatic increase in the saturated amplitude. If the mode lies well below the locking threshold, the mode frequency is equivalent to the natural frequency of the $q = 2$ surface and should vary in a *continuous* manner during the ramp-up.

3.3.4. *The effect of pressure*

Figures 7 and 8 show the pressure correction to the (2, 1) tearing stability index as a function of q_a, for $q_0 = 1.01$ and 1.1. Data are shown for unreconnected and fully reconnected, fixed-boundary and free-boundary modes. It can be seen that for both *fixed-boundary* modes pressure is *destabilizing*, and that the effect peaks for q_a just less than 3. The destabilization of the fully reconnected free-boundary mode around $q_a = 3$, due to interaction with the (3, 1) external-kink mode, is again evident, but is far more marked than in Figs 4 and 5. This indicates that pressure is much more effective at coupling the (2, 1) tearing mode and the (3, 1) external-kink mode than toroidicity. The presence of an unreconnected $q = 3$ surface in the plasma is again found to 'shield' the (2, 1) tearing mode from the destabilizing influence of the (3, 1) external-kink mode.

Figures 9 and 10 show the toroidal/pressure correction to the (2, 1) tearing stability index as a function of

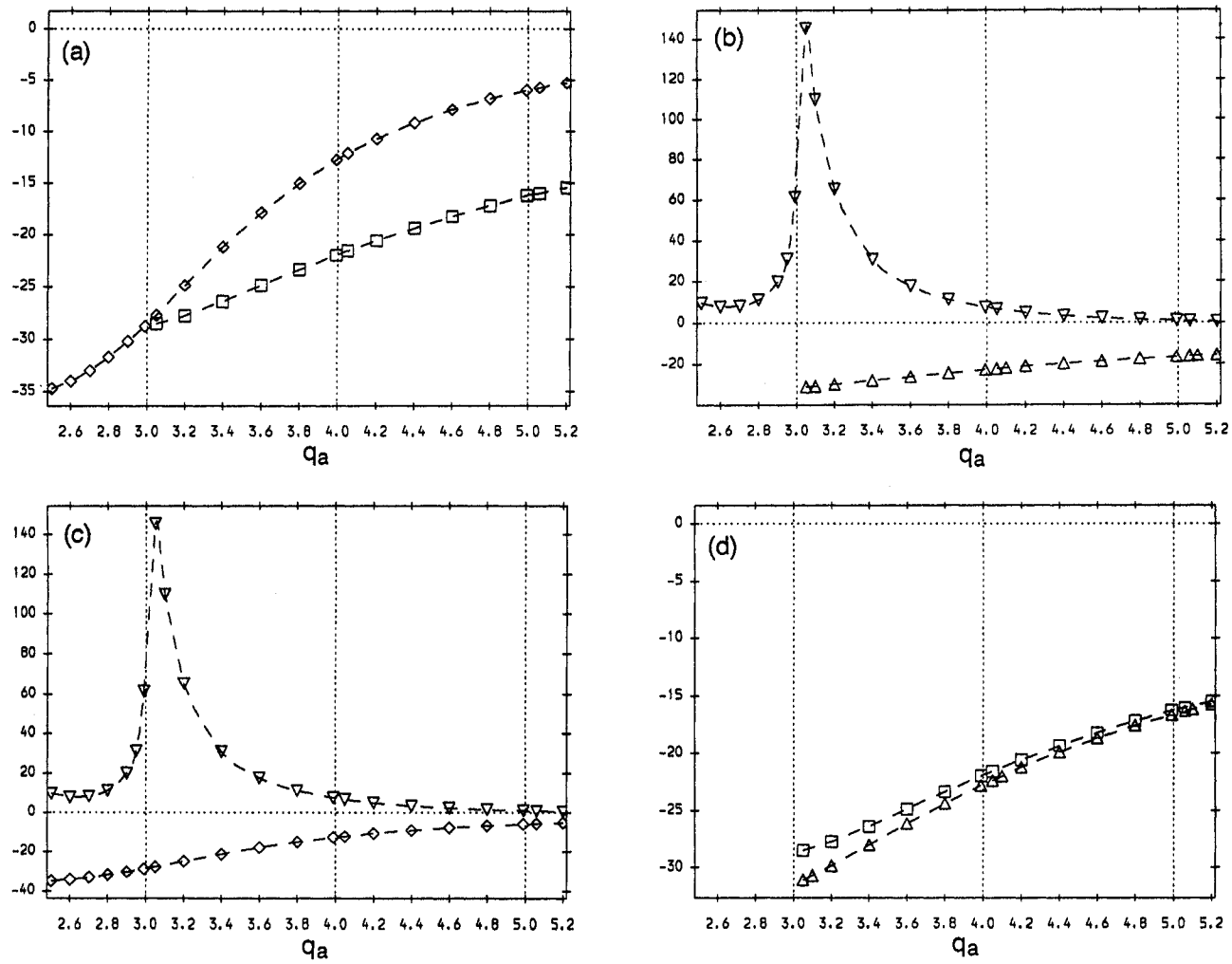

FIG. 5. The toroidal correction (i.e. $\lambda^{(1)}$ in Eq. (58)) to the (2, 1) tearing stability index (normalized to the minor radius of the q = 2 surface) as a function of q_a, for $q_0 = 1.1$ (with k = 4). The data shown are similar to those described in the caption for Fig. 4.

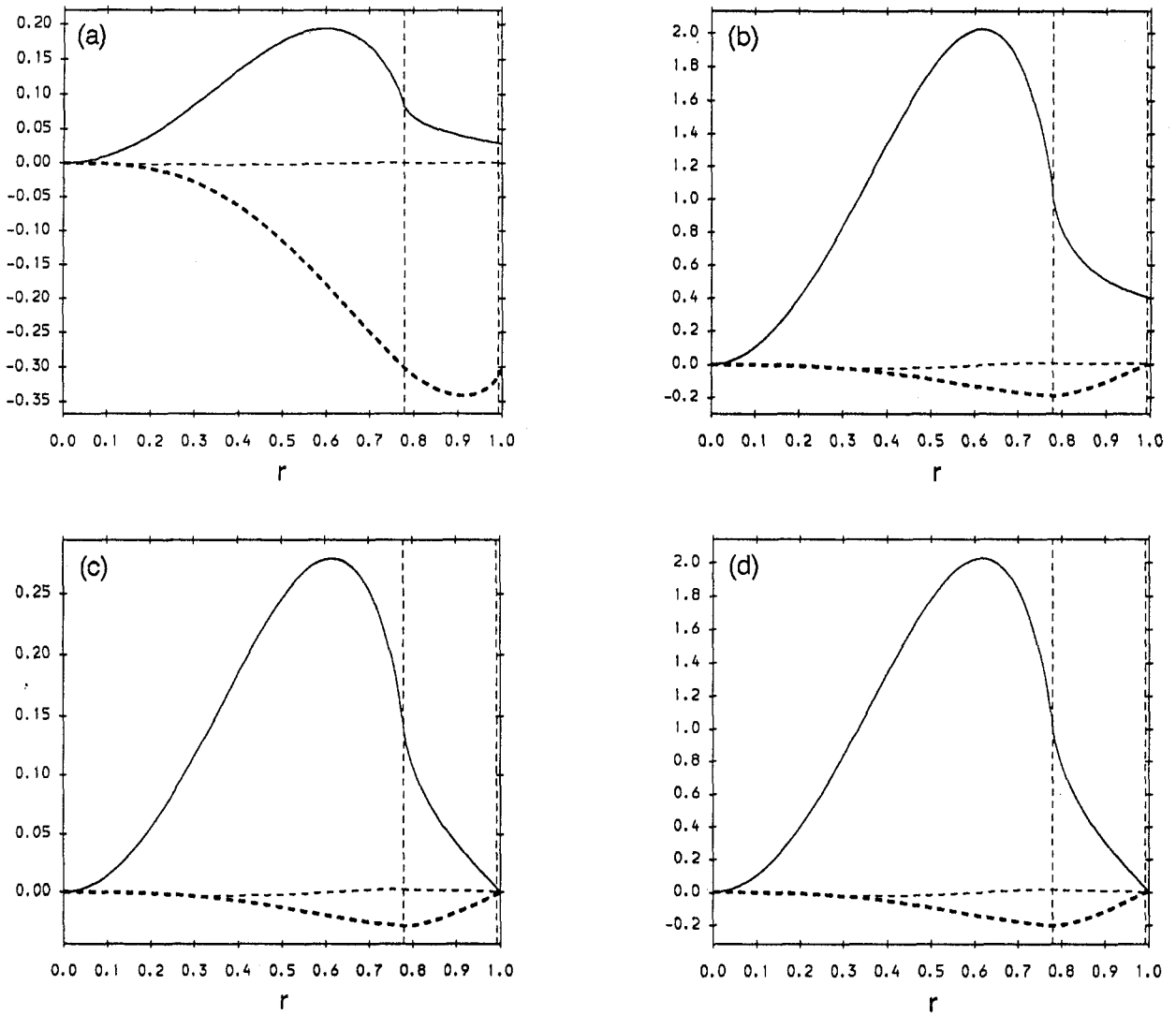

FIG. 6. Typical tearing eigenfunctions for the (2, 1) mode, calculated for $\epsilon = 0.1$, $\beta_p = E_a = T_a = 0.0$, $q_0 = 1.1$, $q_a = 3.05$ *and* $k = 4$. *The solid curves show the* $m = 2$ *harmonic, the heavy dashed curves show the* $m = 3$ *harmonic and the light dashed curve show the* $m = 1$ *harmonic. The positions of the* $q = 2$ *and* $q = 3$ *surfaces are indicated. Subplot (a) shows the eigenfunction for the fully reconnected free-boundary mode, subplot (b) shows the eigenfunction for the unreconnected free-boundary mode, subplot (c) shows the eigenfunction for the fully reconnected fixed-boundary mode and subplot (d) shows the eigenfunction for the unreconnected fixed-boundary mode.*

q_a, for $q_0 = 1.01$ and 1.1. It can be seen that for *fixed-boundary* modes the toroidal/pressure correction is strongly stabilizing at low edge q, and is either weakly stabilizing or destabilizing at high edge q. The behaviour of the *free-boundary* modes is similar to that shown in Figs 7 and 8.

3.3.5. *The effect of flux surface shaping*

Figures 11 and 12 show the ellipticity correction to the (2, 1) tearing stability index as a function of q_a, for $q_0 = 1.01$ and 1.1. It can be seen that for both *fixed-boundary* modes ellipticity is strongly *stabilizing*, and that the effect peaks for q_a just less than 3. For $q_a > 4$, the stability curve for the unreconnected mode (for which the elliptically coupled $m = 4$ harmonic does not reconnect magnetic flux at the $q = 4$ surface) bifurcates from the curve for the fully reconnected mode (for which the $m = 4$ harmonic achieves full reconnection at $q = 4$). The fully reconnected mode again is more unstable than the unreconnected mode. Ellipticity is less stabilizing for the fully reconnected free-boundary mode

than for the corresponding fixed-boundary mode, and is actually destabilizing for $q_a \lesssim 2.8$, owing to interaction with the (4, 1) external-kink mode. However, the presence of an unreconnected $q = 4$ surface in the plasma effectively 'shields' the (2, 1) tearing mode from the influence of the (4, 1) external-kink mode.

Figures 13 and 14 show the triangularity correction to the (2, 1) tearing stability index as a function of q_a, for $q_0 = 1.01$ and 1.1. The behaviour of the triangularity correction is similar in form to that of the ellipticity correction, except that now the coupled $m = 5$ harmonic and the $q = 5$ surface are significant. Triangularity is found to be significantly more stabilizing than ellipticity. Note that for $q_a \gtrsim 3$, there is virtually no difference between the free-boundary and fixed-boundary modes in Figs 13 and 14.

3.4. The critical (2, 1) island width for locking the $q = 3$ surface

Output from the code T7 can be used to calculate the various critical mode amplitudes for locking coupled rational surfaces (see Section 2). As an example of this type of calculation, in this section an estimate is made

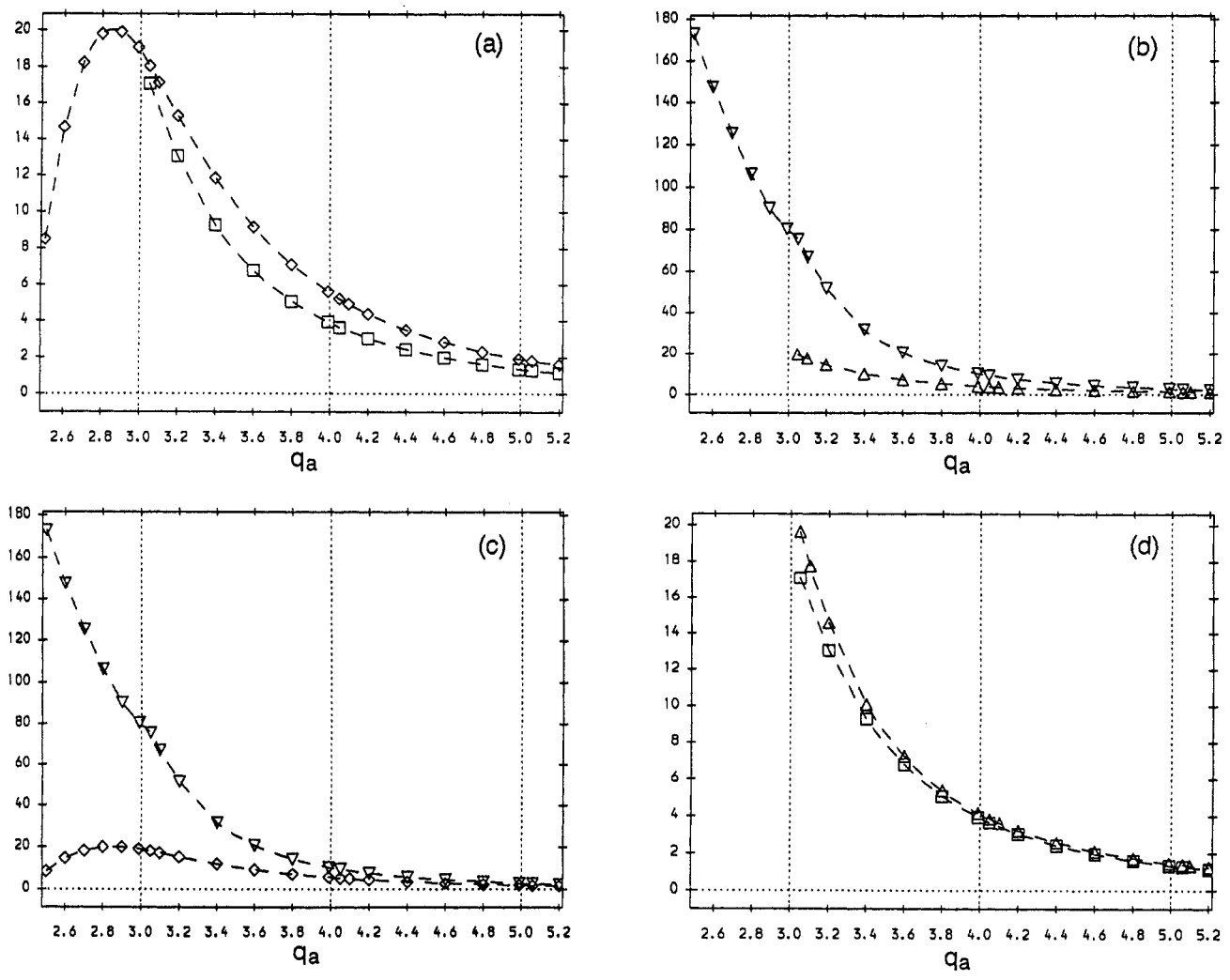

FIG. 7. The pressure correction (i.e. $\lambda^{(2)}$ in Eq. (58)) to the (2, 1) tearing stability index (normalized to the minor radius of the $q = 2$ surface) as a function of q_a, for $q_0 = 1.01$ (with $k = 4$). The data shown are similar to those described in the caption for Fig. 4.

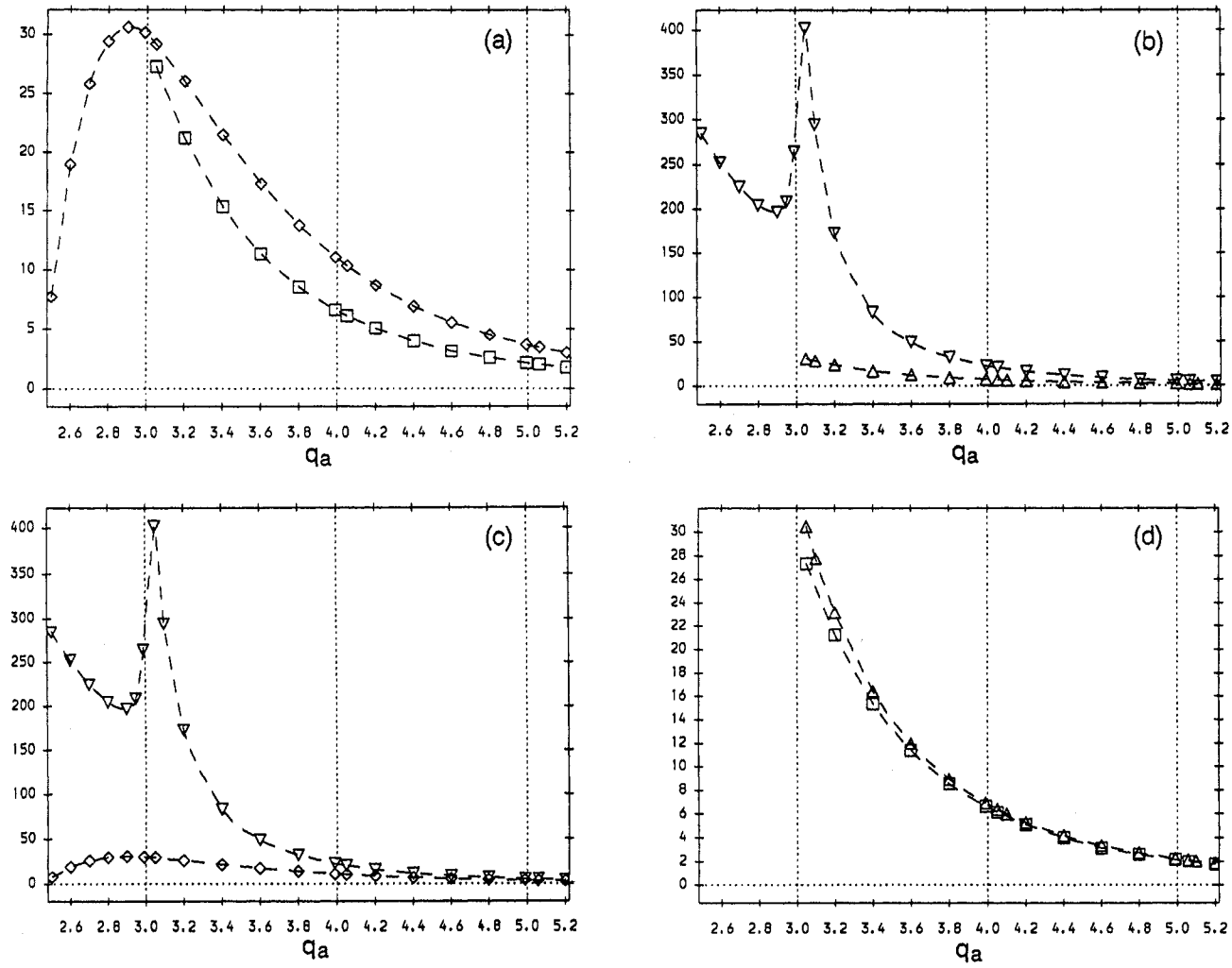

FIG. 8. The pressure correction (i.e. $\lambda^{(2)}$ in Eq. (58)) to the (2, 1) tearing stability index (normalized to the minor radius of the q = 2 *surface) as a function of* q_a, *for* $q_0 = 1.1$ *(with* k = 4*). The data shown are similar to those described in the caption for Fig. 4.*

of the (2, 1) island width needed to lock the $q = 3$ surface in a typical ohmically heated tokamak.

To lowest order, the relationship between the magnitude of the reconnected magnetic flux and the maximum island width at a general rational surface j is (see Ref. [16])

$$W_j \simeq 4 \sqrt{\frac{R_0}{B_0} \frac{m_j \Psi_j}{n s_j}} \tag{59}$$

It follows from Eqs (22), (23) and (59) that the equation governing the mutual locking of the $q = 2$ and $q = 3$ surfaces (assuming the latter surface is intrinsically stable to tearing modes) takes the form

$$\frac{1}{4} \left(\frac{W_1}{W_{\rm lock}} \right)^4 \frac{\hat{\omega}}{\alpha^2 + \hat{\omega}^2} = 1 - \hat{\omega} \tag{60}$$

where

$$\frac{W_{\rm lock}}{a} \simeq \left(2^9 \frac{r_1^2}{\epsilon^2 E_{12}^2} (\omega_1 - \omega_2)^2 \tau_2 \times \frac{\tau_{\rm H}^2(r_1)}{\tau_{\rm V}(r_1)} \Big/ \int_{r_1}^{r_2} \frac{\mu_\perp(r_1)}{r \mu_\perp(r)} \, {\rm d}r \right)^{1/4} \tag{61}$$

Here, surface 1 refers to the $q = 2$ surface and surface 2 to the $q = 3$ surface. According to Eqs (10), (20), (23) and (37), the reconnected flux driven at the $q = 3$ surface is given by

$$\left| \frac{\Psi_2}{\Psi_2^{\rm full}} \right| = \frac{\alpha}{\sqrt{\hat{\omega}^2 + \alpha^2}} \tag{62}$$

For a monotonic q profile, with $q_0 > 1$, the off-diagonal elements of the E matrix can be expressed as

a power series in the various expansion parameters. A general element E_{ij} is written as

$$E_{ij} = \lambda^{(1)}\epsilon + \lambda^{(2)}\epsilon\beta_p + \lambda^{(3)}E_a + \lambda^{(4)}T_a + O(\epsilon^2) \quad (63)$$

If the poloidal mode numbers resonant at surfaces i and j differ by unity, then only $\lambda^{(1)}$ and $\lambda^{(2)}$ are non-zero. If the mode numbers differ by two, or three, then only $\lambda^{(3)}$, or $\lambda^{(4)}$, is non-zero, respectively. If they differ by more than three, then E_{ij} is negligible in the T7 ordering scheme.

Figure 15 shows the off-diagonal element of the E matrix coupling the $q = 2$ and $q = 3$ surfaces (i.e. E_{12}), calculated from the code T7 for $q_0 = 1.01$ (and $k = 4$), as a function of q_a. Data are shown for both free-boundary and fixed-boundary plasmas. It can be seen that the coupling is largest when the $q = 3$ surface lies close to the edge of the plasma, and that the pressure contribution has a far stronger variation with edge q than the toroidal contribution. The coupling in a free-boundary plasma is slightly stronger than that in a fixed-boundary plasma. The coupling also increases with increasing plasma pressure.

The matrix element E_{12} is negative according to Fig. 15, implying that the $m = 2$ and $m = 3$ eigenfunctions lock in a configuration such that they interfere constructively on the low field side of the tokamak (i.e. $\theta = \pi$, see Section A.2) and destructively on the high field side (i.e. $\theta = 0$) (see Section 2.3.7 and also Fig. 6) [23]. This appears, from the code T7, to be a fairly general property of modes coupled by toroidicity

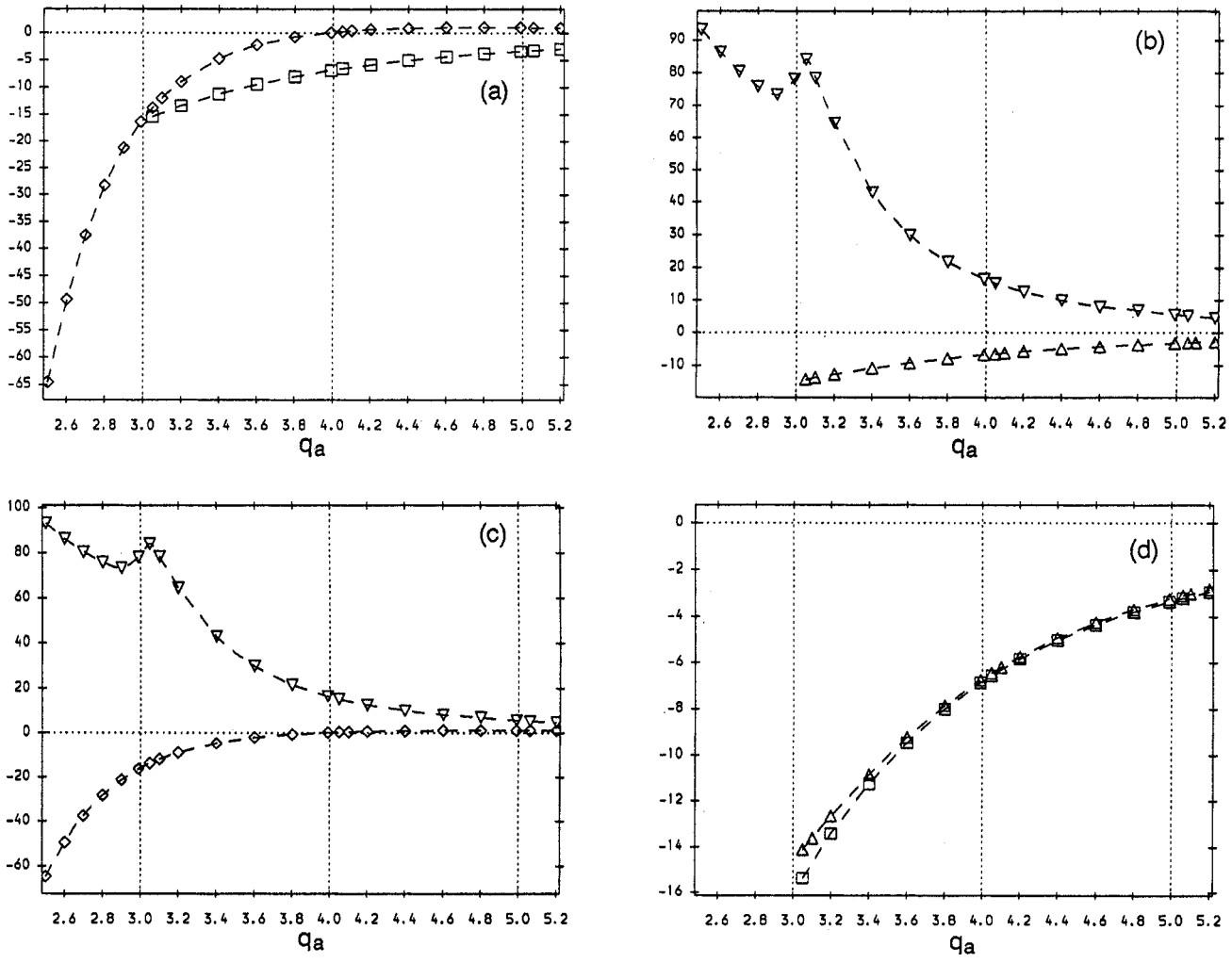

FIG. 9. The toroidal/pressure correction (i.e. $\lambda^{(3)}$ in Eq. (58)) to the (2, 1) tearing stability index (normalized to the minor radius of the q = 2 surface) as a function of q_a, for $q_0 = 1.01$ (with k = 4). The data shown are similar to those described in the caption for Fig. 4.

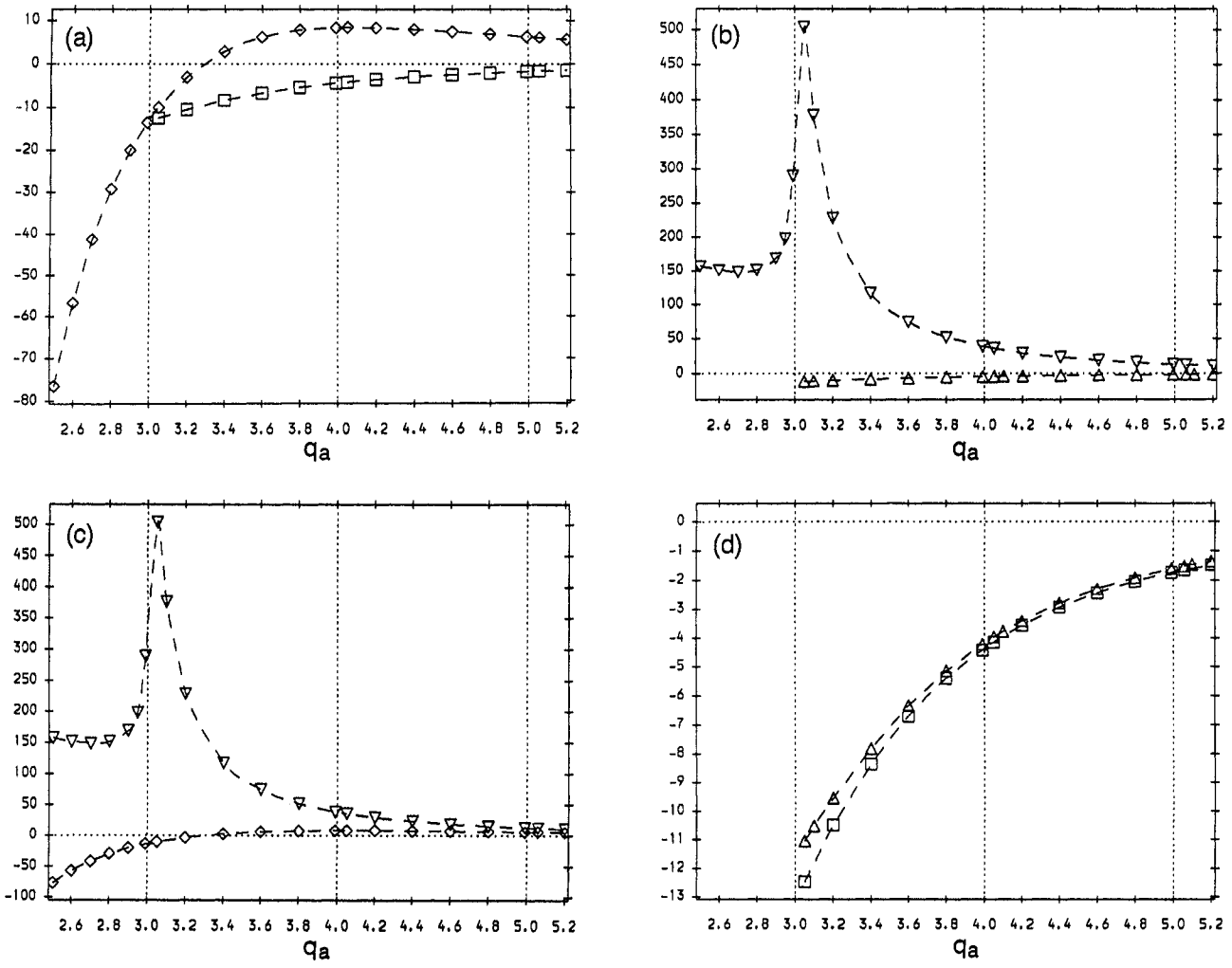

FIG. 10. The toroidal/pressure correction (i.e. $\lambda^{(3)}$ in Eq. (58)) to the (2, 1) tearing stability index (normalized to the minor radius of the q = 2 surface) as a function of q_a, for $q_0 = 1.1$ (with k = 4). The data shown are similar to those described in the caption for Fig. 4.

and pressure. For a conventionally shaped tokamak plasma (i.e. $E_a > 0$ and $T_a > 0$, see Eq. (54) and also Fig. 1), modes coupled by ellipticity tend to lock in a configuration where they interfere constructively on both the high and the low field sides. Finally, modes coupled by triangularity tend to lock in a configuration in which they interfere constructively on the high field side and destructively on the low field side.

The various plasma parameters appearing in Eq. (61) are estimated using the simple scaling model introduced in Ref. [9]. The inverse aspect ratio ϵ is fixed at 0.35, whilst the toroidal field strength scales as $B_0 = 1.35 R_0^{0.7}$ T (R_0 in metres). In general terms, this covers most modern tokamaks of conventional design. For instance, COMPASS-C ($R_0 = 0.56$ m, $a = 0.2$ m, $B_0 = 1.1$ T) [11], DIII-D ($R_0 = 1.67$ m, $a = 0.64$ m, $B_0 = 1.3$ T) [24], JET ($R_0 = 3.0$ m, $a = 1.1$ m, $B_0 = 3.0$ T) [20], ITER (1991) ($R_0 \sim 6.0$ m, $a \sim 2.2$ m, $B_0 \sim 4.9$ T) [25] and ITER (1993) ($R_0 \sim 8.0$ m, $a \sim 2.8$ m, $B_0 \sim 6$ T) [26]. Plausible temperature and density profiles are adopted (i.e. $T(r) \propto (1 - r^2)^2$, $n_e(r) \propto \sqrt{1 - r^2}$). The discharge parameters are $q_0 = 1.01$, $q_a = 4.0$, $k = 4$, $\bar{n}_e = 2 \times 10^{19}$ m^{-3}, $Z_{\rm eff} = 4.0$ and $\beta_p = 0.0$, with deuterium as the fuelling ion species. The central electron temperature is estimated from Ohmic power balance, using the standard neo-ALCATOR energy confinement time-scale [27]. No provision is made for the neoclassical enhancement of resistivity or the shaping of plasma cross-sections, hence the rather high value of $Z_{\rm eff}$ adopted. The viscosity profile is assumed

to be flat (for lack of any better assumption), and the momentum confinement time-scale (i.e. the exponential decay time-scale of an unsupported velocity profile) is set equal to the neo-ALCATOR energy confinement time-scale. The natural mode frequency of the resonant layers is set equal to the local electron diamagnetic frequency. The positions of the $q = 2$ and $q = 3$ surfaces, as determined by the code T7, are $r_1 = 0.674$ and $r_2 = 0.864$, respectively. The code also yields $E_{12} = -6.95\epsilon$ and $E_{22} = -6.36 + O(\epsilon^2)$.

Table I shows various plasma parameters, estimated by the method outlined above, as a function of the major radius, R_0. It can be seen that the visco-resistive time-scale at the $q = 3$ surface increases rapidly with increasing machine dimensions (as the plasma becomes hotter), whereas the frequency mismatch between the $q = 2$ and $q = 3$ surfaces decreases markedly.

The parameter $\alpha \equiv -E_{22}/2\pi\Delta f_{12}\tau_2$ (see Eq. (23a, b)), which governs the nature of the locking process, is O(1) for small tokamaks but becomes significantly less than unity for large tokamaks. Clearly, only comparatively large (i.e. $R_0 \gtrsim 3$ m) ohmically heated tokamaks lie in the $\alpha \ll 1$ regime for mutual mode locking (discussed in detail in Section 2). In fact, in Table I only the cases with $R_0 \geq 6$ m have true bifurcating solutions. In marked contrast, bifurcating solutions are always obtained for the locking of the (2, 1) mode to a static external perturbation [9]. This different

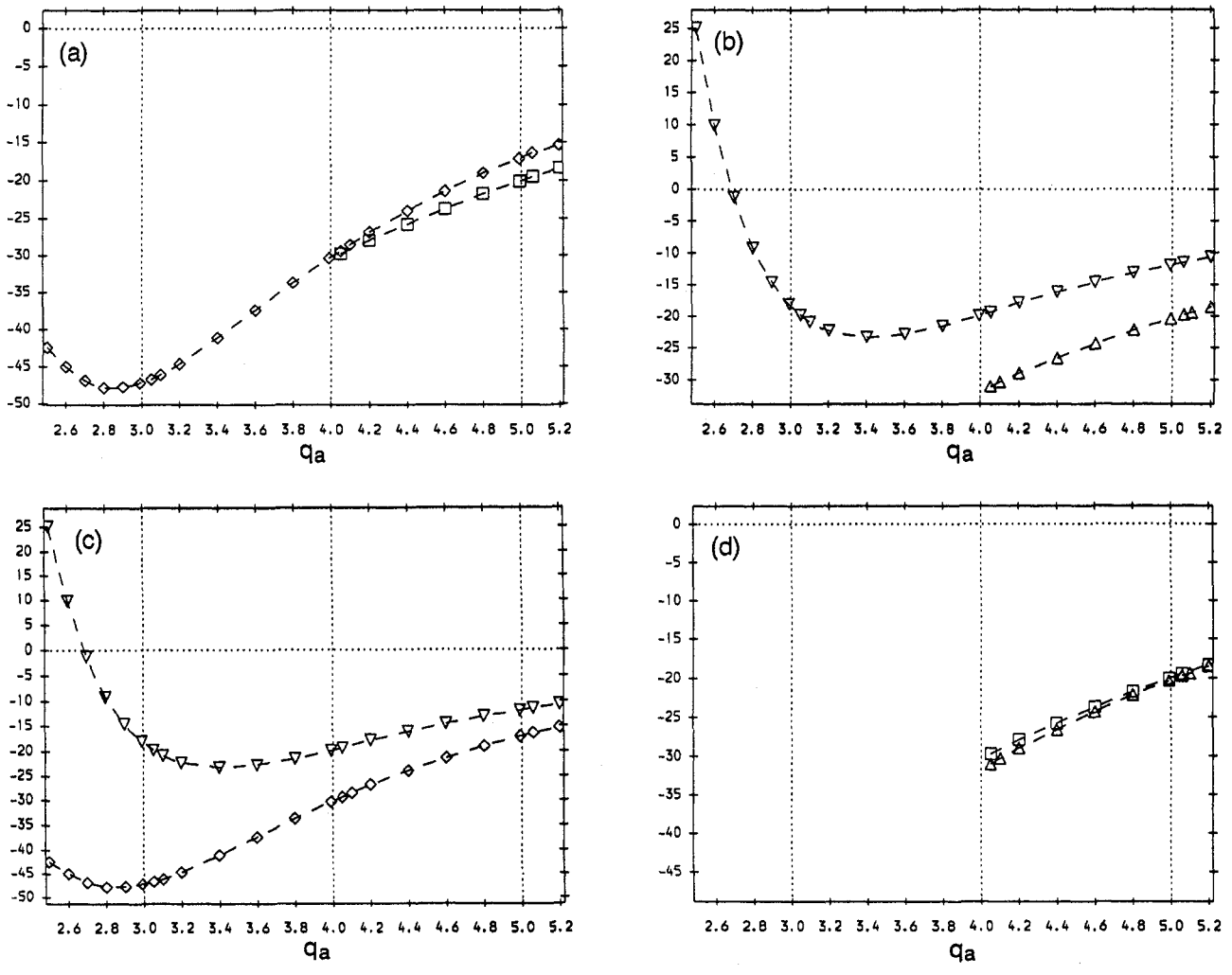

FIG. 11. The ellipticity correction (i.e. $\lambda^{(4)}$ in Eq. (58)) to the (2, 1) tearing stability index (normalized to the minor radius of the $q = 2$ surface) as a function of q_a, for $q_0 = 1.01$ (with $k = 4$). The data shown are similar to those described in the caption for Fig. 4.

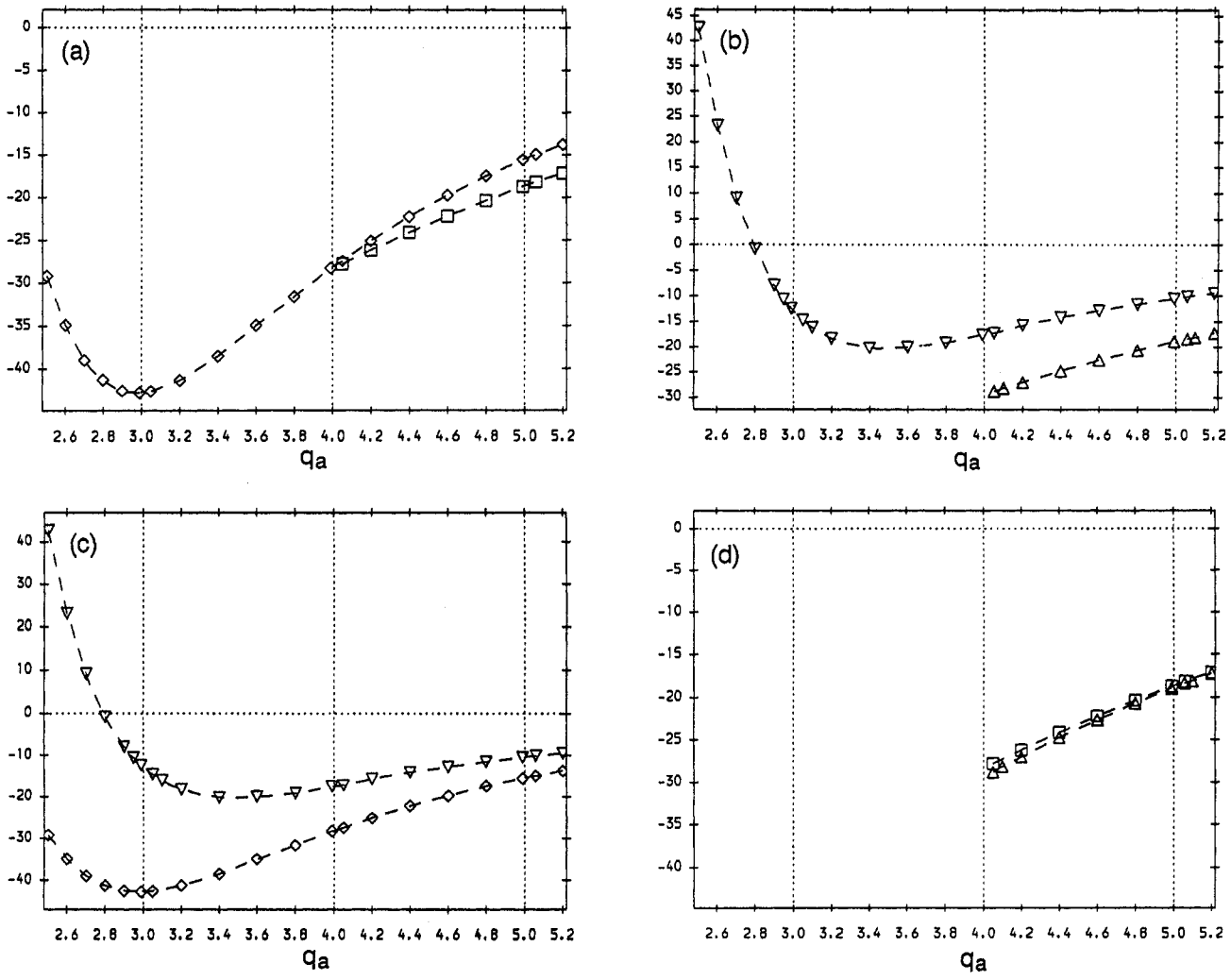

FIG. 12. The ellipticity correction (i.e. $\lambda^{(4)}$ in Eq. (58)) to the (2, 1) tearing stability index (normalized to the minor radius of the $q = 2$ *surface) as a function of* q_a, *for* $q_0 = 1.1$ *(with* $k = 4$*). The data shown are similar to those described in the caption for Fig. 4.*

behaviour is due, firstly, to the much faster reconnection rate at the relatively cold $q = 3$ surface compared with that at the hotter $q = 2$ surface, secondly, to the smaller frequency mismatch between the $q = 2$ and $q = 3$ surfaces compared with that between the $q = 2$ surface and a static perturbation, and, thirdly, to the comparative stability of the (3, 1) mode compared with that of the (2, 1) mode. Auxiliary heated plasmas are much more likely to lie in the $\alpha \ll 1$ regime for the mutual locking of the $q = 2$ and $q = 3$ surfaces, since they are generally significantly hotter than Ohmic plasmas, and τ_2 is consequently much larger. Plasmas heated by unbalanced neutral beam injection (NBI) are almost certain to lie in the $\alpha \ll 1$ regime, since, in addition to the effect of the heating, the plasma rotation (and hence, Δf_{12}) is greatly enhanced [28].

In the $\alpha \ll 1$ regime, there is virtually no reconnection at the $q = 3$ surface if the (2, 1) island width, W_1, lies below the threshold value $W_{\rm lock}$ (see Table I). In this situation, the $q = 3$ surface acts rather like an *ideal* wall as far as the $m = 3$ harmonic is concerned. If W_1 exceeds the threshold value, there is a sudden transition to full reconnection at $q = 3$, which now acts like a vacuum rational surface as far as the $m = 3$ harmonic is concerned. As α becomes O(1), $m = 3$ flux begins to 'leak' through the $q = 3$ surface at small mode amplitudes (see Eq. (62)). In this situation, the surface acts like a *resistive* wall as far as the $m = 3$

harmonic is concerned. The transition to full reconnection at $q = 3$, as the mode amplitude is increased, is far less abrupt than in the $\alpha \ll 1$ regime.

In comparatively small ohmically heated tokamaks, where $\alpha \sim O(1)$, a substantial amount of $m = 3$ flux 'leaks' through the $q = 3$ surface at low mode amplitudes. In this situation, the (2, 1) mode is a hybrid of the unreconnected and the fully reconnected modes. As the machine dimensions increase, and α decreases, the $q = 3$ surface becomes gradually more effective at shielding low amplitude flux, and the (2, 1) mode approximates closer to an unreconnected mode. Since unreconnected modes are generally more stable than fully reconnected modes, this suggests that large tokamaks are likely to be more stable to low amplitude tearing modes than small tokamaks.

Figure 16 shows the critical (2, 1) island width needed to induce full reconnection at $q = 3$, calculated from Eq. (60) using the data in Table I. Here, full reconnection is defined as $\hat{\omega} = 0.1\alpha$ for non-bifurcating solutions (see Eq. (62)). For comparatively small ohmically heated tokamaks, the $q = 3$ surface does not shield $m = 3$ flux very effectively. Nevertheless, some residual shielding persists even at extremely high mode amplitudes. For large tokamaks, on the other hand, the $q = 3$ surface shields $m = 3$ flux quite effectively, but the shielding is suddenly lost (as locking occurs) at comparatively low mode amplitudes. For JET-like dimensions (i.e. $R_0 \sim 3$ m), this loss of shielding occurs when the (2, 1) island width exceeds about 6% of the minor radius. For ITER-like dimensions (i.e. $R_0 \geq 6$ m), the shielding is lost when the (2, 1) island width only

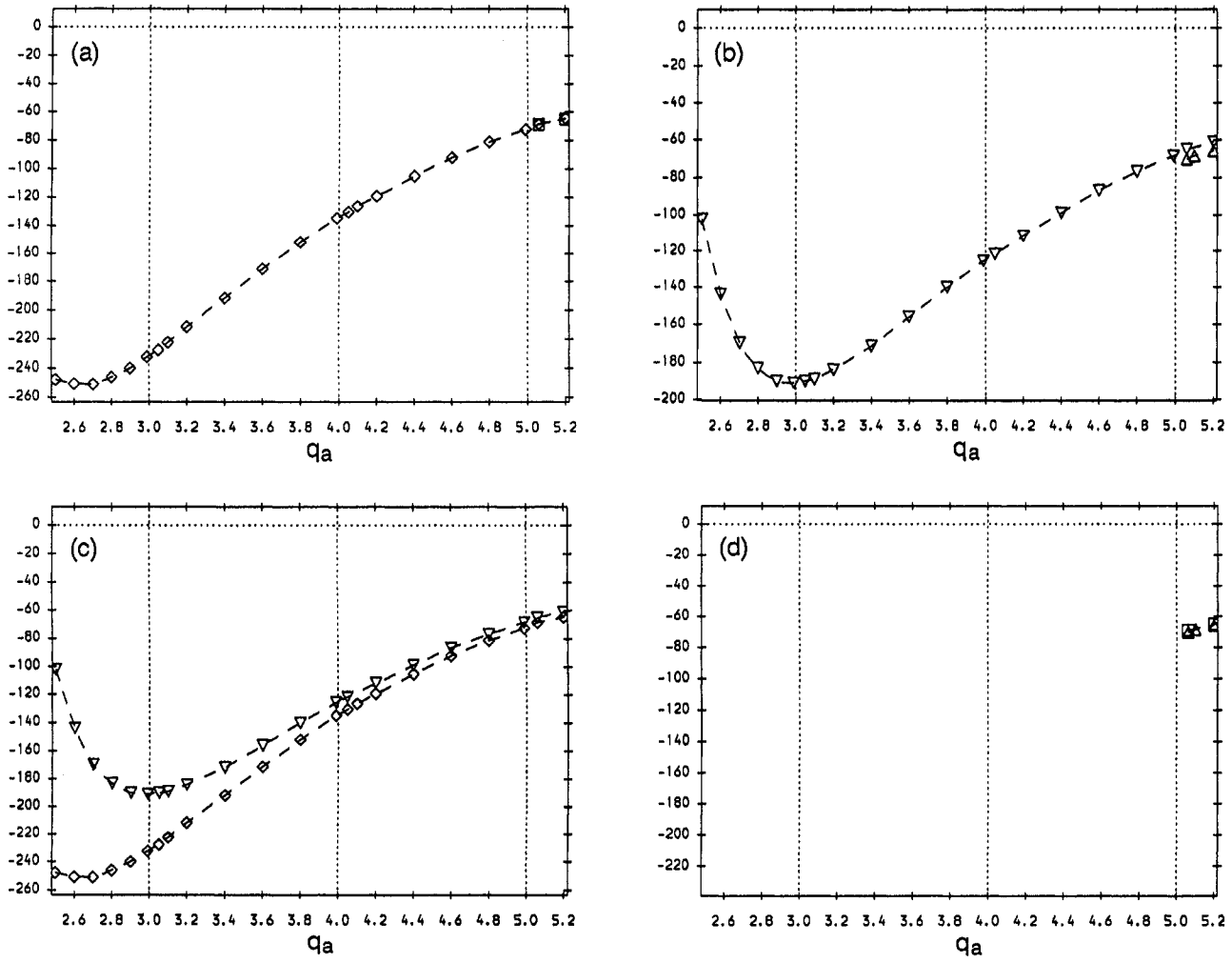

FIG. 13. The triangularity correction (i.e. $\lambda^{(5)}$ in Eq. (58)) to the (2, 1) tearing stability index (normalized to the minor radius of the q = 2 surface) as a function of q_a, for $q_0 = 1.01$ (with k = 4). The data shown are similar to those described in the caption for Fig. 4.

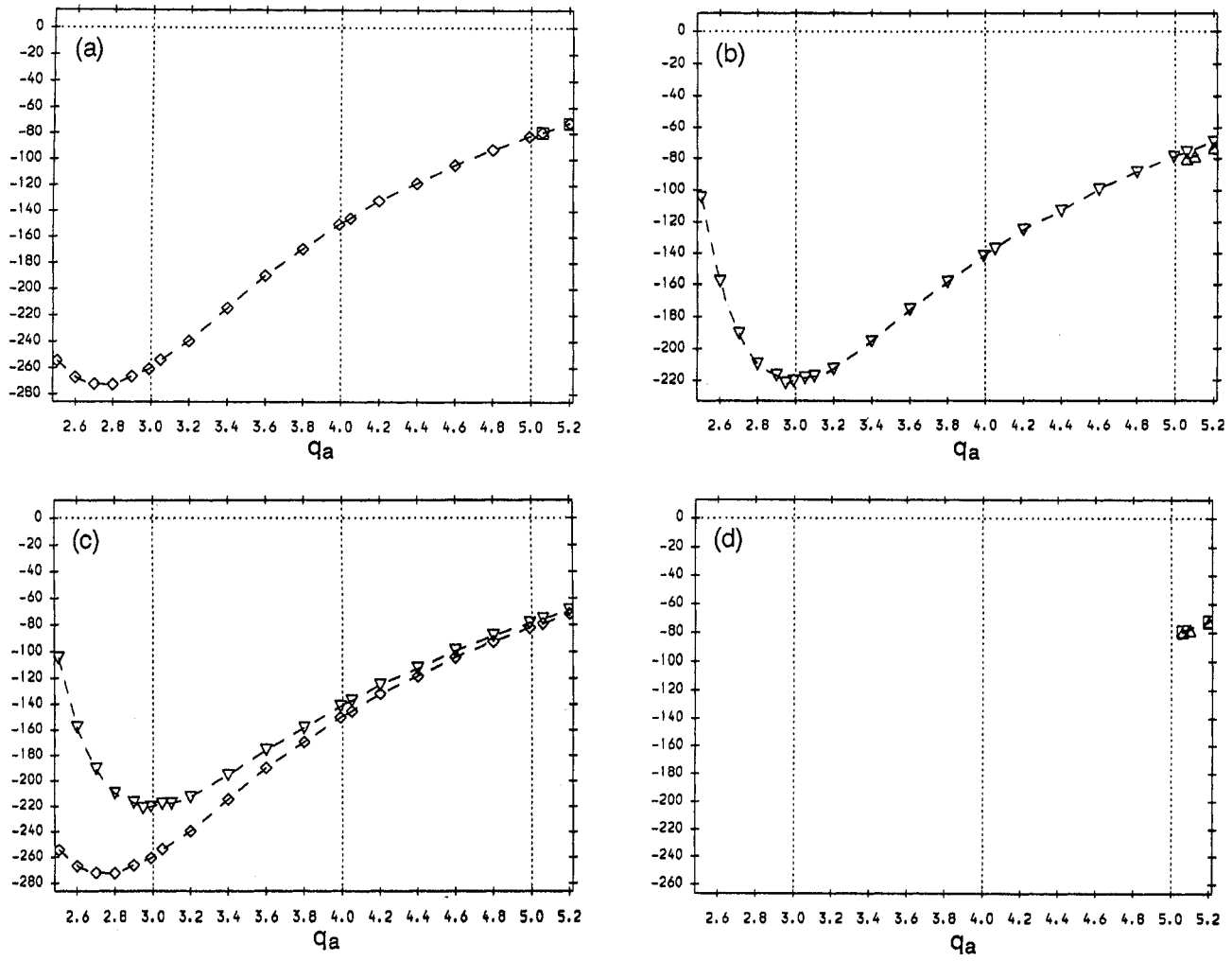

FIG. 14. The triangularity correction (i.e. $\lambda^{(5)}$ in Eq. (58)) to the (2, 1) tearing stability index (normalized to the minor radius of the $q = 2$ *surface) as a function of* q_a, *for* $q_0 = 1.1$ *(with* $k = 4$*). The data shown are similar to those described in the caption for Fig. 4.*

exceeds about 2% of the minor radius. Loss of shielding is accompanied by destabilization of the (2, 1) mode, as it switches from its unreconnected state to its fully reconnected state. It also makes the mode vulnerable to destabilization by the (3, 1) external kink mode.

4. SUMMARY AND CONCLUSIONS

The stability of coupled tearing modes in tokamaks is determined by a dispersion relation of the general form given in Eq. (1). This interrelates the tearing stability indices of the resistive layers located at the various rational surfaces in the plasma via the elements of the E matrix, which is calculated from the solution of the marginally stable ideal MHD equations in the region of the plasma excluding the layers.

No general statements about the properties of coupled tearing modes can be made without first making some assumptions about the nature of the resistive layers. This paper concentrates on one particular property of the layers which has a profound effect on their interaction via the E matrix: i.e. that they only efficiently reconnect magnetic flux which rotates close to a certain characteristic frequency [7]. This frequency is termed the 'natural' frequency of the layer, and is generally determined by the local equilibrium $\boldsymbol{E} \times \boldsymbol{B}$ velocities and by the diamagnetic fluid velocities [8, 9]. The width of the frequency band, centred on the natural frequency, for which magnetic reconnection is efficient

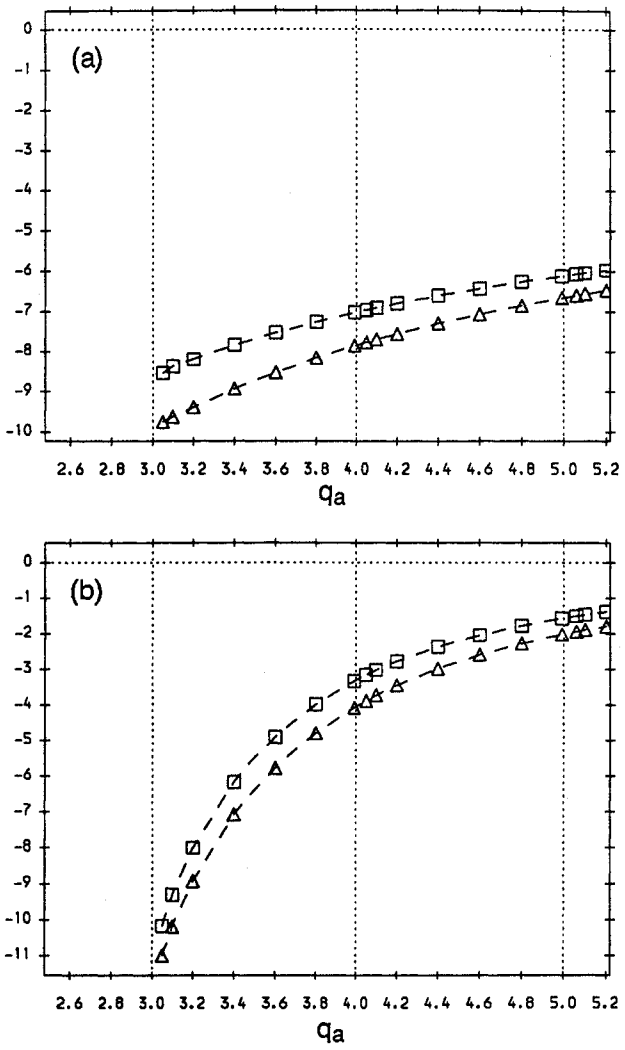

FIG. 15. The off-diagonal element of the E *matrix coupling the* q = 2 *and* q = 3 *surfaces as a function of* q_a, *for* $q_0 = 1.01$ *(with* k = 4*). Data are shown for both fixed-boundary (□) and free-boundary (△) plasmas. Subplot (a) shows the toroidal contribution (i.e.* $\lambda^{(1)}$ *in Eq. (63)) and subplot (b) shows the pressure contribution (i.e.* $\lambda^{(2)}$ *in Eq. (63)).*

is of the order of the typical layer reconnection rate [7]. Fluid flow can also affect the plasma equilibrium, thereby modifying the E matrix, but such effects are only significant when the fluid velocities are comparable with the sound velocity [29, 30], and are neglected in this paper.

In many tokamaks, the differences between the natural frequencies of the various resistive layers are far greater than the typical reconnection rates [9]. It follows that in the linear regime the resistive layers effectively decouple from one another. In fact, linear stability analysis yields a set of modes that reconnect magnetic flux at only one rational surface in the plasma, propagate at the associated natural frequency and effectively behave ideally at all of the other surfaces. These are termed the 'unreconnected' modes, and their stability is determined by the diagonal elements of the E matrix.

In the non-linear regime, electromagnetic torques develop in the vicinity of the rational surfaces. These

TABLE I. PLASMA PARAMETERS ESTIMATED FOR OHMICALLY HEATED TOKAMAKS WITH $a = 0.35R_0$, $B_0(\mathrm{T}) = 1.38R_0^{0.7}(\mathrm{m})$, $q_0 = 1.01$, $q_a = 4.0$ AND $\bar{n}_e = 2 \times 10^{19}$ m^{-3}, INCLUDING THE CENTRAL ELECTRON TEMPERATURE (T_{ec}), THE VISCO-RESISTIVE TIME-SCALE AT THE $q = 3$ SURFACE (τ_2), AND THE DIFFERENCE BETWEEN THE NATURAL FREQUENCIES AT THE $q = 2$ AND $q = 3$ SURFACES (Δf_{12})

R_0(m)	a(m)	B_0(T)	T_{ec}(keV)	τ_2(ms)	Δf_{12}(kHz)	α	W_{lock}/a
0.50	0.18	0.85	0.67	0.16	6.74	0.92	0.199
0.75	0.26	1.13	1.00	0.44	3.35	0.68	0.142
1.00	0.35	1.38	1.32	0.89	2.06	0.55	0.111
1.50	0.53	1.83	1.96	2.40	1.03	0.41	0.079
2.00	0.70	2.24	2.61	4.87	0.63	0.33	0.062
3.00	1.05	2.98	3.89	13.13	0.31	0.25	0.044
4.00	1.40	3.64	4.83	26.49	0.19	0.20	0.034
6.00	2.10	4.84	7.70	71.37	0.10	0.15	0.024
8.00	2.80	5.92	10.2	144.5	0.06	0.12	0.019

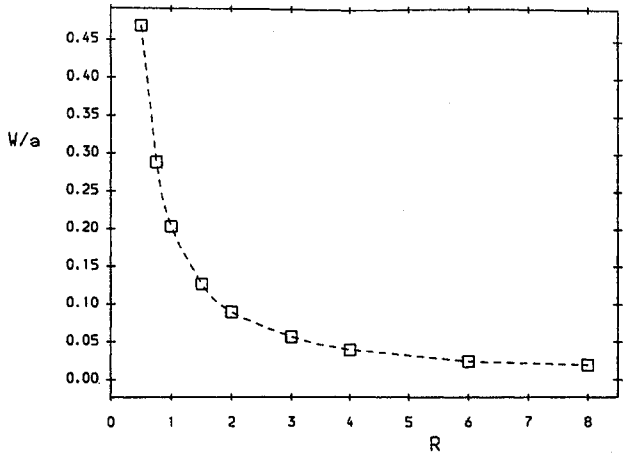

FIG. 16. The critical (2, 1) island width normalized to the minor radius (W/a) *required to induce full reconnection at* q = 3*, as a function of the plasma major radius* (R)*, for a typical ohmically heated tokamak. The discharge parameters are* $q_0 = 1.01$, $q_a = 4.0$, k = 4, $\bar{n}_e = 2 \times 10^{19}$ m^{-3} *and* $Z_{eff} = 4.0$.

torques are associated with the off-diagonal elements of the E matrix and modify the bulk toroidal rotation of the plasma so as to bring the various natural frequencies closer together. Such modifications are opposed by plasma viscosity. In a tokamak plasma with widely dispersed natural frequencies, the balance of electromagnetic and viscous torques at the various rational surfaces gives rise to a system of equations with bifurcated solutions, similar in form to that obtained from a simple induction motor. If the amplitudes of the reconnected fluxes are sufficiently small, then all of the modes in the plasma remain unreconnected. However, above a certain critical amplitude, two or more surfaces can suddenly 'lock' together (i.e. their natural frequencies are suddenly brought into coincidence). This gives rise to a new mode that reconnects magnetic flux simultaneously at all of the locked surfaces, and rotates at the unperturbed natural frequency of the outermost locked surface. This new mode is generally more unstable than any of the unreconnected modes associated with the surfaces that are locked together.

For the special case of a plasma with only one intrinsically unstable rational surface (e.g., surface j), the reconnected flux driven to a coupled surface after locking is termed the 'fully reconnected' flux, and is such as to ensure a vacuum-like behaviour at that surface (i.e. a zero helical sheet current). If the amplitude of the reconnected flux at surface j is sufficiently large to lock all of the coupled surfaces in the plasma, the resulting mode is termed the 'fully reconnected' mode associated with surface j, and its stability is determined by the jth diagonal element of the inverse E matrix.

The significance of unreconnected and fully reconnected modes is illustrated by the results from the code T7, which determines the general coupled tearing-mode dispersion relation for a large aspect ratio tokamak with shaped flux surfaces. The stability of the (2, 1) tearing mode is investigated for $q_0 > 1$. Toroidicity and flux surface shaping are found to have a generally stabilizing effect on the mode, whereas pressure is destabilizing. It is found that the fully reconnected mode is always more unstable than the unreconnected mode. This is particularly the case for free-boundary plasmas, owing to the strong destabilizing influence of external-kink modes. It is found that the presence of an unreconnected $q = 3$ surface external to the $q = 2$ surface completely shields the (2, 1) tearing mode from the destabilizing influence of the (3, 1) external-kink mode. This shielding effect is only overcome if the tearing mode attains sufficient amplitude to lock the $q = 3$ surface, or if the $q = 3$ surface leaves the plasma. The presence of an unreconnected $q = 4$ surface exerts a similar shielding effect with respect to, for example, the (4, 1) external-kink mode.

The implications of many of the above results can be evaluated for ohmically heated tokamaks using a simple scaling model. It is found that for small devices (i.e. $R_0 < 3$ m) the layer reconnection rates on the outermost rational surfaces are too large to allow bifurcated solutions with distinct unreconnected and fully reconnected phases. However, in auxiliary heated plasmas, where the reconnection rates are much smaller (because the plasma is hotter), bifurcated solutions probably occur. Large (i.e. $R_0 > 3$ m) ohmically heated devices are also generally hot enough to allow bifurcated solutions. The critical mode amplitude required to lock coupled rational surfaces is large in small tokamaks, but becomes very small in large tokamaks, owing to the comparatively weak natural mode rotation in the latter devices. For ITER-like dimensions (i.e. $R_0 > 6$ m) the critical mode amplitude for locking corresponds to an island width which is only about 2% of the minor radius.

In conclusion, an examination of the general form of the tearing-mode dispersion relation has yielded some rewarding insights into the behaviour of coupled tearing modes in tokamak plasmas. It is hoped to extend this analysis to cover topics such as the coupling of tearing modes and internal-kink modes, the influence of external resonant magnetic perturbations, and the effect of resistive walls.

Appendix A

DERIVATION OF THE T7 EQUATIONS

A.1. Marginally stable ideal MHD equations

The basic linearized marginally stable ideal MHD equations [4],

$$\nabla\delta p = \delta \boldsymbol{J} \times \boldsymbol{B} + \boldsymbol{J} \times \delta \boldsymbol{B} \tag{64a}$$

$$\delta \boldsymbol{J} = \nabla \times \delta \boldsymbol{B} \tag{64b}$$

$$\delta p = -\boldsymbol{\xi} \cdot \nabla p \tag{64c}$$

represent pressure balance, Ampère's law for the perturbed current $\delta \boldsymbol{J}$ and the equation of state for the perturbed pressure δp, respectively. Here, $\delta \boldsymbol{B}$ is the perturbed magnetic field and $\boldsymbol{\xi}$ is the plasma displacement, whilst the equilibrium current density $\boldsymbol{J}$, magnetic field $\boldsymbol{B}$ and pressure p satisfy the pressure balance equation $\boldsymbol{J} \times \boldsymbol{B} = \nabla p$.

The co-ordinate system (r, θ, ϕ), where r is a flux surface label with dimensions of lengths, θ is an angle-like variable in the poloidal plane and ϕ is the toroidal angle, is chosen so that the magnetic field lines appear to be straight. The Jacobian for these co-ordinates is given (see Ref. [22]) by

$$j = (\nabla r \times \nabla\theta \cdot \nabla\phi)^{-1} = \frac{rR^2}{R_0} \tag{65}$$

where R is the major radius and R_0 is a conveniently chosen average major radius.

For an axisymmetric equilibrium $\boldsymbol{B}$ can be written as

$$\boldsymbol{B} = B_0 R_0 [f(r) \nabla\phi \times \nabla r + g(r) \nabla\phi] \tag{66}$$

where B_0 is the vacuum magnetic field strength at $R = R_0$. The safety factor, the slope of the field lines in the θ–ϕ plane, is then given by

$$q(r) = \frac{rg(r)}{R_0 f(r)} \tag{67}$$

The equilibrium Grad–Shafranov equation takes the form

$$\frac{1}{r}\frac{\partial}{\partial r}(rf|\nabla r|^2) + \frac{1}{r}\frac{\partial}{\partial \theta}(rf \nabla r \cdot \nabla\theta) + \left(\frac{gg'}{f} + \frac{R^2}{R_0^2}\frac{p'}{B_0^2 f}\right) = 0 \tag{68}$$

where primes denote differentiation with respect to r.

Consider ideal perturbations of the equilibrium described by Eq. (68), with toroidal mode number n, satisfying Eqs (64a–c). After some lengthy algebra the following first order coupled differential equations are obtained:

$$r\frac{\partial}{\partial r}\left[\left(\frac{\partial}{\partial\theta} - \mathrm{i}nq\right)y\right] = \frac{\partial}{\partial\theta}\left(Q\frac{\partial z}{\partial\theta}\right) + Sz - \frac{\partial}{\partial\theta}\left[T\left(\frac{\partial}{\partial\theta} - \mathrm{i}nq\right)y + Uy\right] \tag{69a}$$

$$\left(\frac{\partial}{\partial\theta} - \mathrm{i}nq\right)r\frac{\partial z}{\partial r} = -\left(\frac{\partial}{\partial\theta} - \mathrm{i}nq\right)T^*\frac{\partial z}{\partial\theta} + U\frac{\partial z}{\partial\theta} - \left(\frac{\partial}{\partial\theta} - \mathrm{i}nq\right)V\left(\frac{\partial}{\partial\theta} - \mathrm{i}nq\right)y + W\left(\frac{\partial}{\partial\theta} - \mathrm{i}nq\right)y + Xy \tag{69b}$$

Here, the dependent variables are

$$y(r, \theta)\exp(-\mathrm{i}n\phi) = B_0 f \boldsymbol{\xi} \cdot \nabla r$$

and

$$z(r, \theta)\exp(-\mathrm{i}n\phi) = R^2 \delta \boldsymbol{B} \cdot \nabla\phi$$

whilst Q, S, T, U, V, W and X are equilibrium quantities (with T^* being the complex conjugate of T),

$$Q = 1/\mathrm{i}n|\nabla r|^2 \tag{70a}$$

$$S = \mathrm{i}n\frac{r^2}{R_0^2} \tag{70b}$$

$$T = \frac{r\nabla r\cdot\nabla\theta}{|\nabla r|^2} - \frac{1}{in}\frac{1}{|\nabla r|^2}\frac{R_0 g'}{f} \tag{70c}$$

$$U = \frac{1}{|\nabla r|^2}\frac{rp'}{B_0^2 f^2}\frac{R^2}{R_0^2} \tag{70d}$$

$$V = \frac{1}{|\nabla r|^2}\left[in\frac{R_0^2}{R^2} + \frac{1}{in}\left(\frac{R_0 g'}{f}\right)^2\right] \tag{70e}$$

$$W = 2\frac{R_0 g'}{f}\frac{rp'}{B_0^2 f^2}\frac{1}{|\nabla r|^2}\frac{R^2}{R_0^2} - r\frac{\mathrm{d}}{\mathrm{d}r}\left(\frac{R_0 g'}{f}\right) \tag{70f}$$

$$X = in\frac{rp'}{B_0^2 f^2}\left[\frac{\partial}{\partial\theta}\left(T^*\frac{R^2}{R_0^2}\right) + r\frac{\partial}{\partial r}\left(\frac{R^2}{R_0^2}\right) - \frac{R^2}{R_0^2}\frac{r^2}{f}\frac{\mathrm{d}}{\mathrm{d}r}\left(\frac{f}{r}\right) - U\frac{R^2}{R_0^2}\right] \tag{70g}$$

A.2. Metric coefficients for a large aspect ratio tokamak

Consider a tokamak equilibrium in which the (r, θ, ϕ) co-ordinates are related to the cylindrical co-ordinates (R, ϕ, Z) (with Z in the direction of the symmetry axis) via (see Refs [2, 31])

$$R = R_0 - r\cos\omega - \Delta(r) + E(r)\cos\omega + T(r)\cos 2\omega + P(r)\cos\omega \tag{71a}$$

$$Z = r\sin\omega + E(r)\sin\omega + T(r)\sin 2\omega - P(r)\cos\omega \tag{71b}$$

where ω is the poloidal angle about the magnetic axis ($r = 0$), Δ is the Shafranov shift, E is the flux surface ellipticity, T is the flux surface triangularity and P is the departure of the flux surface label r from the 'radius' of flux surfaces. The angle-like variable θ is related to ω by

$$\theta = 2\pi\int_0^\omega \frac{J\,\mathrm{d}\omega}{R}\Big/\oint\frac{J\,\mathrm{d}\omega}{R} \tag{72}$$

where $J = \partial R/\partial\omega\partial Z/\partial r - \partial R/\partial r\partial Z/\partial\omega$ is the Jacobian of the transformation $(R, Z \to r, \omega)$.

In the T7 ordering, the inverse aspect ratio $\epsilon = a/R$ (where $r = a$ corresponds to the outermost plasma flux surface) is assumed to be small. In addition, the relative shift of the centres of the flux surfaces and their departures from circularity are assumed to be such that Δ, E and T are all $\lesssim O(\epsilon a)$. With this ordering the choice

$$P(r) = \frac{1}{8}\frac{r^3}{R_0^2} + \frac{1}{2}\frac{r}{R_0}\Delta - \frac{1}{2}\frac{E^2}{r} - \frac{1}{2}\frac{T^2}{r} + O(\epsilon^3 a) \tag{73}$$

ensures that the Jacobian of the transformation $(r, \theta, \phi \to R, \phi, Z)$ satisfies Eq. (65). Note that $P \sim O(\epsilon^2 a)$, so that the departure of r from the true radius of the flux surfaces is relatively small. To lowest order the Grad-Shafranov equation yields $g = 1 + O(\epsilon^2)$, $f \sim O(\epsilon)$ (assuming $q \sim O(1)$ for a tokamak) and $ap'/B_0^2 \sim O(\epsilon^2)$. The flux surface shaping functions are found to satisfy

$$\Delta'' + (3 - 2s)\frac{\Delta'}{r} + 2\frac{R_0}{r}\frac{p'q^2}{B_0^2} - \frac{1}{R_0} = O(\epsilon^2/a) \tag{74a}$$

$$E'' + (3 - 2s)\frac{E'}{r} - 3\frac{E}{r^2} = O(\epsilon^2/a) \tag{74b}$$

$$T'' + (3 - 2s)\frac{T'}{r} - 8\frac{T}{r^2} = O(\epsilon^2/a) \tag{74c}$$

where $s(r) = rq'/q$ is the magnetic shear. The Shafranov shift of the outermost plasma flux surface is set to zero by convention in T7. Finally, the metric elements are given (see Ref. [31]) by

$$|\nabla r|^2 = 1 - 2\Delta'\cos\theta + 2E'\cos 2\theta + 2T'\cos 3\theta + \left(\frac{3}{4}\frac{r^2}{R_0^2} + \frac{1}{2}\Delta'^2 + \frac{\Delta}{R_0} + \frac{1}{2}E'^2 + \frac{3}{2}\frac{E^2}{r^2} + \frac{1}{2}T'^2 + 4\frac{T^2}{r^2}\right) + O(\epsilon^2) \tag{75a}$$

$$r\nabla r\cdot\nabla\theta = \left(\frac{r}{R_0} + r\Delta'' + \Delta'\right)\sin\theta - \frac{1}{2}\left(rE'' + E' + 3\frac{E}{r}\right)\sin 2\theta - \frac{1}{3}\left(rT'' + T' + 8\frac{T}{r}\right)\sin 3\theta + O(\epsilon^2) \quad (75b)$$

$$\frac{R^2}{R_0^2} = 1 - 2\frac{r}{R_0}\cos\theta - \left(\frac{1}{2}\frac{r^2}{R_0^2} + \frac{r}{R_0}\Delta' + 2\frac{\Delta}{R_0}\right) + O(\epsilon^2) \quad (75c)$$

where θ-varying terms are retained up to $O(\epsilon)$ and secular terms up to $O(\epsilon^2)$. Note that with the scheme set out above, the equilibrium is completely specified by two arbitrary functions, $p'(r)$ and $q(r)$, plus the inverse aspect ratio, ellipticity and triangularity of the outermost plasma flux surface.

A.3. Expansion in poloidal Fourier harmonics

The dependent variables in the perturbed marginally stable ideal MHD equations (69a, b) can be expressed as an infinite sum of poloidal Fourier harmonics. Thus,

$$y(r,\theta) = \sum_m y_m(r)\exp(im\theta) \quad (76a)$$

$$z(r,\theta) = \sum_m z_m(r)\exp(im\theta) \quad (76b)$$

Equations (69a, b) can be transformed into the following infinite set of coupled equations for the Fourier harmonics:

$$r\frac{d}{dr}[(m - nq)y_m] = \sum_{j=-\infty}^{\infty}(B_m^{m+j}z_{m+j} + C_m^{m+j}y_{m+j}) \quad (77a)$$

$$(m - nq)r\frac{dz_m}{dr} = \sum_{j=-\infty}^{\infty}(D_m^{m+j}z_{m+j} + E_m^{m+j}y_{m+j}) \quad (77b)$$

where

$$B_m^{m+j} = \frac{1}{2\pi i}\oint \exp(-im\theta)\left(\frac{\partial}{\partial\theta}Q\frac{\partial}{\partial\theta} + S\right)\exp[i(m + j)\theta]\,d\theta \quad (78a)$$

$$C_m^{m+j} = \frac{1}{2\pi i}\oint \exp(-im\theta)\left[-\frac{\partial}{\partial\theta}T\left(\frac{\partial}{\partial\theta} - inq\right) - \frac{\partial}{\partial\theta}U\right]\exp[i(m + j)\theta]\,d\theta \quad (78b)$$

$$D_m^{m+j} = \frac{1}{2\pi i}\oint \exp(-im\theta)\left[-\left(\frac{\partial}{\partial\theta} - inq\right)T^*\frac{\partial}{\partial\theta} + U\frac{\partial}{\partial\theta}\right]\exp[i(m + j)\theta]\,d\theta \quad (78c)$$

$$E_m^{m+j} = \frac{1}{2\pi i}\oint \exp(-im\theta)\left[-\left(\frac{\partial}{\partial\theta} - inq\right)V\left(\frac{\partial}{\partial\theta} - inq\right) + W\left(\frac{\partial}{\partial\theta} - inq\right) + X\right]\exp[i(m + j)\theta]\,d\theta \quad (78d)$$

A more convenient set of equations is obtained by applying the transformation (see Ref. [5])

$$y_m = \frac{\psi_m}{m - nq} \quad (79a)$$

$$z_m = n\frac{Z_m}{m - nq} - \frac{C_m^m}{B_m^m}\frac{\psi_m}{m - nq} \quad (79b)$$

to the dependent variables. The relationship between the perturbed magnetic field and the new dependent variables, ψ_m and Z_m, is as follows:

$$\delta\boldsymbol{B}\cdot\nabla r = i\frac{R_0^2}{R^2}\sum_m \frac{\psi_m(r)}{r}\exp[i(m\theta - n\phi)] \quad (80a)$$

$$R_0\delta\boldsymbol{B}\cdot\nabla\phi = n\frac{R_0^2}{R^2}\sum_m \frac{Z_m(r) + \lambda_m\psi_m(r)}{R_0(m - nq)}\exp[i(m\theta - n\phi)] \quad (80b)$$

where

$$\lambda_m = \left(m \frac{rp'}{B_0^2 f^2} \left\langle \frac{R^2}{R_0^2} \frac{1}{|\nabla r|^2} \right\rangle - \frac{m}{n} (m - nq) \frac{R_0 g'}{f} \left\langle \frac{1}{|\nabla r|^2} \right\rangle \right) \left(m^2 \left\langle \frac{1}{|\nabla r|^2} \right\rangle + n^2 \frac{r^2}{R_0^2} \right)^{-1} \tag{81a}$$

$$\langle \ldots \rangle \equiv \frac{1}{2\pi} \oint (\ldots) \, \mathrm{d}\theta \tag{81b}$$

Finally, the transformed coupled mode equations are written (see Ref. [32]) as

$$r \frac{\mathrm{d}\psi_m}{\mathrm{d}r} = \frac{L_m^m Z_m}{m - nq} + \sum_{j \neq 0} \frac{L_m^{m+j} Z_{m+j} + M_m^{m+j} \psi_{m+j}}{m + j - nq} \tag{82a}$$

$$(m - nq) r \frac{\mathrm{d}}{\mathrm{d}r} \left(\frac{Z_m}{m - nq} \right) = \frac{P_m^m \psi_m}{m - nq} + \sum_{j \neq 0} \frac{N_m^{m+j} Z_{m+j} + P_m^{m+j} \psi_{m+j}}{m + j - nq} \tag{82b}$$

For the large aspect ratio expanded metric elements described in Section A.2, the coupling coefficients in Eqs (82a, b) take the form

$$L_m^m = m^2 \left(1 - \frac{3}{4} \frac{r^2}{R_0^2} + \frac{3}{2} \Delta'^2 - \frac{\Delta}{R_0} + \frac{3}{2} E'^2 - \frac{3}{2} \frac{E^2}{r^2} + \frac{3}{2} T'^2 - 4 \frac{T^2}{r^2} \right) + n^2 \frac{r^2}{R_0^2} \tag{83a}$$

$$\begin{aligned} P_m^m = {} & (m - nq)^2 \left\{ 1 + \frac{7}{4} \frac{r^2}{R_0^2} + 3 \frac{r}{R_0} \Delta' + \frac{3}{2} \Delta'^2 + \frac{\Delta}{R_0} + \frac{3}{2} E'^2 - \frac{3}{2} \frac{E^2}{r^2} + \frac{3}{2} T'^2 - 4 \frac{T^2}{r^2} \right. \\ & + \frac{1}{m^2} \left[\frac{n}{m} r \frac{\mathrm{d}}{\mathrm{d}r} \left(\frac{r^2}{R_0^2} \frac{2 - s}{q} \right) - \frac{r^2}{R_0^2} \frac{(2 - s)^2}{q^2} - r \frac{\mathrm{d}}{\mathrm{d}r} \left(\frac{rp'}{B_0^2} \right) \right] \Bigg\} + \frac{m - nq}{m} \left\{ -2 \frac{rp'}{B_0^2} (2 - s) \right. \\ & + qr \frac{\mathrm{d}}{\mathrm{d}r} \left[\frac{2 - s}{q} \left(1 - \frac{r^2}{R_0^2 q^2} + \frac{3}{4} \frac{r^2}{R_0^2} - \frac{3}{2} \Delta'^2 + \frac{\Delta}{R_0} - \frac{3}{2} E'^2 + \frac{3}{2} \frac{E^2}{r^2} - \frac{3}{2} T'^2 + 4 \frac{T^2}{r^2} \right) \right. \\ & \left. \left. + \frac{1}{q} \left(\frac{3}{2} \frac{r^2}{R_0^2} + 2 \frac{r}{R_0} \Delta' + \Delta'^2 + E'^2 + 6 \frac{EE'}{r} - 3 \frac{E^2}{r^2} + T'^2 + 16 \frac{TT'}{r} - 8 \frac{T^2}{r^2} \right) \right] \right\} \\ & + 2 \frac{rp'}{B_0^2} (1 - q^2) \end{aligned} \tag{83b}$$

$$L_m^{m \pm 1} = m(m \pm 1) \Delta' \tag{83c}$$

$$L_m^{m \pm 2} = -m(m \pm 2) E' \tag{83d}$$

$$L_m^{m \pm 3} = -m(m \pm 3) T' \tag{83e}$$

$$M_m^{m \pm 1} = \mp m(m - nq) \frac{R_0 p' q^2}{B_0^2} \mp m(m \pm 1 - nq) \left((1 - s) \Delta' - \frac{r}{R_0} \right) \tag{83f}$$

$$M_m^{m \pm 2} = \pm \frac{m}{2} (m \pm 2 - nq) \left((1 - s) E' - 3 \frac{E}{r} \right) \tag{83g}$$

$$M_m^{m \pm 3} = \pm \frac{m}{3} (m \pm 3 - nq) \left((1 - s) T' - 8 \frac{T}{r} \right) \tag{83h}$$

$$N_m^{m \pm 1} = \mp (m \pm 1)(m \pm 1 - nq) \frac{R_0 p' q^2}{B_0^2} \mp (m \pm 1)(m - nq) \left((1 - s) \Delta' - \frac{r}{R_0} \right) \tag{83i}$$

$$N_m^{m \pm 2} = \pm \frac{1}{2} (m \pm 2)(m - nq) \left((1 - s) E' - 3 \frac{E}{r} \right) \tag{83j}$$

$$N_m^{m \pm 3} = \pm \frac{1}{3} (m \pm 3)(m - nq) \left((1 - s) T' - 8 \frac{T}{r} \right) \tag{83k}$$

$$P_m^{m\pm1} = -(1+s)\frac{R_0 p' q^2}{B_0^2} + (m \pm 1 - nq)(m - nq)\left(\Delta' + \frac{r}{R_0}\right) \tag{83l}$$

$$P_m^{m\pm2} = -(m \pm 2 - nq)(m - nq)E' \tag{83m}$$

$$P_m^{m\pm3} = -(m \pm 3 - nq)(m - nq)T' \tag{83n}$$

When $m = 0$ some of the coupling coefficients take on special values,

$$P_0^0 = n^2q^2 - \frac{q^2}{r}\frac{\mathrm{d}}{\mathrm{d}r}\left(\frac{r^2}{q^2}(2-s)\right) - q^2 r \frac{\mathrm{d}}{\mathrm{d}r}\left(\frac{R_0^2 p'}{r B_0^2}\right) + \mathrm{O}(\epsilon^2) \tag{84a}$$

$$M_{\pm1}^0 = \lim_{m\to0} M_{m\pm1}^m \pm (2-s)\Delta' \tag{84b}$$

$$M_{\pm2}^0 = \lim_{m\to0} M_{m\pm2}^m \mp 2(2-s)E' \tag{84c}$$

$$M_{\pm3}^0 = \lim_{m\to0} M_{m\pm3}^m \mp 3(2-s)T' \tag{84d}$$

$$N_0^{\pm1} = \lim_{m\to0} N_m^{m\pm1} \mp (2-s)\Delta' \tag{84e}$$

$$N_0^{\pm2} = \lim_{m\to0} N_m^{m\pm2} \pm 2(2-s)E' \tag{84f}$$

$$N_0^{\pm3} = \lim_{m\to0} N_m^{m\pm3} \pm 3(2-s)T' \tag{84g}$$

$$P_{\pm1}^0 = \lim_{m\to0} P_{m\pm1}^m - (2-s)\left[\pm nq\frac{R_0 p' q^2}{B_0^2} - (1 \mp nq)\left((1-s)\Delta' - \frac{r}{R_0}\right)\right] \tag{84h}$$

$$P_{\pm2}^0 = \lim_{m\to0} P_{m\pm2}^m - \frac{1}{2}(2-s)(2 \mp nq)\left((1-s)E' - 3\frac{E}{r}\right) \tag{84i}$$

$$P_{\pm3}^0 = \lim_{m\to0} P_{m\pm3}^m - \frac{1}{3}(2-s)(3 \mp nq)\left((1-s)T' - 8\frac{T}{r}\right) \tag{84j}$$

$$P_0^{\pm1} = \lim_{m\to0} P_m^{m\pm1} - (2-s)\left[\pm nq\frac{R_0 p' q^2}{B_0^2} - (1 \mp nq)\left((1-s)\Delta' - \frac{r}{R_0}\right)\right] \tag{84k}$$

$$P_0^{\pm2} = \lim_{m\to0} P_m^{m\pm2} - \frac{1}{2}(2-s)(2 \mp nq)\left((1-s)E' - 3\frac{E}{r}\right) \tag{84l}$$

$$P_0^{\pm3} = \lim_{m\to0} P_m^{m\pm3} - \frac{1}{3}(2-s)(3 \mp nq)\left((1-s)T' - 8\frac{T}{r}\right) \tag{84m}$$

The coupling coefficients satisfy the following important symmetry relations:

$$L_{m\pm j}^m = L_m^{m\pm j} \tag{85a}$$

$$M_{m\pm j}^m = -N_m^{m\pm j} \tag{85b}$$

$$N_{m\pm j}^m = -M_m^{m\pm j} \tag{85c}$$

$$P_{m\pm j}^m = P_m^{m\pm j} \tag{85d}$$

The ordering adopted for the T7 equations (82a, b) is consistent with that described in Section A.2 for the metric elements. Thus, a *cylindrical* tearing eigenfunction with poloidal mode number m drives *six* $\mathrm{O}(\epsilon)$ poloidal sidebands: namely, $m \pm 1$ via toroidicity and pressure, $m \pm 2$ via flux surface ellipticity and $m \pm 3$ via flux surface triangularity. These sidebands couple back to produce $\mathrm{O}(\epsilon^2)$ corrections to the original cylindrical mode. It follows that coefficients that describe sideband coupling (e.g., L_m^{m+1}) need only be determined to $\mathrm{O}(\epsilon)$, whereas self-coupling coefficients (e.g., L_m^m) must be determined to $\mathrm{O}(\epsilon^2)$. For the special case of $m = 0$, where L_0^0 is $\mathrm{O}(\epsilon^2)$, P_0^0 need only be determined to $\mathrm{O}(1)$.

Appendix B

PROPERTIES OF THE T7 EQUATIONS

B.1. Behaviour close to the magnetic axis

Consider the expansion of the T7 equations (82a, b) at small r/a. In the T7 ordering scheme, the generalization of a cylindrical tearing eigenfunction with poloidal mode number m is a *septuplet* of coupled eigenfunctions with poloidal mode numbers in the range $m - 3$ to $m + 3$. At small r/a, a well behaved septuplet with central mode number $m > 0$ satisfies the following relations:

$$Z_m(r) \simeq \frac{m - nq}{m}\,\psi_m(r) \tag{86a}$$

$$\psi_{m+1}(r) \simeq -\frac{r}{R_0}\,\frac{(m - nq) - 2R_0^2 p'' q^2/B_0^2}{2(m - nq)}\,\psi_m(r) \tag{86b}$$

$$\psi_{m+2}(r) \simeq \frac{2r^2 q'' E'}{(m - nq)(m + 1)q}\,\psi_m(r) \tag{86c}$$

$$\psi_{m+3}(r) \simeq \frac{2r^2 q'' T'}{(m - nq)(m + 1)q}\,\psi_m(r) \tag{86d}$$

to lowest order, with all other ψ_{m+j} and Z_{m+j} approximately zero. The equivalent septuplet with central mode number $m < 0$ satisfies

$$Z_m(r) \simeq \frac{m - nq}{|m|}\,\psi_m(r) \tag{87a}$$

$$\psi_{m-1}(r) \simeq -\frac{r}{R_0}\,\frac{(m - nq) + 2R_0^2 p'' q^2/B_0^2}{2(m - nq)}\,\psi_m(r) \tag{87b}$$

$$\psi_{m-2}(r) \simeq -\frac{2r^2 q'' E'}{(m - nq)(|m| + 1)q}\,\psi_m(r) \tag{87c}$$

$$\psi_{m-3}(r) \simeq -\frac{2r^2 q'' T'}{(m - nq)(|m| + 1)q}\,\psi_m(r) \tag{87d}$$

with all other ψ_{m+j} and Z_{m+j} approximately zero. For the special case where the central mode number is zero the lowest order solution is

$$Z_0(r) \simeq \text{constant} \tag{88}$$

with all other ψ_j and Z_j approximately zero.

Note from Eqs (86) to (88) that at small r/a only 'outward' coupling (i.e. coupling in the direction away from the $m = 0$ harmonic) is important. However, 'inward' coupling can become effective in the special case where it straddles the $m = 0$ harmonic. Thus, in addition to the couplings described in Eqs (86a–d), an $m = 1$ mode can also drive both $m = -1$ and $m = -2$ sidebands:

$$\psi_{-1}(r) = 2E'\psi_1(r) \tag{89a}$$

$$\psi_{-2}(r) = 2T'\psi_1(r) \tag{89b}$$

Likewise, an $m = -1$ mode can also drive both $m = 1$ and $m = 2$ sidebands:

$$\psi_1(r) = 2E'\psi_{-1}(r) \tag{90a}$$

$$\psi_2(r) = 2T'\psi_{-1}(r) \tag{90b}$$

B.2. Behaviour in the vicinity of rational surfaces

B.2.1. The general case

In the vicinity of a rational surface resonant with poloidal mode number m (defined by $q(r_m) = m/n$, where r_m is the radius of the surface) the most general expressions for the resonant harmonics (see Ref. [32]) are

$$\psi_m \simeq A_L |x|^{\nu_L}(1 + \lambda_L x + \ldots) + A_S \mathrm{sgn}(x)|x|^{\nu_S}(1 + \ldots) + A_C x(1 + \ldots) \tag{91a}$$

$$Z_m \simeq A_L |x|^{\nu_L}(b_L + \gamma_L x + \ldots) + A_S \mathrm{sgn}(x)|x|^{\nu_S}(b_S + \ldots) + B_C x(1 + \ldots) \tag{91b}$$

where $x = r - r_m$. Here, A_L and A_S are the coefficients of the 'large' and 'small' solutions (see Ref. [33]), respectively, whereas A_C and B_C are the coefficients of the 'continuous' solution. The indices ν_L and ν_S are given by

$$\nu_L = \frac{1}{2} - \left(\frac{1}{4} + D\right)^{1/2} \tag{92a}$$

$$\nu_S = \frac{1}{2} + \left(\frac{1}{4} + D\right)^{1/2} \tag{92b}$$

where for the large aspect ratio tokamak ordering described in Section A.2

$$D \simeq \left[2\frac{rp'}{B_0^2 s^2}(1 - q^2)\right]_{r_m} \tag{93}$$

Note that D is related to the well known Mercier stability criterion $1/4 + D > 0$ [34]. The most general expressions for the non-resonant harmonics in the vicinity of the rational surface are

$$\psi_{m+k} \simeq A_L |x|^{\nu_L}(a_k + \ldots) + A_S \mathrm{sgn}(x)|x|^{\nu_S}(\tilde{a}_k + \ldots) + \bar{\psi}_{m+k}(1 + \ldots) \tag{94a}$$

$$Z_{m+k} \simeq A_L |x|^{\nu_L}(b_k + \ldots) + A_S \mathrm{sgn}(x)|x|^{\nu_S}(\tilde{b}_k + \ldots) + \bar{Z}_{m+k}(1 + \ldots) \tag{94b}$$

The constants appearing in Eqs (91a, b) and (94a, b) can be shown to take the following form:

$$b_L = \nu_L / L_0 \tag{95a}$$

$$b_S = \nu_S / L_0 \tag{95b}$$

$$A_C = -\frac{1}{r_m P_0}\sum_{k \neq 0}\frac{1}{k}(N_m^{m+k}\bar{Z}_{m+k} + P_m^{m+k}\bar{\psi}_{m+k})_{r_m} \tag{95c}$$

$$B_C = -\frac{1}{r_m L_0}\sum_{k \neq 0}\frac{1}{k}(L_m^{m+k}\bar{Z}_{m+k} + M_m^{m+k}\bar{\psi}_{m+k})_{r_m} + \frac{A_C}{L_0} \tag{95d}$$

$$\lambda_L = \frac{1}{2r_m}\left[\frac{P_1 L_0}{\nu_L} + T_1 + \nu_L\left(\frac{L_1}{L_0} - 2\right)\right]_{r_m} - \frac{1}{(ms)_{r_m}}\frac{1}{r_m \nu_L}\sum_{k \neq 0}\frac{1}{k}(P_m^{m+k}L_m^{m+k} - M_m^{m+k}N_m^{m+k})_{r_m} \tag{95e}$$

$$\gamma_L = \frac{1}{2r_m}\left[(1 + \nu_L)\left(\frac{P_1}{\nu_L} + \frac{T_1}{L_0} - \frac{\nu_L}{L_0}\right) + P_0\left(\frac{L_1}{L_0} - 1\right)\right]_{r_m} - \frac{1}{(ms)_{r_m}}\frac{1}{r_m L_0}\sum_{k \neq 0}\frac{1}{k}(P_m^{m+k}L_m^{m+k} - M_m^{m+k}N_m^{m+k})_{r_m} \tag{95f}$$

$$a_k = \frac{1}{(ms)_{r_m}}\left(\frac{N_m^{m+k}}{\nu_L} - \frac{L_m^{m+k}}{L_0}\right)_{r_m} \tag{95g}$$

$$\tilde{a}_k = \frac{1}{(ms)_{r_m}}\left(\frac{N_m^{m+k}}{\nu_S} - \frac{L_m^{m+k}}{L_0}\right)_{r_m} \tag{95h}$$

$$b_k = \frac{1}{(ms)_{r_m}}\left(\frac{M_m^{m+k}}{L_0} - \frac{P_m^{m+k}}{\nu_L}\right)_{r_m} \tag{95i}$$

$$\tilde{b}_k = \frac{1}{(ms)_{r_m}}\left(\frac{M_m^{m+k}}{L_0} - \frac{P_m^{m+k}}{\nu_S}\right)_{r_m} \tag{95j}$$

where

$$L_0 = -\left(\frac{L_m^m}{ms}\right)_{r_m} \tag{96a}$$

$$P_0 = -\left(\frac{P_m^m}{ms}\right)_{r_m} \tag{96b}$$

$$L_1 = \lim_{x\to 0}\left(\frac{L_m^m}{m - nq} + \frac{L_m^m}{msx/r}\right) \tag{96c}$$

$$P_1 = \lim_{x\to 0}\left(\frac{P_m^m}{m - nq} + \frac{P_m^m}{msx/r}\right) \tag{96d}$$

$$T_1 = \lim_{x\to 0}\left(\frac{-nqs}{m - nq} - \frac{r}{x}\right) \tag{96e}$$

Note that $D \equiv L_0 P_0$.

One vitally important property of the code T7 is its ability to determine *accurately* the coefficients of the large and small solutions in the vicinity of rational surfaces. This is achieved as follows. First, the continuous components of the non-resonant harmonics are identified via

$$\bar{\psi}_{m+k} \simeq \psi_{m+k}(r_m + \delta) - a_k\psi_m(r_m + \delta) + O(\delta/r_m) \tag{97a}$$

$$\bar{Z}_{m+k} \simeq Z_{m+k}(r_m + \delta) - b_k\psi_m(r_m + \delta) + O(\delta/r_m) \tag{97b}$$

enabling all the quantities in Eqs (95) to be evaluated. The coefficient of the small solution is then given by

$$A_S \simeq \{[Z_m(r_m + \delta) - b_L\psi_m(r_m + \delta)] - \delta(B_C - b_L A_C) - \delta(\gamma_L - b_L\lambda_L)\psi_m(r_m + \delta)\}$$
$$\times [\mathrm{sgn}(\delta)|\delta|^{\nu_S}(b_S - b_L)]^{-1} + O\left(\frac{\delta}{r_m}\right) \tag{98}$$

whilst the coefficient of the large solution satisfies

$$A_L \simeq [\psi_m(r_m + \delta) - A_S\,\mathrm{sgn}(\delta)|\delta|^{\nu_S} - A_C\delta]/[|\delta|^{\nu_L}(1 + \delta\lambda_L)] + O\left(\frac{\delta^2}{r_m^2}\right) \tag{99}$$

B.2.2. The zero pressure limit

In the limit $p'(r_m) \to 0$, or for the special case of a resonant surface located at $q = 1$, the indices ν_L and ν_S become exactly 0 and 1, respectively. In this situation some of the expressions in Eqs (95a–j) become singular, so a special treatment is clearly required. The most general expressions for the resonant harmonics in this case are

$$\psi_m \simeq A_L[1 + \hat{\lambda}_L x(\ln|x| - 1) + \ldots] + A_S x(1 + \ldots) + A_C x(1 + \ldots) + A_D x(\ln|x| - 1 + \ldots) \tag{100a}$$

$$Z_m \simeq A_L(\hat{\gamma}_L x\ln|x| + \ldots) + A_S x(\hat{b}_S + \ldots) + B_D x[\ln|x| + \ldots] \tag{100b}$$

whilst the most general expressions for the non-resonant harmonics are

$$\psi_{m+k} \simeq A_L(\hat{a}_k\ln|x| + \ldots) + A_S x(\hat{a}_k + \ldots) + \bar{\psi}_{m+k}(1 + \ldots) \tag{101a}$$

$$Z_{m+k} \simeq A_L(\hat{b}_k\ln|x| + \ldots) + A_S x(\hat{b}_k + \ldots) + \bar{Z}_{m+k}(1 + \ldots) \tag{101b}$$

The constants appearing in Eqs (100a, b) and (101a, b) can be shown to take the form

$$\hat{b}_S = 1/L_0 \tag{102a}$$

$$A_C = \frac{1}{r_m}\sum_{k\neq 0}\frac{1}{k}(L_m^{m+k}\bar{Z}_{m+k} + M_m^{m+k}\bar{\psi}_{m+k})_{r_m} \tag{102b}$$

$$A_D = \frac{L_0}{r_m}\sum_{k\neq 0}\frac{1}{k}(N_m^{m+k}\bar{Z}_{m+k} + P_m^{m+k}\bar{\psi}_{m+k})_{r_m} \tag{102c}$$

$$B_D = A_D/L_0 \tag{102d}$$

$$\hat{\lambda}_L = \frac{1}{r_m} L_0 P_1 - \frac{1}{r_m} \frac{1}{(ms)_{r_m}} \sum_{k \neq 0} \frac{1}{k} (P_m^{m+k} L_m^{m+k} - M_m^{m+k} N_m^{m+k})_{r_m} \tag{102e}$$

$$\hat{\gamma}_L = \frac{1}{r_m} P_1 \tag{102f}$$

$$\hat{a}_k = \frac{1}{(ms)_{r_m}} (N_m^{m+k})_{r_m} \tag{102g}$$

$$\hat{b}_k = -\frac{1}{(ms)_{r_m}} (P_m^{m+k})_{r_m} \tag{102h}$$

The accurate identification of the coefficients of the large and small solutions is achieved as follows. First, the continuous components of the non-resonant harmonics are calculated via

$$\bar{\psi}_{m+k} \simeq \psi_{m+k}(r_m + \delta) - \psi_m(r_m + \delta)\hat{a}_k \ln|\delta| + O\left(\frac{\delta}{r_m}\right) \tag{103a}$$

$$\bar{Z}_{m+k} = Z_{m+k}(r_m + \delta) - \psi_m(r_m + \delta)\hat{b}_k \ln|\delta| + O\left(\frac{\delta}{r_m}\right) \tag{103b}$$

This enables all of the constants in Eqs (102a–h) to be evaluated. The coefficient of the small solution is then given by

$$A_S \simeq \{Z_m(r_m + \delta) - \delta[B_D + \hat{\gamma}_L \psi_m(r_m + \delta)] \ln|\delta|\}/(\delta \hat{b}_S) + O\left(\frac{\delta}{r_m}\right) \tag{104}$$

whilst the coefficient of the large solution is given by

$$A_L \simeq \{\psi_m(r_m + \delta) - \delta[A_S + A_C + A_D(\ln|\delta| - 1)]\}[1 + \hat{\lambda}_L \delta(\ln|\delta| - 1)]^{-1} + O\left(\frac{\delta^2}{r_m^2}\right) \tag{105}$$

B.2.3. Tearing parity modes

The code T7 is restricted to stability calculations for *tearing parity* modes. For such modes the coefficient of the large solution is continuous across resonant layers, whereas the coefficient of the small solution may be discontinuous. As is discussed in Ref. [4], the restriction to tearing parity modes is justified provided certain very reasonable assumptions can be made about the nature of layers in the inner region. The dimensionless tearing stability index for a layer located at r_m (see Ref. [35]) is

$$\Delta_m = r_m^{\nu_S - \nu_L} \left(\frac{A_{S+} - A_{S-}}{A_L}\right)_{r_m} \tag{106}$$

where

$$A_L = \lim_{|\delta| \to 0} A_L(r_m + |\delta|) = \lim_{|\delta| \to 0} A_L(r_m - |\delta|) \tag{107a}$$

$$A_{S+} = \lim_{|\delta| \to 0} A_S(r_m + |\delta|) \tag{107b}$$

$$A_{S-} = \lim_{|\delta| \to 0} A_S(r_m - |\delta|) \tag{107c}$$

Consider a solution which is completely continuous across the rational surface, so that $\Delta_m = 0$. According to the preceding analysis the continuity conditions for the resonant harmonic can be written as

$$\psi_m(r_m + |\delta|) \simeq \psi_m(r_m - |\delta|) + 2|\delta|[\psi_m(r_m - |\delta|)\lambda_L + A_C] + 2A_{S-}|\delta|^{\nu_S} + O\left(\frac{\delta^2}{r_m^2}\right) \tag{108a}$$

$$Z_m(r_m + |\delta|) \simeq Z_m(r_m - |\delta|) + 2|\delta|[\psi_m(r_m - |\delta|)\gamma_L + B_C] + 2A_{S-}b_S|\delta|^{\nu_S} + O\left(\frac{\delta^2}{r_m^2}\right) \tag{108b}$$

for the general case, and

$$\psi_m(r_m + |\delta|) \simeq \psi_m(r_m - |\delta|) + 2|\delta|[\psi_m(r_s - |\delta|)\hat{\lambda}_L(\ln|\delta| - 1) + A_C + A_D(\ln|\delta| - 1)] + 2A_{S-}|\delta| + O\left(\frac{\delta^2}{r_m^2}\right) \tag{109a}$$

$$Z_m(r_m + |\delta|) \simeq Z_m(r_m - |\delta|) + 2|\delta|[\psi_m(r_m - |\delta|)\hat{\gamma}_L \ln|\delta| + B_D \ln|\delta|] + 2A_{S-}\hat{b}_S|\delta| + O\left(\frac{\delta^2}{r_m^2}\right) \tag{109b}$$

for the special case where the indices ν_L and ν_S are exactly 0 and 1, respectively. For both cases the non-resonant harmonics satisfy

$$\psi_{m+k}(r_m + |\delta|) \simeq \psi_{m+k}(r_m - |\delta|) + O\left(\frac{\delta}{r_m}\right) \tag{110a}$$

$$Z_{m+k}(r_m + |\delta|) \simeq Z_{m+k}(r_m - |\delta|) + O\left(\frac{\delta}{r_m}\right) \tag{110b}$$

Finally, consider a solution which is launched from the rational surface, so that $A_L = A_{S-} = 0$. It follows from the preceding analysis that

$$\psi_m(r_m + |\delta|) \simeq A_{S+}|\delta|^{\nu_S} + O\left(\frac{\delta^2}{r_m^2}\right) \tag{111a}$$

$$Z_m(r_m + |\delta|) \simeq A_{S+}b_S|\delta|^{\nu_S} + O\left(\frac{\delta^2}{r_m^2}\right) \tag{111b}$$

$$\psi_{m+k}(r_m + |\delta|) \simeq A_{S+}\tilde{a}_k|\delta|^{\nu_S} + O\left(\frac{\delta^2}{r_m^2}\right) \tag{111c}$$

$$Z_{m+k}(r_m + |\delta|) \simeq A_{S+}\tilde{b}_k|\delta|^{\nu_S} + O\left(\frac{\delta^2}{r_m^2}\right) \tag{111d}$$

B.3. Toroidal angular momentum conservation

For a tokamak plasma isolated from any external source or sink of toroidal angular momentum (e.g., a resistive vacuum vessel or helical magnetic windings) the volume integrated angular momentum around the toroidal symmetry axis of the equilibrium is a conserved quantity. Thus, the T7 equations ought to conserve the total toroidal angular momentum of an isolated plasma exactly.

The volume integrated toroidal electromagnetic torque acting between the magnetic axis and a flux surface of radius r is given by

$$T_\phi(r) = \int_0^r \oint\oint R^2 \nabla\phi\cdot(\boldsymbol{J} + \delta\boldsymbol{J}) \times (\boldsymbol{B} + \delta\boldsymbol{B}) j\, dr\, d\theta\, d\phi = \int_0^r \oint\oint R^2 \nabla\phi\cdot(\delta\boldsymbol{J} \times \delta\boldsymbol{B}) j\, dr\, d\theta\, d\phi$$

$$= \frac{1}{R_0}\int_0^r \frac{\partial}{\partial r}(rR^4 \delta\boldsymbol{B}\cdot\nabla r\delta\boldsymbol{B}\cdot\nabla\phi)\, dr\, d\theta\, d\phi = \frac{r}{R_0}\oint\oint R^4 \delta\boldsymbol{B}\cdot\nabla r\delta\boldsymbol{B}\cdot\nabla\phi\, d\theta\, d\phi$$

$$= (n\pi^2 R_0)\mathrm{i}\sum_m \frac{(\psi_m Z_m^* - \psi_m^* Z_m)}{m - nq} \tag{112}$$

A trivial manipulation of the T7 equations (82a, b) yields

$$r\frac{d}{dr}\left(\frac{\psi_m Z_m^* - \psi_m^* Z_m}{m - nq}\right) = \sum_{j\neq 0}\frac{(L_m^{m+j}Z_{m+j} + M_m^{m+j}\psi_{m+j})Z_m^* - (L_m^{m+j}Z_{m+j}^* + M_m^{m+j}\psi_{m+j}^*)Z_m}{(m + j - nq)(m - nq)}$$

$$- \sum_{j\neq 0}\frac{(N_m^{m+j}Z_{m+j} + P_m^{m+j}\psi_{m+j})\psi_m^* - (N_m^{m+j}Z_{m+j}^* + P_m^{m+j}\psi_{m+j}^*)\psi_m}{(m + j - nq)(m - nq)} \tag{113}$$

The sum over all poloidal harmonics gives

$$r\frac{dT_\phi}{dr} = (n\pi^2 R_0)i\sum_{m,\,m'}\frac{(L_m^{m'} - L_{m'}^{m})Z_{m'}Z_m^* - (P_m^{m'} - P_{m'}^{m})\psi_{m'}\psi_m^* + (M_m^{m'} + N_{m'}^{m})(\psi_{m'}Z_m^* - \psi_{m'}^*Z_m)}{(m - nq)(m' - nq)} \tag{114}$$

Application of the symmetry relations (85a–d) yields

$$dT_\phi/dr = 0 \tag{115}$$

Thus, the volume integrated toroidal electromagnetic torque is constant between rational surfaces. As will become apparent, the integrated torque can make discontinuous jumps across mode rational surfaces. It follows that net electromagnetic torques can only develop in the vicinity of rational surfaces where ideal MHD breaks down [9, 36].

The net electromagnetic torque $\delta T_\phi(r_j)$ acting in the vicinity of a rational surface of radius r_j is simply given by the discontinuity of T_ϕ across the surface, thus

$$\delta T_\phi(r_j) = \lim_{|\delta|\to 0}[T_\phi(r_j + |\delta|) - T_\phi(r_j - |\delta|)] \tag{116}$$

The total electromagnetic torque acting on the plasma is

$$\Delta T_\phi = \sum_j \delta T_\phi(r_j) = T_\phi(r > r_N) \tag{117}$$

where the sum is taken over the N rational surfaces in the plasma (radii $r_1 < r_2 \ldots < r_N$), and r_N is the radius of the outermost surface. Thus, the criterion for the conservation of the total plasma toroidal angular momentum reduces to

$$T_\phi(r > r_N) = 0 \tag{118}$$

which is clearly a constraint on the boundary conditions applied to the T7 equations at the edge of the plasma ($r = a$).

It is easily demonstrated, using the formalism of Section B.2, that in the vicinity of a rational surface of radius r_j, resonant with poloidal mode number m_j, Eq. (112) reduces to

$$T_\phi(r_j + \delta) \simeq (n\pi^2 R_0)i\left[\left(\frac{r(\nu_S - \nu_L)}{L_{m_j}^{m_j}}\right)_{r_j}(A_L A_S^* - A_L^* A_S)_{r_j+\delta} + \sum_{k\neq 0}\frac{1}{k}(\bar{\psi}_{m+k}\bar{Z}_{m+k}^* - \bar{\psi}_{m+k}^*\bar{Z}_{m+k})_{r_j}\right] \tag{119}$$

It is helpful to define the quantities

$$\Psi_j = r_j^{\nu_L}\left[\frac{\nu_S - \nu_L}{L_{m_j}^{m_j}}\right]_{r_j}^{1/2}(A_L)_{r_j} \tag{120a}$$

$$\Delta\Psi_j = r_j^{\nu_S}\left[\frac{\nu_S - \nu_L}{L_{m_j}^{m_j}}\right]_{r_j}^{1/2}(A_{S+} - A_{S-})_{r_j} \tag{120b}$$

at each rational surface. Here, Ψ_j is the generalization of the familiar cylindrical perturbed poloidal magnetic flux to include the effects of toroidicity, finite pressure and flux surface shaping. It follows from the above that

$$\delta T_\phi(r_j) = (n\pi^2 R_0)i(\Psi_j\Delta\Psi_j^* - \Psi_j^*\Delta\Psi_j) = 2n\pi^2 R_0|\Psi_j|^2\mathrm{Im}(\Delta_j) \tag{121}$$

where from Eq. (106) the tearing stability index at rational surface j satisfies

$$\Delta_j = \Delta\Psi_j/\Psi_j \tag{122}$$

Equation (121) demonstrates that the torque exerted at rational surface j is related to the *imaginary* part of the tearing stability index Δ_j.

Appendix C

EDGE BOUNDARY CONDITIONS

C.1. Matching of equilibrium quantities

The flux surface averaged parallel equilibrium current can be expressed as

$$J_{\|}(r) = \left\langle \frac{R^2}{R_0^2}\frac{\boldsymbol{J}\cdot\boldsymbol{B}}{B_0}\right\rangle = \frac{g^2 B_0}{R_0}\frac{1}{r}\frac{\mathrm{d}}{\mathrm{d}r}\left(\frac{r^2}{q}\langle|\nabla r|^2\rangle\right) \simeq \frac{g^2 B_0}{R_0}\frac{(2-s)}{q}\left(1+\frac{3}{4}\frac{r^2}{R_0^2}-\frac{3}{2}\Delta'^2+\frac{\Delta}{R_0}-\frac{3}{2}E'^2+\frac{3}{2}\frac{E^2}{r^2}\right.$$
$$\left.-\frac{3}{2}T'^2+4\frac{T^2}{r^2}+\mathrm{O}(\epsilon^3)\right)+\frac{g^2 B_0}{R_0}\frac{1}{q}\left(\frac{3}{2}\frac{r^2}{R_0^2}+\Delta'^2+2\frac{r}{R_0}\Delta'-2\frac{R_0 p' q^2}{B_0^2}\Delta'+E'^2+6\frac{EE'}{r}-3\frac{E^2}{r^2}\right.$$
$$\left.+T'^2+16\frac{TT'}{r}-8\frac{T^2}{r^2}+\mathrm{O}(\epsilon^3)\right) \tag{123}$$

whereas the flux surface averaged poloidal equilibrium current takes the form

$$J_\theta(r) = r\left\langle\frac{R^2}{R_0^2}\boldsymbol{J}\cdot\nabla\theta\right\rangle = \frac{B_0}{R_0}\left(\frac{R_0 p'}{B_0^2}+\frac{r}{R_0}\frac{2-s}{q^2}+\mathrm{O}(\epsilon^3)\right) \tag{124}$$

Thus, if the region $r > a$ is a vacuum characterized by $J_{\|} = J_\theta = p = 0$ then

$$s(r>a) = 2+\frac{3}{2}\frac{r^2}{R_0^2}+\Delta'^2+2\frac{r}{R_0}\Delta'+E'^2+6\frac{EE'}{r}-3\frac{E^2}{r^2}+T'^2+16\frac{TT'}{r}-8\frac{T^2}{r^2}+\mathrm{O}(\epsilon^3) \tag{125}$$

It follows from Eqs (74a–c) and (125) that

$$\Delta(r>a) = \Delta_a+\frac{1}{2}\frac{r^2}{R_0}\ln\left(\frac{r}{a}\right)+\frac{1}{2}\left(\frac{r^2}{a^2}-1\right)\left(a\Delta'_a-\frac{1}{2}\frac{a^2}{R_0}\right)+\mathrm{O}(\epsilon^2 a) \tag{126a}$$

$$E(r>a) = \frac{1}{4}(E_a+aE'_a)\left(\frac{r}{a}\right)^3+\frac{1}{4}(3E_a-aE'_a)\frac{a}{r}+\mathrm{O}(\epsilon^2 a) \tag{126b}$$

$$T(r>a) = \frac{1}{6}(2T_a+aT'_a)\left(\frac{r}{a}\right)^4+\frac{1}{6}(4T_a-aT'_a)\left(\frac{a}{r}\right)^2+\mathrm{O}(\epsilon^2 a) \tag{126c}$$

where $\Delta_a = \Delta(a)$, $E_a = E(a)$ and $T_a = T(a)$.

The code T7 requires that the plasma pressure and its first derivative be zero at $r = a$, so that

$$p_a = p'_a = 0 \tag{127}$$

and also that the edge magnetic shear satisfy the constraint

$$s_a = 2+\frac{3}{2}\frac{a^2}{R_0^2}+\Delta'^2_a+2\frac{a}{R_0}\Delta'_a+E'^2_a+6\frac{E_a E'_a}{a^2}-3\frac{E_a^2}{a^2}+T'^2_a+16\frac{T_a T'_a}{a}-8\frac{T_a^2}{a^2}+\mathrm{O}(\epsilon^3) \tag{128}$$

It is clear from the above that these conditions are equivalent to the requirement that the equilibrium plasma current be zero at the edge of the plasma. It is easily demonstrated from the T7 equations (82a, b) that for an equilibrium subject to the constraints (127) and (128) all of the ψ_m and Z_m are continuous across the plasma boundary.

C.2. The vacuum perturbed magnetic field

In vacuum the perturbed magnetic field is written as

$$\delta\boldsymbol{B} = \mathrm{i}\nabla V \tag{129}$$

where the scalar magnetic potential V can be expanded as

$$V(r,\theta,\phi) = \sum_m V_m(r)\exp[\mathrm{i}(m\theta-n\phi)] \tag{130}$$

It follows from Eqs (80a, b) that in the vacuum region $r > a$

$$Z_m(r) = (m - nq)V_m(r) \tag{131}$$

and

$$\psi_m(r) = \sum_k \left\langle \frac{R^2}{R_0^2} |\nabla r|^2 \exp(ik\theta) \right\rangle r \frac{dV_{m+k}(r)}{dr} + \sum_k \left\langle \frac{R^2}{R_0^2} ir\nabla r \cdot \nabla\theta \exp(ik\theta) \right\rangle (m + k)V_{m+k}(r) \tag{132}$$

In vacuum the scalar magnetic potential satisfies Laplace's equation,

$$\nabla^2 V = 0 \tag{133}$$

It is necessary to obtain solutions of Eq. (133) which extend beyond the region of validity of the large aspect ratio ordering (i.e. to regions where $r/R_0 \sim O(1)$). This is achieved using the standard toroidal co-ordinates (μ, η, ϕ), where

$$R = R_0 \frac{\sinh\mu}{\cosh\mu - \cos\eta} \tag{134a}$$

$$Z = R_0 \frac{\sin\eta}{\cosh\mu - \cos\eta} \tag{134b}$$

The most general solution of Laplace's equation in toroidal co-ordinates for a potential that has n periods around the toroidal symmetry axis (see Ref. [37]) is

$$V(\mu, \eta, \phi) = \sum_m A_m \sqrt{\cosh\mu - \cos\eta}\, P^n_{m-\frac{1}{2}}(\cosh\mu) \exp[i(m\eta - n\phi)]$$

$$+ \sum_m B_m \sqrt{\cosh\mu - \cos\eta}\, Q^n_{m-\frac{1}{2}}(\cosh\mu) \exp[i(m\eta - n\phi)] \tag{135}$$

where P^b_a and Q^b_a are standard associated Legendre functions, and A_m and B_m are arbitrary complex constants. The solutions associated with P^b_a are well behaved in the limit $r/R_0 \to \infty$ (i.e. $\mu \to 0$), whereas those associated with Q^b_a are badly behaved.

In the region external to the plasma where the large aspect ratio ordering is valid (i.e. $a < r \ll R_0$), Eq. (135) reduces to

$$V = \sum_m (a_m \hat{P}^m + b_m \hat{Q}^m) \tag{136}$$

where the element $V_k(r)$ of the solution vector V is the kth poloidal harmonic of the scalar potential, so that

$$V(r, \theta, \phi) = \sum_k V_k(r) \exp[i(k\theta - n\phi)]$$

The arbitrary complex constants a_m and b_m are given by

$$a_m = \frac{-2^n |m|! (-\epsilon)^{-|m|}}{\Gamma\left(\frac{|m|}{2} - \frac{n}{2} + \frac{1}{4}\right)\Gamma\left(\frac{|m|}{2} - \frac{n}{2} + \frac{3}{4}\right)} A_m \tag{137a}$$

$$b_m = \frac{(-1)^n \sqrt{\pi}\Gamma(|m| + n + \frac{1}{2})(-\epsilon)^{|m|}}{2^{|m|+\frac{1}{2}}(|m| - 1)!} B_m \tag{137b}$$

for general m, and

$$a_0 = \frac{-2^{n+1}}{\Gamma\left(\frac{1}{4} - \frac{n}{2}\right)\Gamma\left(\frac{3}{4} - \frac{n}{2}\right)} A_0 \tag{138a}$$

$$b_0 = \frac{(-1)^n \sqrt{\pi}\,\Gamma(n - \frac{1}{2})}{\sqrt{2}}\, B_0 \tag{138b}$$

for the special case $m = 0$.

The perturbed poloidal magnetic 'flux' in the region $a < r \ll R_0$ takes the form

$$\psi = \sum_m (a_m \boldsymbol{P}^m + b_m \boldsymbol{Q}^m) \tag{139}$$

where the element $\psi_k(r)$ of the solution vector ψ is the kth harmonic of the poloidal magnetic flux, so that

$$\psi(r, \theta, \phi) = \sum_k \psi_k(r) \exp[\mathrm{i}(k\theta - n\phi)]$$

Note that in the vacuum region the $V_k(r)$ are related to the $\psi_k(r)$ via Eq. (132). The vacuum solution vectors $\boldsymbol{P}^m$ are well behaved as $r/R_0 \to \infty$, whereas the vectors $\boldsymbol{Q}^m$ are badly behaved.

It can be demonstrated, after considerable algebra, that the elements of the vacuum solution vector $\boldsymbol{P}^m$ are

$$P^m_{m-3\sigma}(r) \simeq \left(\frac{r}{a}\right)^{-|m|} \left(1 - \frac{|m|}{3}\right)\left(-\frac{T}{r} + \frac{1}{2}T'\right) \tag{140a}$$

$$P^m_{m-2\sigma}(r) \simeq \left(\frac{r}{a}\right)^{-|m|} \left(1 - \frac{|m|}{2}\right)\left(-\frac{1}{2}\frac{E}{r} + \frac{1}{2}E'\right) \tag{140b}$$

$$P^m_{m-\sigma}(r) \simeq \left(\frac{r}{a}\right)^{-|m|} \left[-\left(\frac{1}{4|m|} + \frac{1}{4}\right)\frac{r}{R_0} - (1 - |m|)\frac{1}{2}\Delta'\right] \tag{140c}$$

$$P^m_m(r) \simeq \left(\frac{r}{a}\right)^{-|m|} (1 + G_0 - |m| G_1 + m^2 G_2) \tag{140d}$$

$$P^m_{m+\sigma}(r) \simeq \left(\frac{r}{a}\right)^{-|m|} (1 + |m|)\left[-\left(\frac{1}{4|m|} + \frac{1}{2}\right)\frac{r}{R_0} - \frac{1}{2}\Delta' - \frac{\Delta}{r}\right] \tag{140e}$$

$$P^m_{m+2\sigma}(r) \simeq \left(\frac{r}{a}\right)^{-|m|} \left(1 + \frac{|m|}{2}\right)\left(\frac{3}{2}\frac{E}{r} + \frac{1}{2}E'\right) \tag{140f}$$

$$P^m_{m+3\sigma}(r) \simeq \left(\frac{r}{a}\right)^{-|m|} \left(1 + \frac{|m|}{3}\right)\left(2\frac{T}{r} + \frac{1}{2}T'\right) \tag{140g}$$

whilst the elements of the associated solution vector $\hat{\boldsymbol{P}}^m$ are

$$\hat{P}^m_{m-3\sigma}(r) \simeq \left(\frac{r}{a}\right)^{-|m|} \left(-\frac{1}{3}\frac{T}{r} + \frac{1}{6}T'\right) \tag{141a}$$

$$\hat{P}^m_{m-2\sigma}(r) \simeq \left(\frac{r}{a}\right)^{-|m|} \left(-\frac{1}{4}\frac{E}{r} + \frac{1}{4}E'\right) \tag{141b}$$

$$\hat{P}^m_{m-\sigma}(r) \simeq \left(\frac{r}{a}\right)^{-|m|} \left(-\frac{1}{4|m|}\frac{r}{R_0} - \frac{1}{2}\Delta'\right) \tag{141c}$$

$$\hat{P}^m_m(r) \simeq -\frac{1}{|m|}\left(\frac{r}{a}\right)^{-|m|} \left[1 + G_3 - |m|\left(G_1 + \frac{1}{2}\frac{\Delta}{R_0}\right) + m^2 G_2\right] \tag{141d}$$

$$\hat{P}^m_{m+\sigma}(r) \simeq \left(\frac{r}{a}\right)^{-|m|} \left[-\left(\frac{1}{4|m|} - \frac{1}{2}\right)\frac{r}{R_0} + \frac{1}{2}\Delta' + \frac{\Delta}{r}\right] \tag{141e}$$

$$\hat{P}^m_{m+2\sigma}(r) \simeq \left(\frac{r}{a}\right)^{-|m|} \left(-\frac{3}{4}\frac{E}{r} - \frac{1}{4}E'\right) \tag{141f}$$

$$\hat{P}^m_{m+3\sigma}(r) \simeq \left(\frac{r}{a}\right)^{-|m|}\left(-\frac{2}{3}\frac{T}{r}-\frac{1}{6}T'\right) \tag{141g}$$

where

$$\sigma = \mathrm{sgn}(m) \tag{142a}$$

$$G_0 = -\left(\frac{(|m|-2)n^2+m^2/4}{4(|m|-1)|m|}\right)\left(\frac{r}{R_0}\right)^2 \tag{142b}$$

for $|m| > 1$ and

$$G_0 = -\left[\frac{n^2}{4}-\frac{1}{8}+\left(\frac{n^2}{2}-\frac{1}{8}\right)\ln\left(\frac{\zeta}{8}\frac{r}{R_0}\right)\right]\left(\frac{r}{R_0}\right)^2 \tag{142c}$$

for $|m| = 1$,

$$G_1 = \frac{1}{4}\frac{r}{R_0}\Delta' + \frac{1}{2}\frac{\Delta\Delta'}{r} + \frac{1}{4}\frac{\Delta}{R_0} + \frac{1}{2}\frac{EE'}{r} + \frac{1}{2}\frac{TT'}{r} \tag{142d}$$

$$G_2 = -\frac{1}{4}\frac{r}{R_0}\Delta' + \frac{1}{4}\frac{\Delta^2}{r^2} - \frac{1}{4}\left(\Delta' + \frac{\Delta}{r}\right)^2 + \frac{1}{4}\frac{E^2}{r^2} - \frac{1}{16}\left(E' + \frac{E}{r}\right)^2 + \frac{1}{4}\frac{T^2}{r^2} - \frac{1}{36}\left(T' + \frac{T}{r}\right)^2 \tag{142e}$$

$$G_3 = -\left(\frac{n^2+(|m|-2)(|m|-\frac{3}{4})}{4(|m|-1)}\right)\left(\frac{r}{R_0}\right)^2 + \frac{1}{4}\frac{r}{R_0}\Delta' + \frac{1}{2}\frac{\Delta}{R_0} \tag{142f}$$

for $|m| > 1$ and

$$G_3 = -\left[\frac{n^2}{4}-\left(\frac{n^2}{2}-\frac{1}{8}\right)\ln\left(\frac{\zeta}{8}\frac{r}{R_0}\right)\right]\left(\frac{r}{R_0}\right)^2 + \frac{1}{4}\frac{r}{R_0}\Delta' + \frac{1}{2}\frac{\Delta}{R_0} \tag{142g}$$

for $|m| = 1$,

$$\zeta = \exp\left(\sum_{i=1}^{n}\frac{2}{2i-1}\right) \tag{142h}$$

The elements of the vacuum solution vectors $\boldsymbol{Q}^m$ and $\hat{\boldsymbol{Q}}^m$ can be obtained via the simple substitution

$$Q^m_{m+j} = P^m_{m-j}(|m| \to -|m|) \tag{143a}$$

$$\hat{Q}^m_{m+j} = \hat{P}^m_{m-j}(|m| \to -|m|) \tag{143b}$$

with the proviso that

$$G_0(|m| \to -|m|) \to \frac{(|m|+2)n^2-m^2/4}{4(|m|+1)|m|}\left(\frac{r}{R_0}\right)^2 \tag{144a}$$

$$G_3(|m| \to -|m|) \to \frac{n^2+(|m|+2)(|m|+\frac{3}{4})}{4(|m|+1)}\left(\frac{r}{R_0}\right)^2 + \frac{1}{4}\frac{r}{R_0}\Delta' + \frac{1}{2}\frac{\Delta}{R_0} \tag{144b}$$

with no exceptions for $|m| = 1$.

For the special case $|m| = 0$,

$$P^0_{\pm 3}(r) \simeq \frac{1}{2}\frac{T}{r} + \frac{1}{2}T' \tag{145a}$$

$$P^0_{\pm 2}(r) \simeq \frac{1}{2}\frac{E}{r} + \frac{1}{2}E' \tag{145b}$$

$$P^0_{\pm 1}(r) \simeq \frac{1}{4}\frac{r}{R_0}\ln\left(\frac{\zeta}{8}\frac{r}{R_0}\right) - \frac{1}{2}\frac{r}{R_0} - \frac{1}{2}\Delta' - \frac{1}{2}\frac{\Delta}{r} \tag{145c}$$

$$P^0_0(r) \simeq 1 + \frac{1}{2}n^2\frac{r^2}{R_0^2}\left[\ln\left(\frac{\zeta}{8}\frac{r}{R_0}\right) - \frac{1}{2}\right] \tag{145d}$$

and

$$\hat{P}^0_{\pm 3}(r) \simeq -\frac{1}{2}\frac{T}{r} \tag{146a}$$

$$\hat{P}^0_{\pm 2}(r) \simeq -\frac{1}{2}\frac{E}{r} \tag{146b}$$

$$\hat{P}^0_{\pm 1}(r) \simeq \frac{1}{4}\frac{r}{R_0}\ln\left(\frac{\zeta}{8}\frac{r}{R_0}\right) + \frac{1}{4}\frac{r}{R_0} + \frac{1}{2}\frac{\Delta}{r} \tag{146c}$$

$$\hat{P}^0_0(r) \simeq \ln\left(\frac{\zeta}{8}\frac{r}{R_0}\right) - \left[\frac{n^2}{4} - \frac{5}{16} - \left(\frac{n^2}{4} + \frac{3}{8}\right)\ln\left(\frac{\zeta}{8}\frac{r}{R_0}\right)\right]\left(\frac{r}{R_0}\right)^2 + \left(\frac{1}{4}\frac{r}{R_0}\Delta' + \frac{1}{2}\frac{\Delta}{R_0}\right)\ln\left(\frac{\zeta}{8}\frac{r}{R_0}\right) + G_1 + \frac{1}{2}\frac{\Delta}{R_0} \tag{146d}$$

with

$$Q^0_{\pm 3}(r) \simeq Q^0_{\pm 2}(r) \simeq 0 \tag{147a}$$

$$Q^0_{\pm 1}(r) \simeq \frac{1}{4}\frac{r}{R_0} \tag{147b}$$

$$Q^0_0(r) \simeq \frac{1}{2}n^2\frac{r^2}{R_0^2} \tag{147c}$$

and, finally,

$$\hat{Q}^0_{\pm 3}(r) \simeq \hat{Q}^0_{\pm 2}(r) \simeq 0 \tag{148a}$$

$$\hat{Q}^0_{\pm 1}(r) \simeq \frac{1}{4}\frac{r}{R_0} \tag{148b}$$

$$\hat{Q}^0_0(r) \simeq 1 + \frac{1}{4}n^2\frac{r^2}{R_0^2} + \frac{3}{8}\frac{r^2}{R_0^2} + \frac{1}{4}\frac{r}{R_0}\Delta' + \frac{1}{2}\frac{\Delta}{R_0} \tag{148c}$$

In Eqs (140) to (148), the principal harmonics are evaluated to $O(\epsilon^2)$ and the sideband harmonics are evaluated to $O(\epsilon)$, in accordance with the basic T7 ordering scheme.

C.3. Angular momentum conservation in the vacuum region

According to Eq. (112), the integrated electromagnetic torque associated with a general vacuum solution is given by

$$T_\phi(r > a) = (n\pi^2 R_0)\mathrm{i}\sum_k [\psi_k(r)V_k^*(r) - \psi_k^*(r)V_k(r)]$$

$$= -n\pi^2 R_0 \sum_{m,l} \{\mathrm{Im}(a_m a_l^*)[\boldsymbol{P}^m, \boldsymbol{P}^l](r) + \mathrm{Im}(b_m b_l^*)[\boldsymbol{Q}^m, \boldsymbol{Q}^l](r) + 2\mathrm{Im}(a_m b_l^*)[\boldsymbol{P}^m, \boldsymbol{Q}^l](r)\} \tag{149}$$

where use has been made of Eqs (136) and (139), and where

$$[\psi^a, \psi^b](r) \equiv \sum_k [\psi_k^a(r)V_k^b(r) - \psi_k^b(r)V_k^a(r)] \tag{150}$$

It can be demonstrated, after considerable algebra, that the vacuum basis solution vectors $\boldsymbol{P}^m$ and $\boldsymbol{Q}^m$ possess the following orthogonality properties:

$$[\boldsymbol{P}^m, \boldsymbol{P}^l](r) = \delta^{ml}O(\epsilon^4) + (1 - \delta^{ml})O(\epsilon^2) \tag{151a}$$

$$[\boldsymbol{Q}^m, \boldsymbol{Q}^l](r) = \delta^{ml}O(\epsilon^4) + (1 - \delta^{ml})O(\epsilon^2) \tag{151b}$$

$$[\boldsymbol{P}^m, \boldsymbol{Q}^l](r) = \delta^{ml}[h_m + O(\epsilon^4)] + (1 - \delta^{ml})O(\epsilon^2) \tag{151c}$$

where

$$h_m = 1 \qquad \text{for } |m| = 0 \tag{152a}$$

$$h_m = 2/|m| \qquad \text{for } |m| > 0 \tag{152b}$$

It follows from Eqs (149) and (151a-c) that, to lowest order,

$$T_\phi(r > a) \simeq -2n\pi^2 R_0 \sum_m \mathrm{Im}(a_m b_m^*) h_m \tag{153}$$

which clearly satisfies the basic angular momentum conservation law (115). In the vacuum region ($r > a$) a general solution vector ψ of the T7 equations can be resolved into elements of the basis solution vectors $\boldsymbol{P}^m$ and $\boldsymbol{Q}^m$ (see Eq. (139)) via

$$a_m \simeq h_m^{-1}[\psi, \boldsymbol{Q}^m](r > a) \tag{154a}$$

$$b_m \simeq -h_m^{-1}[\psi, \boldsymbol{P}^m](r > a) \tag{154b}$$

C.4. Perfect wall boundary conditions

Consider a perfectly conducting wall located on a flux surface at $r_{\mathrm{wall}} > a$. The boundary condition applied to the T7 equations at the wall is simply

$$\psi_m(r_{\mathrm{wall}}) = 0 \tag{155}$$

for all m. This trivially satisfies the global angular momentum conservation constraint (118), since $T_\phi(r_{\mathrm{wall}})$ is clearly zero (see Eq. (149)) and $\mathrm{d}T_\phi(r > r_N)/\mathrm{d}r = 0$ from (115).

C.5. Free-boundary conditions

For a free-boundary problem the solution must be well behaved in the limit $r/R_0 \to \infty$, implying

$$b_m = 0 \tag{156}$$

for all m. This also satisfies the global angular momentum conservation constraint (118), as can be seen from Eq. (153).

Appendix D

CONSTRUCTION OF THE TEARING-MODE DISPERSION RELATION

D.1. Construction of the F matrix

Let there be N rational surfaces in the plasma, with radii r_j ($r_1 < r_2 \ldots < r_N$), resonant with poloidal mode numbers m_j. The construction of a solution vector of the T7 equations associated with rational surface j and satisfying the selected edge boundary conditions proceeds as follows [4].

First, *seven* linearly independent solution vectors $\psi_j^{(1)}, \ldots, \psi_j^{(7)}$ are launched from the magnetic axis ($r = 0$). These are constructed in accordance with Section B.1, with $\psi_j^{(1)}$ consisting only of the $m_j - 3$ poloidal harmonic in the cylindrical circular flux surface limit, $\psi_j^{(2)}$ consisting only of the $m_j - 2$ harmonic in this limit, and so on. Any poloidal harmonics lying outside the range $m_j - 3$ to $m_j + 3$ are discarded in accordance with the basic T7 ordering scheme. The seven solution vectors are integrated forward in r using the T7 equations (82a, b). The integration is stopped at a small distance $|\delta|$ before each rational surface, and restarted again at a distance $|\delta|$ beyond the surface, using the jump condition (108a, b) and (110a, b). This ensures that $\Delta\Psi_k = 0$ at each rational surface ($k = 1$ to N) in the plasma (see Eq. (120b)). In this manner, the solution vectors are integrated to the edge of the plasma ($r = a$)

and are there resolved into coefficients of the well behaved basis vacuum solution vectors $\boldsymbol{P}^m$ and the badly behaved basis vacuum solution vectors $\boldsymbol{Q}^m$ using Eqs (154a, b). Thus, in the vacuum region

$$\psi_j^{(l)}(r > a) = \sum_{k=-3}^{+3} [a^{(l)}_{m_j+k,j} \boldsymbol{P}^{m_j+k}(r) + b^{(l)}_{m_j+k,j} \boldsymbol{Q}^{m_j+k}(r)] \tag{157}$$

for $l = 1$ to 7.

Next, an eighth solution vector $\psi_j^{(8)}$ is launched as a purely 'small' solution from rational surface j, with $\Psi_j = 0$ and $\Delta\Psi_j = 1$, using Eqs (111a–d) and (120b). This solution vector is integrated to the plasma boundary and resolved there into coefficients of the basis vacuum solution vectors in the manner described above. In the vacuum region

$$\psi_j^{(8)}(r > a) = \sum_{k=-3}^{+3} [a^{(8)}_{m_j+k,j} \boldsymbol{P}^{m_j+k}(r) + b^{(8)}_{m_j+k,j} \boldsymbol{Q}^{m_j+k}(r)] \tag{158}$$

Finally, a linear combination of the eight solution vectors,

$$\psi_j^{\text{full}}(r) = \sum_{l=1}^{7} c_{(l)} \psi_j^{(l)}(r) + \psi_j^{(8)}(r) \tag{159}$$

is formed which satisfies the selected edge boundary conditions. For the case of a perfectly conducting wall located at r_{wall} the boundary conditions reduce to

$$\psi^{\text{full}}_{m_j+k,j}(r_{\text{wall}}) = 0 \tag{160}$$

for $k = -3$ to $+3$ (see Section C.4). Here, $\psi^{\text{full}}_{m_j+k,j}(r)$ are the elements of the solution vector $\psi_j^{\text{full}}(r)$, with

$$\psi_j^{\text{full}}(r, \theta, \phi) = \sum_{k=-3}^{+3} \psi^{\text{full}}_{m_j+k,j}(r) \exp\{\mathrm{i}[(m_j + k)\theta - n\phi]\} \tag{161}$$

If there is no wall, the boundary conditions reduce to

$$b^{\text{full}}_{m_j+k,j} \equiv \sum_{l=1}^{7} c_{(l)} b^{(l)}_{m_j+k,j} + b^{(8)}_{m_j+k,j} = 0 \tag{162}$$

for $k = -3$ to $+3$ (see Section C.5). Since there are seven constraints (i.e. Eq. (160) or Eq. (162)) and seven unknowns (i.e. $c_{(1)}$ to $c_{(7)}$) the solution vector ψ_j^{full} can always be constructed.

Now, ψ_j^{full} is denoted the 'fully reconnected' solution vector associated with the rational suface j. By construction it possesses the property

$$\Delta\Psi_k = \delta_{kj} \tag{163}$$

for $k = 1$ to N: i.e. the tearing stability index Δ_k is zero at every rational surface except the rational surface j (see Eq. (122)). Note that the functions $\psi^{\text{full}}_{m_j+k,j}(r)$ which make up ψ_j^{full} are *real* since the T7 equations (82a, b) contain no complex coefficients. The values of the reconnected flux Ψ_k at each rational surface of the plasma associated with ψ_j^{full} form column j of the so called F matrix. Thus, for ψ_j^{full},

$$\Psi_k = F_{kj} \tag{164}$$

for $k = 1$ to N. The F matrix is a *real* $N \times N$ matrix and is completely determined after ψ_j^{full} has been constructed for every rational surface in the plasma (i.e. for $j = 1$ to N).

A general solution vector ψ of the T7 equations can be built up from a linear combination of the N fully reconnected solution vectors. Thus,

$$\psi = \sum_{j=1}^{N} \Delta\Psi_j \psi_j^{\text{full}} \tag{165}$$

where the arbitrary complex constants $\Delta\Psi_j$ specify the amplitudes and phases of the helical 'sheet' currents at each rational surface in the plasma (see Eq. (120b)). Using Eqs (164) and (165), the reconnected flux at each rational surface is given by

$$\Psi_k = \sum_{j=1}^{N} F_{kj} \Delta\Psi_j \tag{166}$$

for $k = 1$ to N. It follows from Eq. (122) that the tearing-mode dispersion relation can be written as

$$(\mathbf{F}\Delta - \mathbf{I})\Psi = \mathbf{0} \tag{167}$$

where $\mathbf{F}$ is the real matrix of elements F_{kj}, $\mathbf{I}$ is the $N \times N$ unit matrix, Δ is a complex $N \times N$ diagonal matrix of elements Δ_j, Ψ is the $1 \times N$ column vector of complex elements Ψ_j and $\mathbf{0}$ is a $1 \times N$ column of zeros.

It follows from Eq. (121) that the net toroidal electromagnetic torque acting in the vicinity of rational surface j is given by

$$\delta T_\phi(r_j) = 2n\pi^2 R_0 \sum_{k=1}^{N} F_{jk}\,\mathrm{Im}(\Delta\Psi_j \Delta\Psi_k^*) \tag{168}$$

Conservation of toroidal angular momentum implies that the total toroidal electromagnetic torque acting on the plasma is zero (see Section B.3). Thus, summing Eq. (168) over rational surfaces yields

$$\Delta T_\phi = \sum_{j=1}^{N} \delta T_\phi(r_j) = n\pi^2 R_0 \sum_{j,k} (F_{jk} - F_{kj})\,\mathrm{Im}(\Delta\Psi_j \Delta\Psi_k^*) = 0 \tag{169}$$

which holds for arbitrary $\Delta\Psi_j$. Clearly, this implies that

$$F_{jk} = F_{kj} \tag{170}$$

for all j and k. Thus, as a consequence of angular momentum conservation, the F matrix must be *symmetric*.

D.2. Construction of the E matrix

Consider the new set of basis solution vectors

$$\psi_j^{\mathrm{unrc}} = \sum_{k=1}^{N} E_{jk}\,\psi_j^{\mathrm{full}} \tag{171}$$

where the E_{jk} are elements of

$$\mathbf{E} \equiv \mathbf{F}^{-1} \tag{172}$$

Here, $\mathbf{E}$ is a *real symmetric* $N \times N$ matrix referred to as the E matrix. It is easily demonstrated that ψ_j^{unrc}, the so called 'unreconnected' solution vector for rational surface j, has the following properties:

$$\Psi_k = \delta_{kj} \tag{173a}$$

$$\Delta\Psi_k = E_{kj} \tag{173b}$$

for $k = 1$ to N: i.e. the reconnected flux Ψ_k is zero at every rational surface except surface j. The tearing-mode dispersion relation (167) can be rewritten (see Ref. [5]) as

$$(\Delta - \mathbf{E})\Psi = \mathbf{0} \tag{174}$$

A general solution vector ψ of the T7 equations can be built up from a linear combination of the N unreconnected solution vectors. Thus,

$$\psi = \sum_{j=1}^{N} \Psi_j \psi_j^{\mathrm{unrc}} \tag{175}$$

where the arbitrary complex constants Ψ_j specify the amplitudes and orientations of the magnetic islands at each rational surface in the plasma. Using Eqs (173) and (175), the $\Delta\Psi_k$ at each rational surface are given by

$$\Delta\Psi_k = \sum_{j=1}^{N} E_{kj}\,\Psi_j \tag{176}$$

for $k = 1$ to N. It follows from Eq. (121) that the net electromagnetic torque acting in the vicinity of rational surface j is given by

$$\delta T_\phi(r_j) = 2n\pi^2 R_0 \sum_{k=1}^{N} E_{jk}\,\mathrm{Im}(\Psi_k \Psi_j^*) \tag{177}$$

Conservation of the toroidal angular momentum of the plasma is guaranteed by the symmetry of the E matrix.

ACKNOWLEDGEMENT

This work was jointly funded by Euratom and the UK Department of Trade and Industry.

REFERENCES

[1] FURTH, H.P., et al., Phys. Fluids **6** (1963) 459.
[2] CONNOR, J.W., HASTIE, R.J., The Effect of Shaped Plasma Cross Sections on the Ideal Kink Mode in a Tokamak, Rep. CLM-M106, Culham Laboratory, Abingdon (1985).
[3] GRIMM, R.C., et al., in Plasma Physics and Controlled Nuclear Fusion Research 1982 (Proc. 9th Int. Conf. Baltimore, 1982), Vol. 3, IAEA, Vienna (1983) 35.
[4] CONNOR, J.W., et al., Phys. Fluids **31** (1988) 577.
[5] CONNOR, J.W., et al., Phys. Fluids B **3** (1991) 1532.
[6] COWLEY, S.C., HASTIE, R.J., Phys. Fluids **31** (1988) 426.
[7] FITZPATRICK, R., HENDER, T.C., Phys. Fluids B **3** (1991) 644.
[8] FITZPATRICK, R., in Theory of Fusion Plasmas (Proc. Joint Varenna-Lausanne Int. Workshop, Varenna, 1992), Editrice Compositori, Bologna (1992) 147.
[9] FITZPATRICK, R., Nucl. Fusion **33** (1993) 1049.
[10] BONDESON, A., PERSSON, M., Nucl. Fusion **28** (1988) 1887.
[11] HENDER, T.C., et al., Nucl. Fusion **32** (1992) 2091.
[12] LA HAYE, R.J., et al., Nucl. Fusion **32** (1992) 2119.
[13] GIMBLETT, C.G., PECKOVER, R.S., Proc. R. Soc. London, Ser. A Math. Phys. Sci. **368** (1979) 75.
[14] JENSEN, T.H., et al., Phys. Fluids B **5** (1993) 1239.
[15] CONNOR, J.W., et al., Plasma Phys. Control. Fusion **29** (1987) 919.
[16] RUTHERFORD, P.H., Phys. Fluids **16** (1973) 1903.
[17] WANG, X., BHATTACHARJEE, A., Phys. Fluids B **4** (1992) 1795.
[18] BOOZER, A.H., Phys. Fluids **27** (1984) 2055.
[19] MIRNOV, S.V., SEMENOV, I.B., Sov. At. Energy **30** (1971) 22.
[20] WESSON, J.A., et al., Nucl. Fusion **29** (1989) 641.
[21] WESSON, J.A., Nucl. Fusion **18** (1978) 87.
[22] BUSSAC, M.N., et al., Phys. Rev. Lett. **35** (1975) 1638.
[23] HENDER, T.C., et al., in Plasma Physics and Controlled Nuclear Fusion Research 1986 (Proc. 11th Int. Conf. Kyoto, 1986), Vol. 1, IAEA, Vienna (1987) 291.
[24] SCOVILLE, J.T., et al., Nucl. Fusion **31** (1991) 875.
[25] TOSCHI, R. (presented by), in Plasma Physics and Controlled Nuclear Fusion Research 1990 (Proc. 13th Int. Conf. Washington, DC, 1990), Vol. 3, IAEA, Vienna (1991) 225.
[26] HUGUET, M., in Steady-State Operation of Fusion Plasmas (Proc. 11th Eur. Tokamak Workshop, Noordwijk, 1993), FOM-Institute for Plasma Physics "Rijnhuizen", Nieuwegein (1993) 547.
[27] POST, D.E., et al., in ITER Physics, ITER Documentation Series No. 21, IAEA, Vienna (1991).
[28] STORK, D., et al., in Controlled Fusion and Plasma Physics (Proc. 14th Eur. Conf. Madrid, 1987), Vol. 11D, Part I, European Physical Society, Geneva (1987) 306.
[29] BHATTACHARJEE, A., in Theory of Fusion Plasmas (Proc. Workshop Varenna, 1987), CEC, Brussels (1987) 47.
[30] BONDESON, A., IACONO, R., in Theory of Fusion Plasmas (Proc. Course Joint Varenna-Lausanne Int. Workshop, Chexbres, 1988), Editrice Compositori, Bologna (1988) 57.
[31] FITZPATRICK, R., et al., Plasma Phys. Control. Fusion **34** (1992) 161.
[32] MARTIN, T.J., et al., Computer Codes for Toroidal Tearing Mode Calculations, Rep. AEA-FUS-91, AEA Fusion, Culham Laboratory, Abingdon (1991).
[33] NEWCOMB, W.A., Ann. Phys. (N.Y.) **10** (1960) 232.
[34] MERCIER, C., Nucl. Fusion **1** (1960) 47.
[35] GLASSER, A.H., et al., Phys. Fluids **18** (1975) 875.
[36] RUTHERFORD, P.H., in Basic Physical Processes of Toroidal Fusion Plasmas (Proc. Course and Workshop Varenna, 1985), Vol. 2, CEC, Brussels (1986) 531.
[37] MORSE, P.M., FESHBACH, H., Methods in Theoretical Physics, Vol. 2, McGraw-Hill, New York (1953) 1301.

(Manuscript received 10 May 1993
Final manuscript received 26 July 1993)